# Anionic:Cationic Surfactant Mixtures at the Oil-Water Interface

by

Konnor K. Jones

A dissertation accepted and approved in partial fulfillment of the

requirements for the degree of

Doctor of Philosophy

in Chemistry

Dissertation Committee:

Jim Prell, Chair

Lawrence Scatena, Advisor

Julia Widom, Core Member

Jayanth Banavar, Institutional Representative

University of Oregon

Winter 2025

DISSERTATION ABSTRACT

Konnor K. Jones

Doctor of Philosophy in Chemistry

Title: Anionic:Cationic Surfactant Mixtures at the Oil-Water Interface

Anionic:cationic surfactant mixtures are unique in that they synergistically enhance and largely govern the properties of the oil-water interface, even when one surfactant is present in trace amounts. These behaviors of the mixtures have significant implications for various industries. For instance, in oil-related industries wherein these mixtures are used to create oil-tolerant foams, small quantities of surfactants can be used to form these important foams. On the other hand, when such enhanced interfacial properties are undesirable, as in the case that foams need to be unstable in the presence of oil, trace amounts of ionic surfactant impurities can detrimentally affect a product's performance. In both scenarios, this oil tolerance is dependent on the mixture's composition: the surfactant mixing ratio as well as the anionic and cationic surfactant themselves. Hence, it is challenging to predict which mixture compositions create oil-tolerant foams since the underlying behaviors that govern a foam's oil tolerance is unclear.

In order to judiciously employ these anionic:cationic surfactant mixtures, it is necessary to characterize the structure-function property relationship of their monolayers that lend to oil-tolerant foams. This thesis helps elucidate this relationship by employing interfacial tensiometry in tandem with vibrational sum frequency spectroscopy to determine the composition (surfactant population and anionic:cationic ratio) and structure (surfactant alkyl tail conformation) of monolayers prepared at the oil-water interface by SDS:DTAB (sodium dodecyl sulfate:dodecyltrimethylammonium bromide) mixtures across a range of surfactant mixing ratios and total surfactant concentrations. These measurements reveal that the interfacial surfactant

density of SDS:DTAB mixtures greatly exceeds that of pure SDS and DTAB at similar concentrations, up to and beyond their respective critical micelle concentration. The enhanced interfacial adsorption of these mixtures is due to the adsorption of stoichiometric 1:1 SDS:DTAB surfactant pairs that form through the attractive electrostatic interactions between surfactant headgroups. We find that the mixed SDS:DTAB monolayers predominantly contain these paired surfactants and a diminutive number of unpaired surfactants. The unpaired surfactants likely act as point defects that disrupt the tight packing of the adsorbed surfactant monolayers. Additionally, we find that the SDS tail is more conformationally ordered than the DTAB tail, even though they are expected to be conformationally identical along the entire tail since they are likely conjoined through van der Waals interactions. This leads to the conclusion that the surfactant pairs are in a staggered arrangement at the interface. These findings also uncover molecular-level factors that may contribute to the enhanced oil tolerance of foams stabilized by anionic:cationic surfactant mixtures and its dependence on the mixture's composition.

This work contains published and unpublished co-authored material.

CURRICULUM VITAE

NAME OF AUTHOR: Konnor K. Jones

GRADUATE AND UNDERGRADUATE SCHOOLS ATTENDED:

University of Oregon, Eugene, OR
Western Kentucky University, Bowling Green, KY

DEGREES AWARDED:

Doctor of Philosophy, Chemistry, 2025, University of Oregon
Master of Science, Chemistry, 2018, Western Kentucky University
Bachelor of Science, Chemistry, 2018, Western Kentucky University

AREAS OF SPECIAL INTEREST:

Lasers
Nonlinear Optics
Vibrational Spectroscopy
Interfacial Science
Physical Chemistry

GRANTS, AWARDS, AND HONORS:

Western Kentucky University Scholars in Service Scholarship: Konnor Jones, 2017

Habitat for Humanity Campus Chapter State Farm Matching Grant Memorandum of Understanding: Rodney Goodman, Konnor Jones, Bryan Reaka, 2016-2017

Western Kentucky University Faculty-Undergraduate Student Engagement Grant, 2016

Western Kentucky University Student Government Association Organizational Aid: Kirsten Banks, Konnor Jones, 2016

University of Oregon three-minute thesis competition people's choice award, May 2022

Western Kentucky University American Institute of Chemists Outstanding graduate student award, 2018

Western Kentucky University Ogden College of Science and Engineering Outstanding Graduate Student award honorable mention, 2018

Kentucky Academy of Science Analytical/Physical Chemistry graduate oral presentation 2nd place, 2017

Western Kentucky University Analytical Chemistry award, 2017

Department of Defense Science, Mathematics, and Research for Transformation scholarship semifinalist, 2015 and 2016

Kentucky Academy of Science Analytical/Physical Chemistry undergraduate oral presentation 3rd place, 2016

Western Kentucky University Freshman Achievement in Chemistry award, 2015

Western Kentucky University Ward C. Sumpter Undergraduate scholarship award, 2015

PUBLICATIONS:

Jones, K. K.; Scatena, L. F. "Molecular Composition and Structure of Anionic:Cationic Surfactant Mixtures at the Oil-Water Interface" *Langmuir*, Under review

Jones, K. K.; Scatena, L. F. "A Tale of Two Tails: Tail Ordering of Stoichiometric 1:1 DTAB:SDS Pairs Adsorbed at the Oil-Water Interface." *Langmuir*, **2024***, 40,* 27445–27454

Tran, E.; Jones, K. K.; Cano, G.; Moore, F. G.; Scatena, L. F. "Synergistic Adsorptive Behavior of Cationic/ Anionic Surfactant Mixtures at the Oil-Water Interface." *J. Phys. Chem. B,* **2022**, 126, 7720-7730**.**

Altman, M. R.; Christoffersen, L. E.; Jones, K. K.; Geraldine, R. L. "Playing Favorites: Preferential Adsorption of Nonionic over Anionic Surfactants at the Liquid/Liquid Interface." *Langmuir* **2021**, 37, 12213-12222.

Carpenter, A. P.; Foster, M. J.; Jones, K. K.; Geraldine, R. L. "Effects of Salt-Induced Charge Screening of AOT Adsorption to the Planar and Nanoemulsion Oil-Water Interfaces." *Langmuir* **2021**, 37, 8658-8666.

Jones, K. K.; Eckler, L. H.; Nee, M. J. "Effect of Ionic Strength on Solvation Geometries in Aqueous Nitrate Ion Solutions." *J. Phys. Chem. A* **2017**, 121, 2322-2330.

ACKNOWLEDGMENTS

Fourteen years ago, I decided to earn a Ph.D. in chemistry, using nonlinear spectroscopy. That journey has finally concluded. *Many* people have helped me during that period. Unfortunately, I do not remember everyone at this time; however, I want to thank those who come to mind.

**To my family:** Ken, Rachel, Kolton, and Anna—I am truly appreciative and grateful for your support throughout my life. I would not have made it to this point without you three. Additionally, thank you to my "co-author" Anna for, at times, falling asleep in my arms, allowing me to write this dissertation.

**To my wife:** Chelsea—thank you for your support while I pursued my Ph.D. You have been there for me during the entire journey. I would not have finished this if you were not there.

**To my high school chemistry teacher:** Mrs. Olson—thank for fostering my curiosity and encouraging me to pursue my passion for chemistry.

**To my first chemistry advisor:** Dr. Matthew Nee—I am extremely grateful and appreciative for your mentorship and encouragement. You played an integral role in preparing me to accomplish my dream of earning a Ph.D.

**To the Richmond lab:** Dr. Geraldine Richmond, Dr. Andrew Carpenter, Dr. Rebecca Altman, Dr. Brandon Schabes, Dr. Regina Ciszewski, Dr. Bri Gordon, Marc Foster, Evan Christoffersen, Dr.

Emma Tran, Dr. Ashely Mapile, Dr. Fred Moore, and Priscilla Lewis —I could not have done this without you all. Geri, I am very appreciative that you allowed me to join your lab. Working in your lab was my dream ever since I learned of your work two years before I enrolled at the University of Oregon. Dr. Larry Scatena, thank you for your friendship, mentorship, and for stepping in as my advisor during Geri's tenure as the Under Secretary for Science and Innovation at the Department of Energy. I have heard people say your grad school advisor significantly influences you as a scientist; I am very appreciative of how you have influenced me as a scientist. Moreover, thank you for guidance as I completely rebuilt my laser. Dr. Fred Moore, I am grateful for the time you spent with the lab and your aid and willingness to help in any way possible. Priscilla, thank you for always being there to lend an ear, support, and guidance.

**My dissertation committee**—Dr. Jim Prell, Dr. Julia Widom, and Dr. Jayanth Banavar: Thank you for your support and willingness to aid me during this journey.

For God.

For my mom who saw the beginning of this journey, but not the end.

TABLE OF CONTENTS

LIST OF FIGURES

Figure Page

LIST OF TABLES

Table Page

# CHAPTER I:

# Introduction

Liquid interfaces are omnipresent in both natural and commercial settings. Some examples of natural liquid interfaces include the oil-water interface at oceanic petroleum seeps,[1] the air-water interface of atmospheric aerosols,[2] and the air-water interface of the quasi-liquid layer on glaciers.[3] In commercial settings, liquid interfaces commonly appear as the air-water interface of liquid foams,[4-7] the oil-water interface of emulsions,[8-10] and the air-water interface of paints and coatings.[11-13] Many commercial processes and materials involve both air-water and oil-water interfaces, particularly in the form of mixed foam-oil systems.[14-16] In many instances, these mixed systems are encountered in the form of oil-based formulations (chemical defoamers)[17] being added to foams to suppress the foam volume. These oil-based defoamers are commonly used because foam tends to readily destabilize and collapse in the presence of oil.[14,17,18] While the low oil intolerance of foams is advantageous in applications where foams are unwanted like water treatment processes[19] and paints/coatings applications,[20] it becomes a hindrance in oily environments such as with enhanced oil recovery[21] and fire suppression,[22] where foam stability is critical. Because the factors and mechanisms that drive the oil intolerance of foams are largely unclear, it is thus challenging to judiciously tune the oil tolerance of foams for specific applications. Consequently, it is difficult to exploit the full capabilities of liquid foams in oily environments. This challenge underscores the critical need to elucidate the factors and mechanisms that drive foam instability/stability in the presence of oil.

At the macroscopic scale, a liquid foam is a collection of gas cells whose walls consist of thin liquid films called lamellae, which meet at junctions known as Plateau borders, as depicted in Figure 1.1. Although the lamellae and Plateau borders constitute only 1-10% of a foam's

volume,[23,24] this liquid network predominantly governs its characteristics and traits.[25] The lamella, being highly susceptible to destabilizing and rupturing, is the principal focus of liquid foam stability research.[25-29] The primary aim of this work is to characterize the factors and mechanisms that drive foam stability/instability. While liquid foam destabilization processes are complex and can occur through multiple pathways, the processes are generally categorized into three mechanisms: coarsening, drainage, and coalescence.[17] Coarsening, also known as Ostwald ripening, is the process wherein gas diffuses from smaller to larger bubbles through the intervening lamella, which is driven by the pressure differential between adjoining bubbles. The second process, drainage, refers to the transfer of water from the lamellae to the Plateau borders, driven by both gravitational and capillary forces. Lastly, coalescence is the merging of bubbles when their adjoining lamella ruptures. All three mechanisms are interrelated, with drainage playing a particularly critical role as it induces lamella thinning, which in turn facilitates and accelerates both coarsening and coalescence.[30]

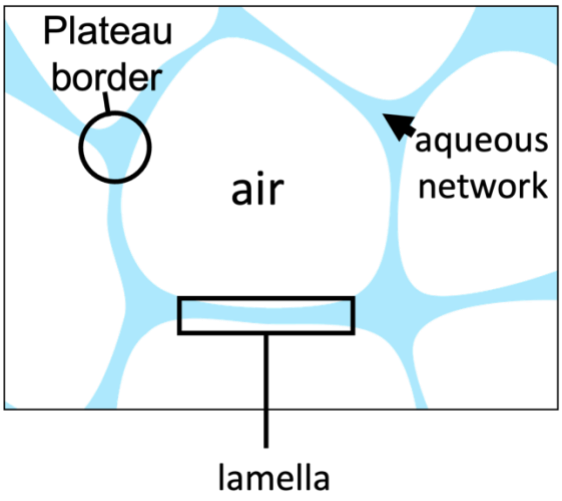


**Figure 1.1.** Cross-sectional view of a liquid foam.

Foam destabilization becomes more complex and interrelated when the foam is introduced into an oily environment. In addition to coarsening, drainage, and coalescence, oil-foam interactions tend to further destabilize lamellae and make the foam more prone to collapse (lamellae rupture). For an oil globule located within the lamella, the specific interactions are unclear. However, the oil-induced foam destabilization process is believed to proceed through three general steps: entry of oil droplet into the lamella's air-water interface,[31,32] oil spreading on the air-water interface,[33] and formation of an unstable oil bridge across the lamella.[34] The bubble collapses once the oil bridge ruptures. The thermodynamic feasibility of these steps is commonly evaluated by a collection of parameters known as the entering, spreading, and bridging coefficients,[31] which are calculated from the equilibrium interfacial tension values of surfactant solution (foaming agent) at the air-water, oil-water, and oil-air interfaces, respectively. While these coefficients provide valuable information about mixed oil-foam systems, they do not always accurately predict whether a foam will readily collapse in the presence of oil.[35,36] This inconsistency is attributable to three primary causes. First, the coefficients are calculated using equilibrium tension values, whereas foams are metastable[37] and never reach thermodynamic equilibrium. Second, the composition of the interfacial layers at each of the interfaces is unknown, particularly for mixtures; this point is discussed below. It is thus not possible to correctly identify which interfacial tension values to use when calculating the coefficients. Lastly, the coefficients do not reflect the kinetics of each destabilization step. It is therefore possible that the coefficients indicate these destabilization processes occur, but the foam is considered oil tolerant because the processes occur slowly. These limitations of the entering, spreading, and bridging coefficients[31] highlights the lack of understanding regarding the oil tolerance/intolerance of liquid.

Additional investigations into oil-induced foam destabilization mechanisms reveal that oil entering the lamella's air-water interface is principally dependent on the stability of the pseudoemulsion film, the thin aqueous film that forms between the lamella surface and an approaching oil globule.[38] Since this finding, studies that investigate oil tolerant/intolerant foam have largely focused on the factors and mechanisms that regulate the stability/instability of the pseudoemulsion film.[38-41] These works have focused on both the air-water and oil-water interface since they constitute a large percentage of the pseudoemulsion film. Selectively studying the pseudoemlusion film interfaces is experimentally not feasible due to the film's diminutive thickness (several nanometers), asymmetrical structure, intricate morphology, and dynamic behavior caused by drainage. Therefore, model oil-water and air-water interfaces formed between bulk fluids are typically examined instead.[29,30,42,43] These model interfaces enable the oil-water and air-water interfaces to be isolated and thus selectively studied with traditional interfacial techniques such as tensiometry, rheology, thin film pressure balance, and optical techniques. While these model interfaces likely are not perfect proxies for the oil-water and air-water interfaces of the pseudoemulsion film, due to water confinement effects[44,45] that likely occur within the film, they still provide invaluable information that helps to reveal the molecular-level details of the pseudoemulsion film. Moreover, this selectivity is invaluable when studying how surfactants contribute to the stability/instability of the pseudoemulsion film since their behavior at the two interfaces can be distinctly different.[46-48] Hence, it starts to become possible to identify how the air-water and oil-water interfaces individually contribute to the overall stability/instability of the pseudoemulsion film.

Given the complexity of the pseudoemulsion film, initial investigations into the molecular factors and mechanisms that regulate their stability/instability have focused on the single (pure)

surfactant systems.[40,49,50] Initial investigations generally found that surfactants confer strong interfacial rheological properties (i.e., high viscosity and elasticity) and high disjoining pressures. Interfacial rheological properties are particularly critical to foam stability[42] since it enables foam films to resist deformation and maintain structure. This resistance hampers the lamella from rupturing during drainage and coarsening, which continually occur.

When much of the liquid has been expelled from the lamella (lamella thickness less than 100 nm), disjoining pressure plays a critical role in foam stability.[43] The disjoining pressure is the sum of long-range repulsive electrostatic interactions as well as short-range steric and van der Waals interactions between two interfaces. In the case of the pseudeomulsion film, the two interfaces are the oil-water and air-water interface of the oil globule and the lamella, respectively. Because repulsive electrostatic interactions are strong, they significantly contribute to the disjoining pressure and thus presumably stabilize the pseudoemulsion film when pure surfactants are used as foam stabilizers.

Although pure surfactants can enhance the stability and longevity of foams in the presence of oil, they are often unsuitable for practical applications due to their high concentration requirements and sensitivity to environmental conditions. Stabilizing foams with pure surfactants typically requires large quantities of surfactants, as exemplified by dodecyltrimethylammonium bromide (DTAB), which forms stable foams only at bulk concentrations exceeding its critical micelle concentration.[43] While the exact mechanisms are not understood, this behavior is partly attributed to the fact that the interfacial rheological properties required for foam stabilization are achieved only at high concentrations. At industrial scales, these high surfactant requirements can result in prohibitively high manufacturing costs. Furthermore, foams stabilized by pure surfactants are not environmentally robust: their performance is significantly influenced by environmental

conditions[37] (e.g., temperature, pH, ionic strength). Given these limitations, there is a pressing need to develop cost-effective and environmentally robust foaming agents for practical applications. This is particularly critical for industries such as enhanced oil recovery and fire suppression, where stable foams in challenging environments would greatly expand their utility and effectiveness.

Anionic:cationic surfactant mixtures have been proposed as new oil tolerant foaming agents for two primary reasons. The first is that these surfactant mixtures are used in nearly all cases that surfactant are used, whether it is intentional or unintentional. Surfactant mixtures are intentionally employed since they synergistically alter the properties of liquid interfaces, leading to ultra-low interfacial tension,[51] very high disjoining pressure,[43] and strong interfacial elasticities,[42] all of which can improve the oil tolerance of foams. On the other hand, the most common reasons surfactant mixtures are unintentionally used is the use of impure chemical reagents and/or utilizing contaminated mixing containers. Regardless of how the mixtures are created, they engender unique and complex interfacial behaviors that can dominate and thus significantly influence the interfacial behaviors. Hence, it is imperative to study how surfactant mixtures behave at the pseudoemulsion film interfaces and how those behaviors translate to their macroscopic properties such as oil tolerance. The second reason is these surfactant mixtures exhibit outstanding oil tolerance compared to pure anionic and cationic surfactants, as evidenced by foam column measurements.[35] These studies determine foam stability by monitoring the decreasing foam volume with time. Complementary rheology measurements[42] suggest that the enhanced tolerance of mixed anionic:cationic surfactant stabilized foams originate from the mixtures' ability to enhance the interfacial dilatational elasticity and viscosity beyond what pure anionic and cationic surfactants can achieve. However, the enhanced rheological properties fail to

explain enhanced oil tolerance of these foams. This becomes clear as one considers foam films measurements of sodium dodecyl sulfate:dodecyltrimethylammonium bromide (SDS:DTAB) mixtures across a range of anionic:cationic surfactant mixing ratios are significantly dependent on whether the anionic or cationic surfactant is in excess. Even though the rheological properties are the same for mixtures that contain excess SDS (SDS-rich) and DTAB (DTAB-rich), the SDS-rich films are stable whereas the DTAB-rich films are unstable and rupture.[43] This observation thus indicates that unidentified molecular-level factors drive the oil tolerance of foams stabilized by anionic:cationic surfactant mixtures.

The molecular-level nuances of the surfactant monolayers are largely uncharacterized due to the technical challenges in selectively probing liquid interfaces with molecular specificity, especially buried liquid-liquid interfaces. This is exemplified by considering techniques that are commonly used to study liquid interfaces. For example, interfacial tensiometry and rheology are commonly employed techniques that probe the interactions and properties at and near a liquid interface without any molecular specificity. Lack of specificity means the molecular details about the system can only be inferred from these measurements. Solution theory,[52,53] a thermodynamic model, was developed in order to discern the composition of surfactant monolayers adsorbed at these interfaces from interfacial tension measurements. However, the assumptions of the model restrict its application to nearly saturated monolayers and to bulk anionic:cationic surfactant mixing ratios that range from 2:8 to 8:2, if accurate results are desired. On the other hand, X-ray[54-56] and neutron[57-59] reflectometry are powerful, interface specific techniques that can provide detailed structural and compositional information about surfactant monolayers at liquid interfaces. However, interpreting the results from these techniques heavily relies on modeling the interface (e.g. interface roughness), the interfacial surfactant layers, and the generated reflectivity profile,

which makes them more prone to inaccuracies. In contrast, linear spectroscopies (e.g., attenuated total reflectance Fourier transform infrared (ATR-FTIR) spectroscopy) are chemically specific but are not interface specific (probe molecules at *and* near the interface) due to the generated evanescent field. Consequently, the signal from molecules at and near the interface cannot be distinguished. These techniques highlight the difficulty in directly interrogating liquid interfaces with molecular specificity under ambient conditions.

Nonlinear spectroscopies, however, can be interface specific (can exclusively probe molecules at an interface) and have demonstrated to be powerful tools for studying the molecular-level details of liquid interfaces, including buried liquid-liquid interfaces (e.g., the oil-water interface), under ambient conditions. Vibrational sum frequency spectroscopy (VSFS) is one of these techniques that essentially provides a vibrational spectrum of interfaces. The interface specificity of VSFS stems from its selection rule that a VSFS response originates exclusively from non-centrosymmetric environments.[60] Unlike spectra from linear spectroscopies, interpretation of VSF spectra is not straight forward due to the coherent nature of the VSF signal that engenders interference effects which distorts both the visual appearance and frequency of each vibrational mode lineshape.[61] Concurrently, this complexity can be leveraged to provide direct insight into the composition and polar orientation of molecules at an interface, which is largely unobtainable with other techniques.

The ability to determine the composition of interfacial layers is invaluable when studying Gibbs monolayers. It is difficult to determine the composition of such monolayers since it is not necessarily equivalent to the bulk, particularly when dealing with mixtures. In surfactant mixtures, the relative interfacial activity and the bulk concentration of the surfactants dictates the relative interfacial population of each species, which itself is difficult to determine. This challenge is

exceptionally more difficult when surfactants in the mixture non-ideally mix by interacting with one another, such as is the case of anionic:cationic surfactant mixtures.[53] In these specific mixtures, the challenge is further compounded by the formation of stoichiometric 1:1 anionic:cationic surfactant pairs (paired surfactants). The paired surfactant association constant is finite,[62,63] meaning these anionic:cationic surfactant mixtures contain three distinct surfactant species (i.e., unpaired SDS, unpaired DTAB, and paired surfactants) that have different interfacial activities. Considering these complexities, it is clear why a detailed molecular picture of Gibbs monolayers formed by anionic:cationic surfactants is lacking.

To help fill the knowledge gap about these mixed surfactant monolayers, anionic:cationic surfactant mixtures, principally SDS:DTAB mixtures, are studied in this dissertation. Specifically, Wilhelmy plate tensiometry in tandem with VSFS are employed to provide a molecular-level perspective of the composition and structure of mixed anionic:cationic surfactant monolayers adsorbed at a model oil-water interface. Carbon tetrachloride was chosen as the oil phase because of its optical transparency in both the infrared and visible spectra. Before delving into these details, Chapter II discusses VSFS theory and the spectral fitting routine used to analyze VSFS spectra. Chapter III provides a detailed description of the instruments, apparatuses, materials, and experimental procedures employed in this work.

Chapter IV elucidates the composition (surfactant population and anionic:cationic ratio) and structure (surfactant alkyl tail conformation) of monolayers prepared at the oil-water interface by 1:1 (equimolar) SDS:DTAB mixtures. The prepared surfactant monolayers are found to be largely composed of paired surfactants and very few unpaired surfactants. In the paired surfactant, the SDS tail is more ordered compared to the DTAB tail, which indicates that the local packing environments of the two tails are different. This finding provides insight into the relative

headgroup immersion depths into the aqueous phase. These findings serve as the foundational knowledge that is needed for understanding the more complicated interfacial behavior of non-equimolar SDS:DTAB mixtures. This work is published with Dr. Lawrence Scatena as the principal investigator.

Chapter V builds on the work in Chapter IV to the more complex non-equimolar SDS:DTAB mixtures. For these experiments, the paired surfactant concentration is fixed while the unpaired surfactant concentration is varied. Varying the unpaired surfactant concentration changes the unpaired surfactants adsorbed at the interface. Similar to the equimolar mixtures, the prepared surfactant monolayers are found to contain very few unpaired surfactants across all surfactant mixing ratios, even when the unpaired surfactant concentration is exceedingly larger compared to the paired surfactant concentration. This behavior is attributed to the exceptionally high interfacial activity of the paired surfactants. The interfacial activity of unpaired SDS and DTAB is also found to be another notable factor given that unpaired surfactants in the mixed SDS:DTAB monolayers can disrupt the interfacial surfactant packing by acting as point defects. These findings and those from Chapter IV provide valuable molecular-level insights into the interfacial behavior of anionic:cationic surfactant mixtures adsorbed at the oil-water interface, which helps develop the structure-function property relationship that is needed to judiciously enhance the oil tolerance of foams for the fire suppression and oil recovery industries. This chapter contains material currently under review for publication with Dr. Lawrence Scatena as the principal investigator.

Lastly, Chapter VI presents a summary of the work discussed in this dissertation and its implications to the stability of liquid foams in the presence of oil. This chapter additionally details future studies that could be carried out to more rigorously assess and build upon the findings of this dissertation.

# CHAPTER II:

## Vibrational Sum Frequency Theory

Vibrational spectroscopy is an indispensable analytical technique due to its ability to reveal molecular-level information of materials. Linear vibrational spectroscopies (IR and Raman) are widely employed and used to study bulk materials. To examine a material's surface/interface, these techniques are configured to interface-sensitive geometries, such as total internal/external reflection geometry. However, in this geometry, the signal still contains contributions from both the interface and the bulk, which are indistinguishable.[64] To exclusively probe molecular vibrations of interfacial molecules, surface-specific nonlinear spectroscopic techniques (e.g., VSFS) are required.[61] VSFS is a second-order nonlinear optical technique that in essence measures the vibrational spectrum of molecules solely at an interface. Only a brief overview of the interface specificity of VSFS is provided here while a more rigorous description is provided elsewhere.[60,65,66]

As light interacts with a molecule, the electromagnetic wave exerts a force on the electrons, inducing an electric dipole, $\vec{\mu}$. For low intensity light, the electric dipole is expressed by

$$\vec{\mu} = \vec{\mu}_0 + \alpha\vec{E} \tag{2.1}$$

where $\vec{\mu}_0$ is the static dipole of the molecule, $\alpha$ is the polarizability of the electrons of the molecule, and $\vec{E}$ is the electric field of the incident light. For an ensemble of molecules, this gives rise to a net dipole moment per unit volume, known as the bulk polarization of the material ($\vec{P}$)

$$\vec{P} = \epsilon_0\chi^{(1)}\vec{E} \tag{2.2}$$

where $\epsilon_0$ is the permittivity of free space and $\chi^{(1)}$ is the first-order susceptibility. For high intensity light (e.g., a laser pulse), nonlinear contributions become significant, and the induced dipole is more accurately represented as

$$\vec{\mu} = \vec{\mu}_0 + \alpha\vec{E} + \beta\vec{E}^2 + \gamma\vec{E}^3 + \cdots \tag{2.3}$$

where $\beta$ and $\gamma$ are the first- and second-order nonlinear hyperpolarizabilities, respectively. Consequently, equation 2.2 becomes

$$\vec{P} = \epsilon_0\left(\chi^{(1)}\vec{E} + \chi^{(2)}\vec{E}^2 + \chi^{(3)}\vec{E}^3 + \cdots\right) \tag{2.4}$$

$$= \vec{P}^{(1)} + \vec{P}^{(2)} + \vec{P}^{(3)} + \cdots \tag{2.5}$$

where $\chi^{(2)}$ and $\chi^{(3)}$ are the second- and third-order nonlinear susceptibility tensors, and $\vec{P}^{(2)}$ and $\vec{P}^{(3)}$ are the second- and third-order nonlinear polarizations.

If two distinct, high intensity electric fields are temporally and spatially overlapped on a sample (as done in this dissertation), the induced polarization state of the material may be accurately expressed by the first two terms of equation 2.5. $\vec{P}^{(2)}$ is the principal focus in this thesis and gives rise to four different optical processes: sum frequency generation (SFG), difference frequency generation, second harmonic generation, and optical rectification.[60] Only SFG is discussed since the spectrometer employed is optimized to measure SFG signal. The SFG response can be expressed as

$$\vec{P}_i(\omega_0) = \chi^{(2)}_{ijk}\vec{E}_j(\omega_1)\vec{E}_k(\omega_2) \tag{2.6}$$

where $\vec{E}_{\mathrm{j}}$ and $\vec{E}_{\mathrm{k}}$ are the electric fields of the incident beams oscillating at frequencies $\omega_1$ and $\omega_2$, respectively. For vibrational sum frequency generation spectroscopy (VSFS), which is employed in this dissertation, the electric fields are an infrared (IR) and a visible (Vis) pulse. This induced

polarization in equation 2.6 oscillates at a frequency that is equal to the sum of the frequencies of the two incident beams ($\omega_{\mathrm{VSF}} = \omega_{\mathrm{IR}} + \omega_{\mathrm{Vis}}$).

Second-order nonlinear optical processes (e.g., sum frequency generation, VSF) are forbidden in centrosymmetric environments (typical of the bulk phase) but permitted in non-centrosymmetric environments (typical of planar interfaces).[60] To understand the origin of this property, it is necessary to recognize that $\chi^{(2)}$ is a third-rank tensor containing 27 elements. Reversing the coordinate system ($i, j, k \rightarrow -i, -j, -k$) of odd-ranked tensors reverses the sign of the tensor:

$$\chi^{(2)}_{ijk} = -\chi^{(2)}_{-i-j-k} \tag{2.6}$$

In contrast, reversing the axis system in a centrosymmetric environment does not change the sign of the tensor:

$$\chi^{(2)}_{ijk} = \chi^{(2)}_{-i-j-k} \tag{2.7}$$

In order for both equations 2.6 and 2.7 to be true, $\chi^{(2)}_{ijk}$ must equal zero:

$$\chi^{(2)}_{ijk} = -\chi^{(2)}_{-i-j-k} = \chi^{(2)}_{-i-j-k} = 0 \tag{2.8}$$

Hence, VSF is forbidden in the centrosymmetric bulk phase. On the other hand, in a non-centrosymmetric environment (e.g., an interface), reversing the coordinate system changes the sign of the tensor (as expressed in equation 2.6), meaning $\chi^{(2)}_{ijk}$ may contain non-zero elements. The number of non-zero elements is dictated by the symmetry of the environment. A planar interface, which is considered in this thesis, posses $C_{\infty v}$ symmetry in the plane of the interface. Under the constraints of this symmetry group and the electric dipole approximation, there are 7 potentially non-zero tensor elements (listed in Table 2.1) that can potentially generate a VSF response.[60] Only four elements are uniquely independent due the x- and y-axes being equivalent (i.e., x = y).

Each non-zero tensor element can be selectively probed by changing the polarization of the incident beams and the generated VSF signal to be either perpendicular (S-polarized) or parallel (P-polarized) to the plane of incidence.[60] Table 2.1 list the polarization combination that probes each of the non-zero tensor element. Polarization combinations are reported in order of increasing wavelength: VSF, Vis, IR, respectively. The different polarization combinations probes components of the transition dipole moments oriented perpendicular (SSP), parallel (SPS, PSS), or both perpendicular and parallel (PPP) to the interface. The SSP combination is exclusively used in this thesis.

**Table 2.1.** The seven non-zero $\chi^{(2)}_{ijk}$ tensor elements of an interface with $C_{\infty v}$ symmetry and the VSF signal, incident visible, incident IR beam polarization combinations that probe each tensor element.

| Non-zero $\chi^{(2)}_{ijk}$ | Polarization combinations (VSF, Vis, IR) |
|---|---|
| $\chi^{(2)}_{xxz}$ | SSP |
| $\chi^{(2)}_{xzx}$ | SPS |
| $\chi^{(2)}_{zxx}$ | PSS |
| $\chi^{(2)}_{zzz}$, $\chi^{(2)}_{yyz}$, $\chi^{(2)}_{yzy}$, $\chi^{(2)}_{zyy}$ | PPP |

Intensity of the VSF signal in any polarization combination is proportional to the $\chi^{(2)}_{ijk}$ and the incident Vis ($I_{Vis}$) and infrared ($I_{IR}$) beam intensities, as expressed in equation 2.9.

$$I_{VSF} \propto \left|\chi^{(2)}\right|^2 I_{IR} I_{Vis} \tag{2.9}$$

The $\chi^{(2)}$ term consist of a non-resonant $\left(\chi^{(2)}_{NR}\right)$ and resonant $\left(\chi^{(2)}_{R}\right)$ contribution:

$$\chi^{(2)} = \chi^{(2)}_{NR} + \sum_{\nu} \chi^{(2)}_{R,\nu} \tag{2.10}$$

The non-resonant contribution is largely constant[67,68] while the resonant term is dependent on the interfacial number density ($N$) and macroscopic average of the molecular hyperpolarizability ($\langle\beta_\nu\rangle$) of probed vibrational modes of molecules at an interface:

$$\chi_{\mathrm{R}}^{(2)} \propto \frac{N}{\epsilon_0}\langle\beta_\nu\rangle \tag{2.11}$$

In order to be VSF active, a vibrational mode must be both IR and Raman active, as expressed by the molecular hyperpolarizability:

$$\beta_{abc}^{(2)} = \frac{A_\gamma M_{\alpha\beta}}{\omega_\nu - \omega_{\mathrm{IR}} - i\Gamma_\nu} \tag{2.12}$$

where $A\gamma$ and $M_{\alpha\beta}$ are the IR and Raman transition moments, respectively, $\omega_\nu$ is the frequency of the vibrational mode, $\omega_{\mathrm{IR}}$ is the IR beam frequency, and $\Gamma_\nu$ is the homogenous line width. Combining equations 2.9 – 2.12 yields equation 2.13.

$$\mathrm{I_{VSF}} \propto \left|\chi_{\mathrm{NR}}^{(2)} + \frac{N}{\epsilon_0}\left\langle\frac{A_\gamma M_{\alpha\beta}}{\omega_\nu - \omega_{\mathrm{IR}} - i\Gamma_\nu}\right\rangle\right|^2 \mathrm{I_{IR}I_{Vis}} \tag{2.13}$$

Inspection of equation 2.13 reveals that a VSF signal will be generated when visible and IR pulses are spatially and temporally overlapped at an interface, irrespective of the IR frequency. Hence, when the IR frequency is off-resonant with an interfacial vibrational mode, the VSF signal will be a non-zero constant. Once the IR beam is resonant with a vibrational mode of a molecule at the interface, $\omega - \omega_{IR}$ goes to zero, the VSFS signal intensity enhanced, giving rise a positive feature in the VSF power spectrum. Thus, the VSF spectrum yields a vibrational spectrum of molecules exclusively at an interface.

**Spectral Fitting Routine**

Since VSFS is a coherent technique, VSF signal emitted from overlapping vibrational modes and the nonresonant response constructively/destructively interfere, which distorts the lineshape and frequency of the spectral features. Thus, VSF spectra must be fit to deconvolute the individual VSF response from each resonant vibrational mode and the nonresonant contribution to the spectrum. The fitting routine implemented here has been discussed in previous publications from

this lab[69,70] and was developed by Bain et al.[71] This model (equation 2.14) represents $\chi^{(2)}$ as a convolution of a Lorentzian and Gaussian distribution, which accounts for homogenous and inhomogeneous broadening, respectively. The inhomogeneous broadening originates primarily from the distribution of surfactant tail conformations and the Gaussian frequency profile of the laser pulses. The first term in equation 2.13 represents the nonresonant signal as an amplitude ($A_{\mathrm{NR}}$) with an associated phase ($\phi_{\mathrm{NR}}$). The second term represents the signal of the resonant vibrational modes and includes terms for the vibrational amplitude ($A_\nu$), phase ($\phi_\nu$), frequency ($\omega_\nu$), as well as Gaussian ($\Gamma_\nu$) and Lorentzian ($\Gamma_L$) linewidths.

$$\left|\chi^{(2)}\right|^2 \propto \left| A_{\mathrm{NR}} e^{i\phi_{\mathrm{NR}}} + \sum_\nu \int_{-\infty}^{+\infty} \frac{A_\nu e^{i\phi_\nu}\, e^{-\left[\omega_{\mathrm{L}} - \frac{\omega_\nu}{\Gamma_\nu}\right]^2}}{\omega_{\mathrm{L}} - \omega_{\mathrm{IR}} + i\Gamma_{\mathrm{L}}} \mathrm{d}\omega_{\mathrm{L}} \right|^2 \tag{2.14}$$

Spectra are either individually or globally fit, as appropriate. All fit parameters and associated errors are in the Appendixes A and B. Spectra that are fit are an average of at least three spectra that are collected on different days.

# CHAPTER III:

# Experimental

## Materials

**Chapter IV**. *Chemicals used:* Dodecyltrimethylammonium bromide (DTAB, 99% purity) was purchased from Acro Organics. Sodium dodecyl sulfate (SDS, ion pair chromatography, LiChropur, ≥ 99.0% purity) was purchased from Millipore Sigma. Hexadecyltrimethylammonium bromide (CTAB, BioXtra, ≥ 99% purity) as well as fully deuterated DTAB (d-DTAB, 98% D) and SDS (d-SDS, ≥ 98% D) were purchased from Sigma Aldrich. DTAB with a deuterated headgroup ($d_9$-DTAB, 98.5% D) was purchased from Cambridge Isotopes Laboratories, Inc. 1,4-Bis(trimethylsilyl) benzene (BTMSB, 98.0% purity) was purchased from Sigma Aldrich. All surfactants and BTMSB were used as received. The oil phase is carbon tetrachloride ($CCl_4$, for HPLC, ≥ 99.9% purity), was purchased from Sigma Aldrich and fractionally distilled twice before being used. The aqueous phase is either $D_2O$ (99.9% D) purchased from Cambridge Isotopes Laboratories, Inc. or ultrapure $H_2O$ (18.2 MΩ ·cm) dispensed from a Barnstead E-pure purification system.

**Chapter V.** *Chemicals used:* The purity, supplier/source, and preparation of DTAB, SDS, d-DTAB, d-SDS, $CCl_4$, $D_2O$, and $H_2O$ are consistent with Chapter IV. CTAB (99+% purity) and dodecylamine hydrochloride (DAC, 99% purity) were purchased from Thermo Fisher Scientific. Both CTAB and DAC were used as received.

## Cleaning Procedure

All glassware used to prepare and contain the samples, the vibrational sum frequency spectroscopy (VSFS) polychlorotrifluoroethylene (Kel-F) cells, associated fluoroelastomer (FKM) O-rings, and ultraviolet (UV) fused silica window were soaked in concentrated sulfuric acid bath containing

NOCHROMIX oxidizer (Godax Labs, Inc.) bath mixture then ultrapure water for at least 12 hr in each bath. The calcium fluoride ($CaF_2$) window of the VSFS cell was placed in the acid mixture for only 15 min to prevent the window from corroding. All items were copiously rinsed with ultrapure water before and after being immersed in the water bath. The glassware was then dried in a 140 ℃ oven.

### Sample Preparation of Surfactant Mixtures

All anionic:cationic surfactant mixtures were prepared by sequentially diluting an aliquot of the cationic and anionic stock solutions in water. The solutions were swirled in the sample vial by hand for 30 sec after each aliquot was added. Samples were immediately transferred to a sample container: a glass well for the interfacial tension measurements or a Kel-F cell for the VSFS measurements.

### Interfacial Tension Measurements

A force balance (Biolin Scientific) with a platinum plate (Biolin Scientific) was used to measure the interfacial tension of the oil-water interface. To prepare the interface, $CCl_4$ and water were sequentially added to a glass well. For the pure surfactants, a concentrated aliquot of SDS or DTAB was added to the well to create a 5 μM solution before being covered. The interfacial tension was recorded after the sample equilibrated for 30 min. In the same manner, the surfactant concentration was increased and allowed to equilibrate before measuring the interfacial tension. For the SDS:DTAB mixtures, the platinum plate was removed after the interfacial tension of the neat oil-water interface was measured. A concentrated aliquot of a SDS:DTAB mixture was then added to the well to achieve the desired total surfactant concentration before being set aside and covered. The interfacial tension was measured after samples equilibrated for 24 hr. Before each measurement, the platinum plate was cleaned with a continuous stream of ultrapure water for 10

min then flame dried. Interfacial tension measurements are reported as interfacial pressure ($IP$), which is the difference in the interfacial tension ($\gamma_{ow}$) of the interface without and with surfactants ($\gamma_s$).

$$IP = \gamma_{ow} - \gamma_s \tag{2.1}$$

**Vibrational Sum Frequency Spectroscopy Measurements**

In order to perform the vibrational sum frequency spectroscopy (VSFS) experiments described herein, a commercially available VSFS spectrometer (purchased from Ekspla) was employed. The system consists of four main components: a laser, a harmonic generation unit, an optical parametric generation unit (OPG), and a collection hood. Figure 3.1 displays a schematic of the spectrometer. Each stage is briefly described.

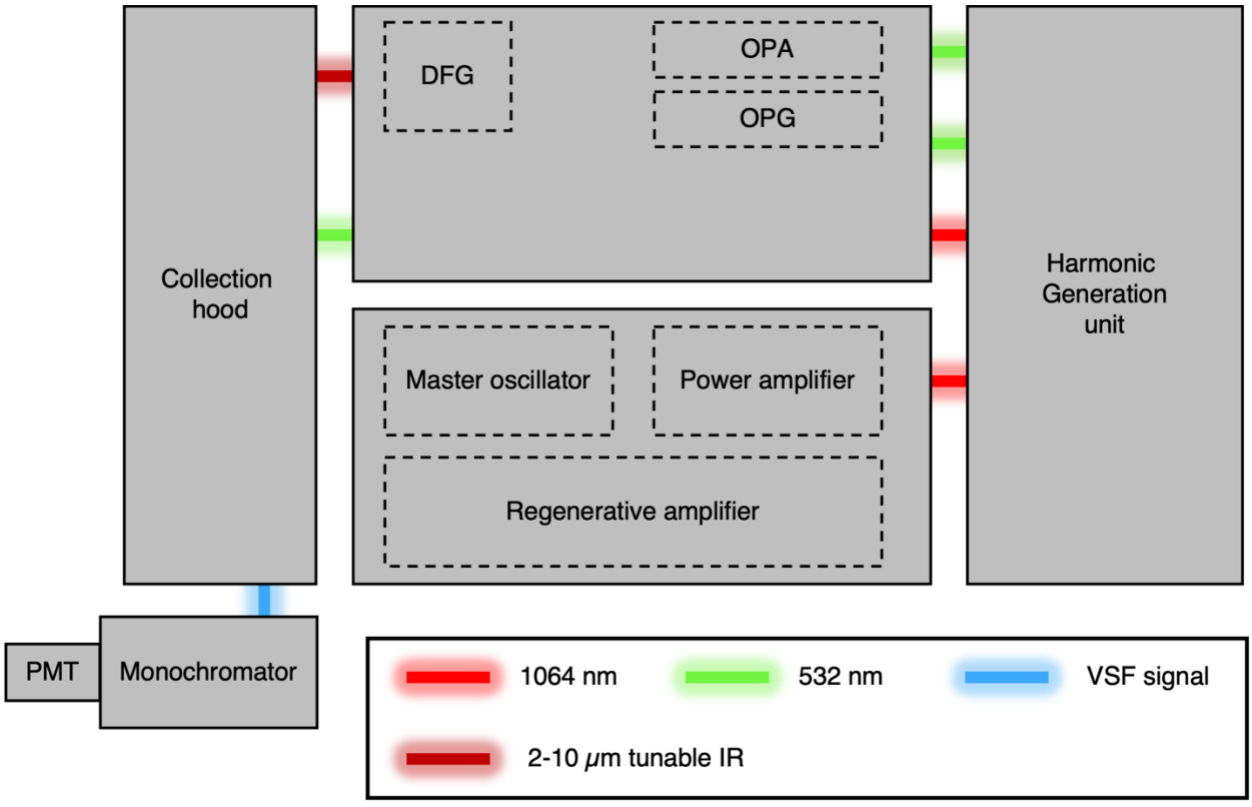


**Figure 3.1.** VSFS spectrometer schematic.

The laser (Ekspla, PL-2250) is comprised of three functional parts: a master oscillator, a regenerative amplifier, and a power amplifier. The master oscillator houses a diode pumped Nd:YAG rod and a solid-state saturable absorber to passively mode-lock the intracavity pulses. The ~30 ps pulses are dumped injected into the regenerative amplifier at a repetition rate of 50 Hz. In the regenerative amplifier, the pulses are amplified by means of a larger Nd:YAG crystal, pumped by a diode. The pulses are subsequently amplified in a double-pass power amplifier, comprised of a yet larger Nd:YAG crystal pumped by flashlamps. The laser beam is directed into the harmonic generation unit (Ekspla, SFG H500) where the fundamental beam is split three ways, two of which are frequency doubled to 532 nm in K*DP nonlinear crystals. One 532 nm beam is sent along a delay stage before being sent directly to the oil-water interface and is referred as the visible beam. The remaining 532 and 1064 nm beams are sent into an OPG. The 532 nm beam is split into two parts referred to as Vis A and Vis B. The Vis A is passed through a BBO nonlinear crystal to generate a signal and idler. The idler is combined with the Vis B in a second BBO crystal to generate a second signal (signal 2) and idler (idler 2). Idler 2 is mixed with the 1064 nm beam to generate a narrowband mid-IR (2–10 μm) beam in a $AgGaS_2$ crystal through different frequency generation (DFG). The frequency of the mid-IR beam is tuned by concurrently adjusting the angles of the three nonlinear crystals according to a calibration curve. The mid-IR beam spatially and temporally overlaps with the visible beam at the oil-water interface. The mid-IR beam is incident on the interface at ~76° while the visible beam concurrently totally internally reflects at 68°, relative to interface normal, to generate a VSF response. Beam angles were selected to maximize the VSF signal intensity in the C-H stretching spectral region, which is the principal focus of the measurements in this thesis. The pulses incident at the interface are ~30 ps. The energy of the visible pulses is 9 μJ and the maximum energy of the IR pulses is ~270 μJ. A series of filters,

waveplates, a polarizer, and a monochromator (SOL instruments, MS 2001i) isolate the VSF signal before being detected by a photomultiplier tube. Resolution of the VSFS spectrometer is 7 $cm^{-1}$.

Figure 3.2 displays a schematic of the VSFS cell contained the samples for the VSFS measures. The cell was machined from a solid piece of Kel-F and incorporates uncoated calcium fluoride ($CaF_2$) and UV fused silica windows as the entrance and exit windows, respectively. The windows were sealed with FKM O-rings. The cell and O-ring materials was selected due to their chemical resistivity, which enables these objects to be scrupulously cleaned and mitigates the leaching of contaminates. $CaF_2$ and UV fused silica windows were selected due to their optical transparency in the mid-IR and visible spectral regions, respectively, and their low solubility in water. The bottom-up cell/beam geometry is employed because it enables the interfacial water spectral region to be examined, with the oil being the subphase. This is critical for the measurements in this thesis since the interfacial water response is monitored in this thesis.

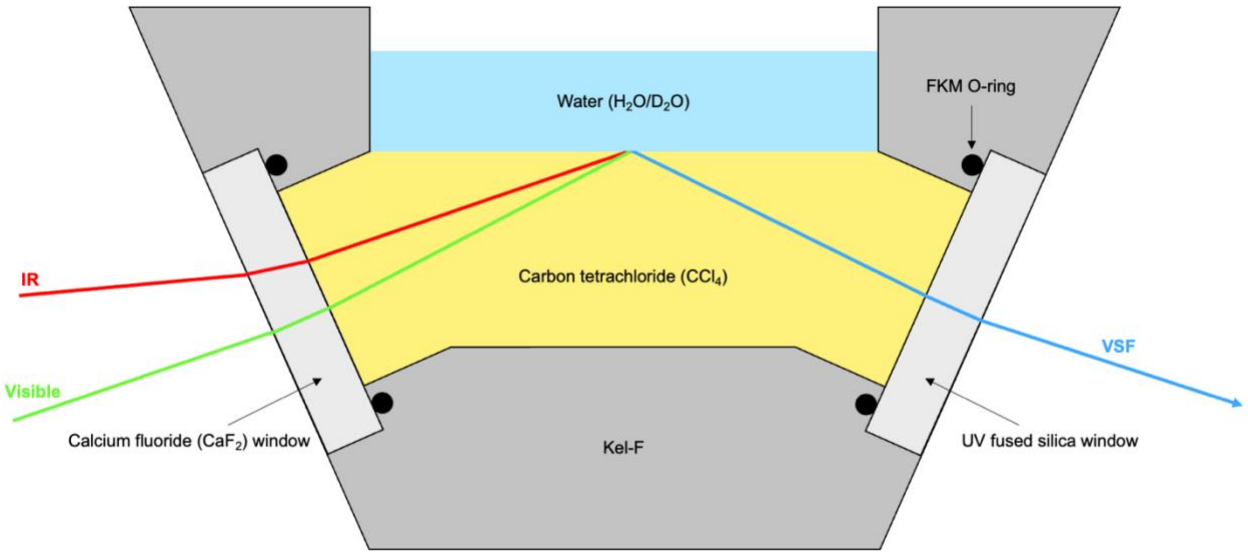


**Figure 3.2.** A side-view schematic of the vibrational sum frequency spectroscopy (VSFS) sample cell with the incident and outgoing beams. The cell was machined from a solid piece of Kel-F and incorporates uncoated calcium fluoride ($CaF_2$) and ultraviolet (UV) fused silica windows, respectively. The windows were sealed with fluoroelastomer (FKM) O-rings.

The SSP polarization scheme (VSF signal, incident visible, incident IR beam polarizations) was used to probe components of transition dipole moments oriented perpendicular to the interface. Spectra were collected with step size of 5 $cm^{-1}$ and 550 pulses/step. Measured spectra are normalized to the nonreonsant VSF response that is measured from an unprotected gold mirror submerged in $CCl_4$ to account for changes in the energy of the IR beam incident at the interface across the scanned spectral regions.

The oil-water interface was created by sequentially adding $CCl_4$ and water to the VSFS cell. Carbon tetrachloride is used as a model oil because of its optical transparency in the visible and IR spectra. While using a model oil may slightly alter the surfactants' behavior, this work is expected to provide valuable insights into molecular-level details not found in literature and establish a foundation to investigate oils that are encountered in practical applications. The VSF spectrum of the neat oil-water interface was used to confirm that no surfactants were adsorbed at the interface before a sample was added. Once the interface was confirmed to be bare, the water layer was replaced with an 8 ml of surfactant sample at the desired concentration. The cell was subsequently set aside and covered. Spectra were collected after the sample equilibrated for 18 hr. Shorter equilibration times led to inconsistent results due to notable changes in the relative intensity of the C-H spectral features among samples with the same composition.

**Fourier Transform Infrared Spectroscopy Measurements**

Samples were prepared in a 1 cm path length UV Fused Quartz cuvette. The cuvette was filled with 2 ml of $CCl_4$ followed by 1 ml of a 30 μM 1:1 DTAB:SDS mixture. The cuvette opening was covered with a Teflon cap and subsequently sealed with Parafilm before being set aside for 24 hr. Proceeding the equilibration period, a Fourier transform infrared spectrometer (ThermoFischer Scientific, Nicolet 6700 IR) was used to collect a spectrum of the $CCl_4$. The sample compartment

was purged with $N_2$ gas for 5 min before a spectrum was collected. The spectrum is an average of 64 scans with a resolution of 2 $cm^{-1}$.

### Quantitative $^1H$ Nuclear Magnetic Resonance Spectroscopy

In order to accurately quantify the surfactant concentration in the $CCl_4$, the sample was prepared in a separatory funnel. This procedure assured the analyzed $CCl_4$ aliquot was not artificially enriched with surfactants, which occurs when the aliquot is obtained by pipetting through the sample's aqueous phase air-water and oil-water interfaces. To closely reproduce the interfacial areas and volume fractions of the IFT and VSFS experiments, 25 ml of $CCl_4$ and 100 ml of $D_2O$ were sequentially added to a separatory funnel. A concentrated 1:1 DTAB:SDS mixture was then diluted to 25 μM in the $D_2O$ before the funnel opening was covered. A $CCl_4$ aliquot was collected after the sample equilibrated for 24 hr. To minimize contamination, the aliquot was collected after most of the $CCl_4$ was dispensed but before $D_2O$ was expelled.

NMR spectra of the aliquots were collected on a Bruker AVANCE III HD spectrometer operating at 600.01 MHz and equipped with a Bruker Prodigy Cryoprobe. Spectra were collected using the Bruker zg30 pulse sequence with 16,000 points collected at an offset frequency of 900 Hz and a 5.00 ppm signal width. Each spectrum was the average of 5,000 scans with a recycle delay of 1 sec. The internal standard was 1 μM BTMSB. A sealed glass capillary tube containing $D_2O$ inserted into the NMR tube was used as the internal lock reference for the $CCl_4$ sample.

# CHAPTER IV:

## Interfacial Behavior of Equimolar SDS:DTAB Mixtures

This work is in press in the journal *Langmuir*: Jones, K. K.; Scatena, L. F. A Tale of Two Tails: Tail Ordering of Stoichiometric 1:1 DTAB:SDS Pairs Adsorbed at the Oil-Water Interface. Konnor Jones identified the study's obejctives, designed and performed the experiments, analyzed and interpreted the data, and wrote the manusript. Geraldine Richmond was the principal investigator for this work and provide general guidance prior her leave of absence that began on Nov. 8, 2021, serving as Undersecretary of Science and Innovation, Department of Energy. Larry Scatena served as the principal investigator during Dr. Richmond's leave, overseeing the project through completion by providing general feedback and editorial assistance.

### Introduction

Surfactant mixtures play a critical role in a myriad of industries including oil,[35,72] gas,[18,73] detergents,[74,75] firefighting,[22,76] pharmaceuticals,[77,78] cosmetics,[79,80] personal care,[81,82] and food.[83,84] Compared to pure (unmixed) surfactants, mixtures are commonly used because of their unique interfacial behaviors and enhanced ability to adsorb at and alter the properties of interfaces. These notable behaviors drive a range of desirable properties including strong interfacial viscoelasticity,[30,42,43] ultra-low interfacial tension,[42,43,85,86] high disjoining pressure,[30,43] and decreased critical micelle concentration.[43,85] These properties promote the formation and inhibit the destabilization of both foams and emulsions. Foam and emulsion stability is particularly important to oil recovery,[10,73] gas production,[73,87] and fire suppression.[22,88]

Foams are gas bubbles separated by liquid films called lamellae, and maintaining sufficient stability while they are deployed is a critical challenge to optimizing their efficacy. This is particularly difficult in applications that involve oil, as it tends to destabilize foam by rupturing

the lamellae.[17,18,21,35,42,72] It is therefore important to identify surfactant mixtures and their interfacial behaviors that enhance foam stability in the presence of oil. This requires identifying surfactant mixtures that sufficiently stabilize the pseudoemulsion film, the aqueous film that separates oil and the air-water interface of a foam, which is believed to be the primary determinant of foam stability in an environment where oil is present.[35,40,89-91] Because the pseudoemulsion film contains both air-water and oil-water interfaces, it is necessary to characterize the structure-property relationship of surfactant mixtures at these interfaces to provide a better understanding of their collective effects on these films.

Selectively studying pseudoemulsion film interfaces is exceptionally difficult because of the film's minute thickness and intricate morphology. Therefore, oil-water and air-water interfaces formed between bulk fluids are used as model interfaces. Interfacial rheology, interfacial tension, and thin film measurements[30,43] are commonly performed at these planar interfaces since they are efficient and relatively easy means to study the behavior and properties of adsorbed surfactants. These measurements, in conjunction with foam stability studies,[30,35] show that stable foams have tightly packed interfacial surfactant monolayers, characterized by strong interfacial viscoelasticity, ultra-low interfacial tension, and high disjoining pressure. Anionic:cationic surfactant mixtures exhibit these properties.[30,35,43] This presumably is the reason foams stabilized by these mixtures are more oil tolerant compared to pure anionic and cationic surfactants. The net neutral charge and van der Waals interactions of stoichiometric 1:1 anionic:cationic surfactant pairs drive the enhanced adsorption (interface activity) and interfacial packing of these mixed surfactant systems. However, a detailed understanding is necessary as the aforementioned techniques do not report on the composition, structure, or net charge of surfactant monolayers with any type of molecular-level specificity. Consequently, molecular-level details about the surfactant mixtures are lacking and it

is difficult to elucidate the structure-property relationship necessary to design surfactant mixtures to more effectively stabilize foams in oil-related applications.

In an effort to understand and efficiently advance the state-of-the-art of foam stabilization, this work provides molecularly specific details regarding the composition, molecular conformation, and headgroup immersion depths of surfactant monolayers prepared by a 1:1 anionic:cationic surfactant mixtures at the oil-water interface. The molecular-level details of these mixed surfactant systems at an oil-water interface are limited since few experimental techniques can specifically probe buried liquid-liquid interfaces with molecular specificity. Only the 1:1 ratio is examined herein as it serves as a foundation for ongoing investigations into the more complex behavior observed at other surfactant mixing ratios. This work, in conjunction with other work of anionic:cationic surfactant mixtures at the air-water interface,[92-98] provide a more comprehensive understanding of the driving forces that define oil-tolerant foams.

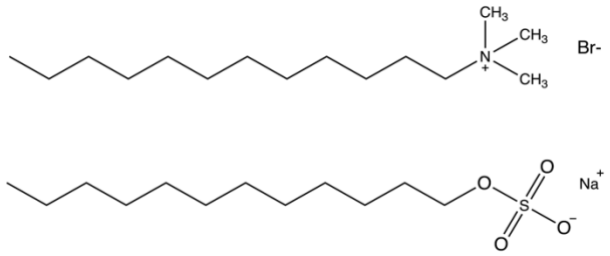


**Figure 4.1.** Molecular structure of DTAB (top) and SDS (bottom).

The system examined herein is composed of a model surfactant mixture and oil. The mixture is composed of sodium dodecyl sulfate (SDS) and dodecyltrimethylammonium bromide (DTAB). Their simple molecular structures (Figure 4.1) and the considerable amount of experimental and theoretical work[47,51,96,98-101] performed with this mixture and the individual surfactants makes it an ideal model to investigate the interfacial behavior of 1:1 anionic:cationic mixtures at an oil-water interface. Moreover, both surfactants are commonly used in foaming

agents and their mixtures create more oil tolerant foams compared to pure SDS and DTAB.[35,43] This lab has also extensively characterized the interfacial behavior of these pure surfactants at the oil-water interface.[102-105] Carbon tetrachloride is used as a model oil because of its optical transparency in the visible and IR spectra. Although a model oil may slightly alter the surfactants' behavior, this work is expected to provide valuable insights into molecular-level details not found in literature and establish a foundation to investigate oils that are encountered in practical applications. Interfacial tensiometery is employed to examine the population, general molecular packing, and the 2D phase (gas-, liquid-, or solid-like) of the adsorbed surfactants as a function of concentration. Concurrently, vibrational sum frequency spectroscopy (VSFS) is employed to determine the composition of the monolayer by monitoring the intensity of the charge sensitive VSF response of water while the individual SDS and DTAB conformations are deconvoluted by selectively deuterating the surfactants in the 1:1 SDS:DTAB mixture. It is found that at all concentrations studied, the prepared monolayers are largely composed of paired SDS and DTAB surfactants and few, if any, unpaired surfactants. Although the conformational ordering of both the SDS and DTAB tails of the paired surfactants increases with bulk concentration, interestingly, the SDS tail is more ordered at all concentrations. These findings provide a fundamental understanding of how 1:1 anionic:cationic surfactant mixtures are adsorbed at the oil-water interface, which is crucial to strategically employ anionic:cationic surfactant mixtures to create oil tolerant foams.

**Synergistic Interfacial Adsorption of 1:1 SDS:DTAB Mixtures**

Figure 4.2 compares the measured interfacial pressure isotherm of 1:1 SDS:DTAB mixtures (blue circles) to the interfacial pressure values of pure 25 μM SDS (solid black line) and DTAB (dashed black line). The relatively low interfacial pressures (population of adsorbed surfactants) of 0.01–1 μM 1:1 SDS:DTAB mixtures indicate that few surfactants are adsorbed at the interface at these

concentrations. Pure SDS and DTAB reach a similar interfacial pressure at a much larger, nearly 25–2500 times greater, concentration of 25 μM. In turn, this comparison exemplifies the increased interface activity of the 1:1 SDS:DTAB mixtures, commensurate with the enhanced interfacial behavior of anionic:cationic surfactant mixtures.[85,92,106]

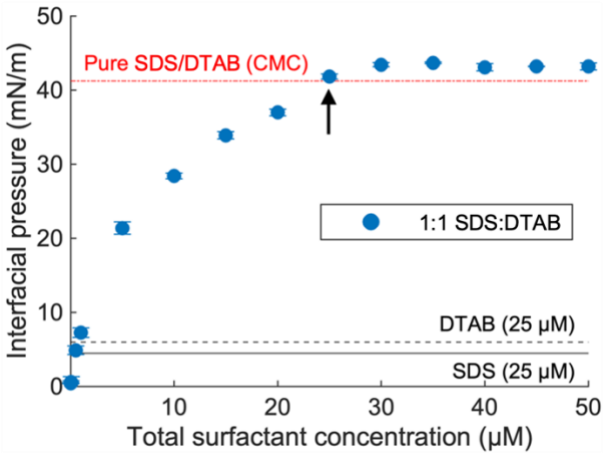


**Figure 4.2.** Interfacial pressure isotherm for 1:1 SDS:DTAB mixtures as well as interfacial pressure values for pure 25 μM SDS (solid black line) and DTAB (dashed black line). Interfacial pressures of pure SDS and DTAB at their CMC (dash-dotted red line) are within error and thus represented by a single line. Error bars for the 1:1 SDS:DTAB mixtures are the standard deviation of at least three measurements performed on separate days.

The enhanced adsorption behavior of the 1:1 SDS:DTAB mixtures is also observed at higher concentrations, most notably around the critical micelle concentration (CMC). The measured interfacial pressure of the mixed surfactant system at 25 μM is greater than pure 8.1 mM SDS and 14.6 mM DTAB (dash-dotted red line), which is the CMC of the pure surfactants and the point of full monolayer coverage.[107,108] The disparity in interface coverage between the mixture and pure surfactants is observed at all concentrations but is the largest at ~30 μM, which is the CMC of the 1:1 SDS:DTAB mixture, as determined from the isotherm in Figure A.1. This value agrees well with the CMC that is determined from surface tension measurements at the air-water interface,[43] suggesting the surfactant concentration in the oil phase is negligible, as discussed in Appendix A. This result is substantiated by Fourier transform infrared (FTIR) and quantitative $^{1}$H

nuclear magnetic resonance (qHNMR) spectroscopic measurements (details provided in Appendix A), which conjointly show surfactants are present in the $CCl_4$ at concentrations well below 1 μM and therefore within experimental error. The disparity in interface coverage is due to the adsorption of highly interface active stoichiometric 1:1 SDS:DTAB pairs that are net neutrally charged.[43,85] These paired surfactants form through attractive electrostatic interactions between the SDS and DTAB headgroups and have an association constant that is on the order of $10^6$.[62] Because of their net neutral charge, short-range steric and van der Waals interactions regulate their interfacial packing and promote tight packing. The tight packing reduces the average interfacial area per surfactant (headgroup area) compared to pure surfactants at comparable concentrations, as evidenced by the larger interfacial pressures of the mixtures in Figure 4.2. This behavior contrasts pure SDS and DTAB monolayers in which long-range repulsive electrostatic interactions regulate interfacial packing and results in a relatively large headgroup area. Consequently, the loose packing of the pure SDS and DTAB monolayers limits the population of adsorbed surfactants compared to the increased interface densities of 1:1 SDS:DTAB mixtures. The remarkably high interfacial pressures of these 1:1 SDS:DTAB mixtures at relatively low total surfactant concentrations exemplify their enhanced adsorption properties that arise from the net neutral charge of the paired surfactant headgroup.

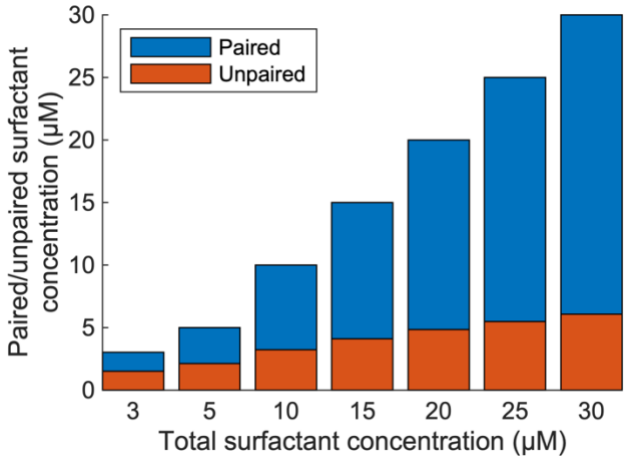


**Figure 4.3.** Concentration of paired and unpaired surfactants in 3–30 μM 1:1 $SDSO_3$:DAC mixtures.

To provide additional insight into the interfacial behavior of the mixtures, we consider how the association behavior of the SDS:DTAB pairs influence the composition of the surfactant monolayer. Although the association constant of the SDS:DTAB mixture is unknown, it is likely finite, as found for similar anionic:cationic surfactant mixtures.[62,63] Thus, SDS:DTAB mixtures contain unpaired surfactants that are presumably co-adsorbed at the interface. To appreciate the percentage of unpaired SDS and DTAB in the mixtures, we consider the $SDSO_3$:DAC (sodium dodecyl sulfonate:dodecylammonium chloride) mixture whose association constant is $1.3 \times 10^6\ M^{-1}$.[62] The $SDSO_3$:DAC mixtures is a reasonable proxy, considering the similarities between the surfactants in the two mixtures. Figure 4.3 shows the percentage of unpaired surfactants in the 3–30 μM 1:1 $SDSO_3$:DAC mixtures range from 50–20%, respectively. While these values are only a proxy, they indicate that the SDS:DTAB mixtures contain a considerable number of unpaired surfactants, which is likely reflected in the surfactant monolayer composition. However, due to the interface activity coefficient of the unpaired SDS (0.22 L/mmol) and DTAB (0.21 L/mmol) being nearly 300 times smaller than the 1:1 SDS:DTAB pair (62.5 L/mmol),[109] the percentage of unpaired surfactants at the interface is presumably much smaller compared to the bulk. The

magnitude of this disparity in interface coverage is unclear since thermodynamic methods like interfacial tensiometry cannot distinguish between unpaired and paired surfactants, highlighting the need for complimentary VSFS measurements to more accurately elucidate the composition of surfactant monolayers, which are discussed later.

**Presence of Unpaired Surfactants at the Interface**

In order to further examine the general composition of the monolayers prepared by the 1:1 SDS:DTAB mixtures, we use the Gibbs[110] and Frumkin[53] equations (details described in the Appendix A) to recast the interfacial pressure values as headgroup areas. Figure 4.4 shows the headgroup area isotherm for the 1:1 SDS:DTAB mixture. We first focus on the 5–50 μM 1:1 SDS:DTAB mixtures of the isotherm since the headgroup areas at these concentrations are markedly smaller compared to maximally packed pure SDS and DTAB monolayers (Figure 4.4); the marked reduction in headgroup area is particularly informative for understanding the composition of the monolayers. The headgroup areas of the 5–50 μM 1:1 SDS:DTAB mixtures range from 34–40 $Å^2$, which are approximately two times smaller than the saturated headgroup areas of pure SDS (59 $Å^2$, solid line)[102] and dodecyltrimethylammonium chloride (DTAC, 88 $Å^2$, dashed line).[102] DTAC is expected to be an accurate proxy for DTAB as a different counterion is unlikely to significantly alter the interfacial packing of the $DTA^+$ ion.[111] The headgroup areas of monolayers formed by pure SDS, pure DTAB, or a SDS:DTAB mixture can be smaller than these saturated headgroups only when the repulsive electrostatic interactions among the headgroups are diminished, as with a pure surfactant/salt mixture,[111] or in our case, a paired surfactant. The markedly smaller headgroup areas of the 1:1 SDS:DTAB mixtures compared to pure SDS and DTAB therefore suggest that predominantly paired surfactants are adsorbed at the interface. Additionally, the headgroup areas of the mixtures (34–40 $Å^2$) are similar to the cross-sectional

area of the SDS (30 Å$^2$)[112] and DTAB (28 Å$^2$)[113] headgroups, suggesting the interface is covered with paired surfactants. This finding is commensurate with what has been postulated about 1:1 SDS:DTAB mixtures at other oil-water[86,114] interfaces and the air-water[43,85] interface. Due to the finite association constant of the paired surfactants, unpaired surfactants are also in solution[62,63] and thus may also be adsorbed at the interface. However, these headgroup area measurements do not have the fidelity to reveal if the mixed SDS:DTAB monolayers also contain unpaired surfactants.

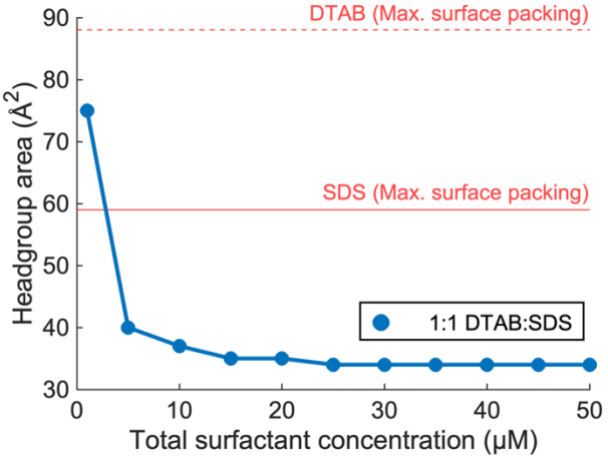


**Figure 4.4.** Headgroup area isotherm for 1:1 DTAB:SDS mixtures, obtained from interfacial pressure measurements in Figure 4.2. The headgroup areas of pure SDS (solid red line) and DTAB (dashed red line) at maximum interfacial packing are also included. The solid blue line is a guide to the eye.

The presence of unpaired surfactants adsorbed at the interface of 1:1 SDS:DTAB mixtures can be assessed by examining the VSF water spectrum. The hydrogen bonding network of interfacial water molecules is very sensitive to the interfacial charge[103,115] and can thus be used to determine the relative number of charged unpaired surfactants in the mixed SDS:DTAB monolayers. Figure 4.5a shows the VSF spectra of the neat oil-water interface and 3–30 μM 1:1 d-SDS:h-DTAB mixtures at the $CCl_4$-$H_2O$ interface. The two broad spectral features in the O-H stretching region (3000–3500 cm$^{-1}$) are assigned to coordinated water molecules[108] while the sharp

features in the C-H stretching region (2800–3000 $cm^{-1}$) originate from the h-DTAB alkyl tail.[116] The other spectral features are not discussed in this chapter and therefore only mentioned in Table A.3. with their assignments.

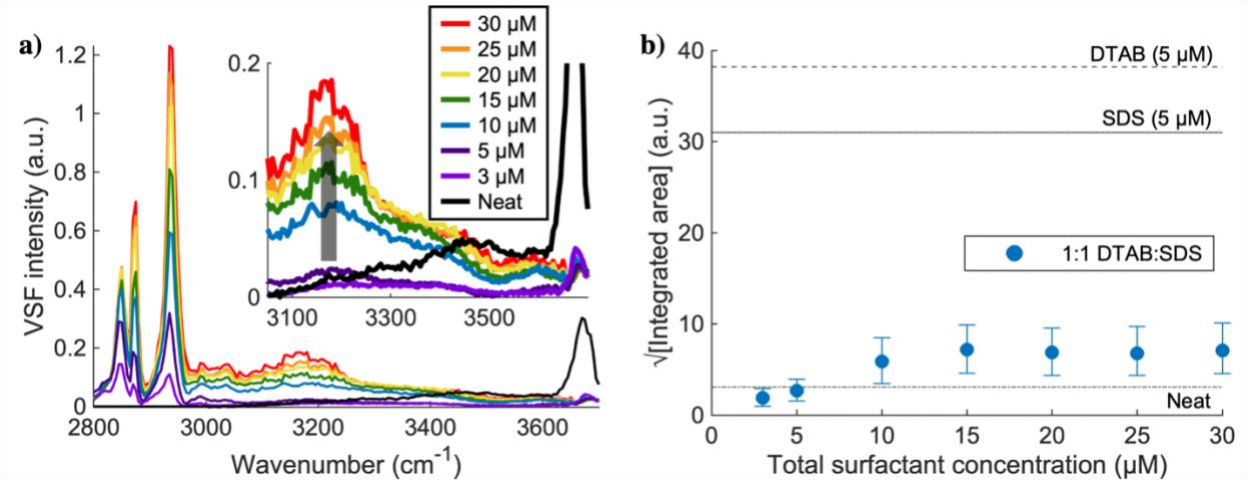


**Figure 4.5.** (a) VSF spectra of the neat $CCl_4$-$H_2O$ interface and 3–30 μM 1:1 d-SDS:h-DTAB mixtures at the $CCl_4$-$H_2O$ interface. (b) Square root of integrated areas of fits to the coordinated water features in panel a. The integrated areas of the neat $CCl_4$-$H_2O$ interface (black dash-dotted line) as well as pure 5 μM SDS (solid black line) and DTAB (dashed black line) are also included. Error bars are the integrated areas that are calculated using the upper and lower bounds of the fit parameters.

The coordinated water features of the 1:1 SDS:DTAB mixtures in Figure 4.5a are generally more redshifted and have larger integrated areas compared to the neat oil-water interface. These spectral changes result from the strengthening and restructuring of the hydrogen bonding network of the Stern layer or the entire electric double layer. In the Stern layer, charge-dipole and hydrogen bond interactions with surfactant headgroups orient the water molecules while in the diffuse layer, the potential setup by charged unpaired surfactants at the interface orient the water. This enhanced structure in both layers strengthens the hydrogen-bonding network, leading to a redshift and increase in integrated area proportional to the network's strength. The shift is smaller for water in the Stern layer since the surfactant headgroup-water interaction is weaker than the water-water interactions in the diffuse layer. For the 1:1 SDS:DTAB mixtures, the net neutrally charged paired

surfactants likely orient water exclusively within the Stern layer, as observed for zwitterionic surfactants,[117] which essentially act as electroneutral paired surfactants. The magnitude of the redshift from water directly interacting with 1:1 SDS:DTAB pairs can be gauged by comparison to the VSF spectrum of the zwitterionic lipid, 1-palmitoyl-2-oleoyl-sn-glycero-3-phosphocholine (POPC).[117] The POPC headgroup contains phosphate and choline moieties, which are similar to the SDS the DTAB headgroups, respectively. Thus, the features from water directly interacting with the headgroups of POPC and 1:1 SDS:DTAB pair should appear at similar frequencies. However, fits indicate the water features in the 1:1 SDS:DTAB mixtures appear at markedly lower frequencies than POPC (Table A.6), suggesting the signal predominantly originates from water in the diffuse layer, aligned by unpaired SDS and/or DTAB adsorbed at the interface. The contribution from water in the Stern layer is likely buried within the broad water spectral features of the diffuse layer.

The relative population of adsorbed unpaired surfactants may be gauged by utilizing the integrated areas of the coordinated water features, which is typically proportional to the number of charged unpaired surfactants adsorbed at the interface.[118] The square root of the areas is examined since the VSF signal scales quadratically with number density. This analysis assumes the average orientation of the interfacial water molecules does not change with electric field strength. This assumption is reasonable given that the intensity of the coordinated water spectrum between the power spectrum (measured with homodyne VSFS, which is employed herein) and the imaginary spectrum (measured with heterodyne VSFS) are similar;[119] molecular orientation does not influence the intensity of the imaginary spectrum. Figure 4.5b shows that the integrated areas of the coordinated water features for 1:1 SDS:DTAB mixtures at concentrations exceeding 5 μM are larger than that of the neat interface**.** To associate these areas to the relative number of unpaired

surfactants in the mixed SDS:DTAB monolayers, we consider the monolayers prepared by pure surfactants for which the number of unpaired surfactants adsorbed at the interface is known. The integrated area of pure 5 μM SDS and DTAB is roughly 30 and 40, respectively. These relatively large integrated areas correspond to a few unpaired surfactants adsorbed at the interface, evident from their low interfacial pressure of 1 (~2% interface coverage) and 0.3 mN/m (~1% interface coverage),[103] respectively. Considering areas of 30 and 40 correspond to very few surfactants, this indicates that integrated areas below 10 correspond to less than 1% of the interface being covered with unpaired surfactants. Thus, the VSF water spectra suggest that mixed SDS:DTAB monolayers contain very few unpaired surfactants. Notably, the coordinated water integrated areas could be so small because counterions in the electric double layer reduce the Debye screening length, limiting the number of water molecules that are oriented by the interfacial electric field. However, this is unlikely given that the counterion concentrations ranges from 3—30 μM, meaning the interfacial electric field is negligibly screened. Hence, these measurements indicate that monolayers prepared by the 1:1 SDS:DTAB mixture at all concentrations contain a negligible number of unpaired surfactants and the interfacial SDS:DTAB ratio can be considered 1:1 for all practical purposes. This finding further elucidates the extent to which the relative interface activity of the paired/unpaired surfactants influences the composition of the adsorbed surfactant monolayer, as briefly explored in Figure 4.3. Moreover, this finding corroborates work by Fauser and coworkers who, based on the inability of 1:1 SDS:DTAB mixtures to form electrostatically stabilized foam films, surmised the surfactant monolayers formed by these mixtures have a null surface charge density,[86] presumably due to the absence of unpaired surfactants.

Notably, our findings at the oil-water interface contrast VSFS measurements of 1:1 SDS:DTAB mixtures at the air-water interface.[120] Contrary to our observations in Figure 4.5, the

coordinated water features at the air-water interface are significantly enhanced and even comparable to pure 50 μM SDS/DTAB. Such an enhancement typically results from charged unpaired surfactants adsorbed at the interface that aligns water within the diffuse layer. Although momentum-dependent VSFS is needed to unequivocally assign water features to the Stern or both the Stern and diffuse layers,[115] thus defining if unpaired surfactants are adsorbed at the air-water interface, we believe differences between the two works is due to differences in equilibration times. Our surface tension and VSFS measurements show 1:1 SDS:DTAB mixtures require approximately 18 hr to equilibrate; at the air-water interface, spectra were collected after the sample equilibrated for a few minutes. Saha, et al. show the coordinated water features for a 1:1 anionic:cationic surfactant mixtures at the air-water interface are significantly enhanced shortly after the sample is prepared and become suppressed at later times during the equilibration process.[120] Presumably, the water features are initially enhanced due to the presence of unpaired surfactants adsorbed at the interface. Based on Saha's observations of an unequilibrated system, the most likely reason for the enhanced water signal at the air-water interface is unpaired surfactants are adsorbed at the interface. However, differences in the sample preparation procedures precludes a direct comparison of the 1:1 SDS:DTAB's behavior at the oil-water and air-water interfaces.

**Interfacial Packing of 1:1 SDS:DTAB Mixtures**

Since paired surfactants are predominantly adsorbed at the interface in the 1:1 SDS:DTAB mixtures, it is reasonable to expect the monolayers to be in an optimally packed, solid-like state (depicted in Figure 4.6a) in which packing is limited by steric interactions at concentrations near the CMC. To identify the 2D phase of the monolayers (gas-, liquid-, or solid-like), we revisit the headgroup areas of the 1:1 SDS:DTAB mixtures in Figure 4.4. The headgroup area of 15 and 25

(partial interface coverage) as well as 30 μM (full interface coverage) mixtures is 34 Å$^2$, comparable to that of optimally packed 1:1 SDS:DTAB mixtures at the hexane-water[114] and air-water interfaces.[92] This suggest that these 15–50 μM mixtures form solid-like monolayers at the $CCl_4$-water interface. These monolayers presumably are tightly packed domains, which have been observed for SDS:CTAB mixtures at the air-water interface.[121] Conversely, below 15 μM, the headgroup areas in Figure 4.4 increase with decreasing concentration, which is typical of loosely packed, liquid-like monolayers, which is depicted in Figure 4.6b. The change in headgroup areas of this mixture near 15 μM is also observed at the air-water interface and is due to the monolayer undergoing a phase transition.[92] Thus, Figure 4.4 shows the 1:1 SDS:DTAB mixtures at the oil-water interface transitions between a solid-like state and a liquid-like state at ~15 μM.

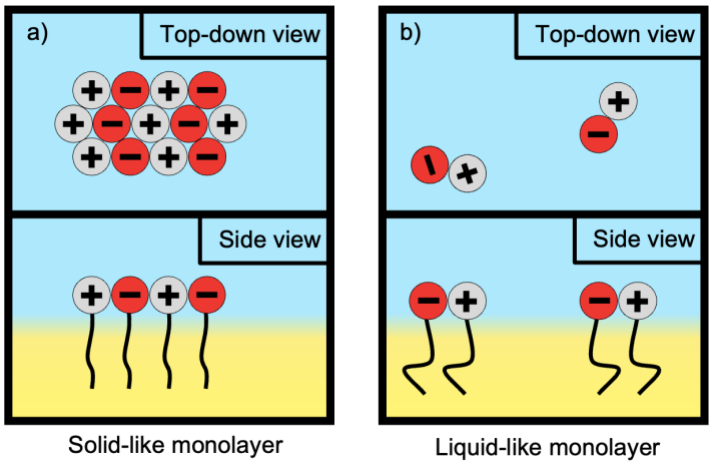


**Figure 4.6.** Cartoon depiction (a) liquid-like and (b) solid-like surfactant monolayers.

### Tail Conformation of 1:1 SDS:DTAB Pairs

To determine how changes in the interfacial surfactant packing manifest on a molecular level, we selectively examine the conformation of the SDS and DTAB alkyl tails with VSFS. This approach is used because the number of gauche defects along the tail is inversely proportional to the surfactant's local packing environment: the number of gauche defects decreases with a tighter

packing environment. In order to isolate the surfactant C-H stretching features of the surfactants' alkyl tails, $D_2O$ is used as the aqueous phase since the O-D stretching features are redshifted outside the C-H stretching region. Additionally, one surfactant in the 1:1 SDS:DTAB mixtures is selectively deuterated so the features in the spectra originate only from the hydrogenated (h-) surfactant tail. Either the headgroup ($d_9$-) or the headgroup and tail of DTAB are deuterated (d-) while only the tail of SDS is deuterated (d-).

Figure 4.7 shows VSF spectra of 3–30 μM 1:1 h-SDS:d-DTAB (SDS tail, Figure 4.7a) and d-SDS:$d_9$-DTAB (DTAB tail, Figure 4.7b) and mixtures at the $CCl_4$-$D_2O$ interface. Peak assignments are reported in Table A.1 and are consistent with literature.[116,122] Inspection of the spectra in Figures 3.6a and 6b clearly reveals that the intensity of the methyl symmetric stretch ($A_{r+}$, 2875 $cm^{-1}$) increases while the methylene symmetric stretch ($A_{d+}$, 2850 $cm^{-1}$) decreases with increasing bulk concentration for both SDS and DTAB tails in the mixtures. The amplitudes of these two features are of particular importance since their relative amplitude ratio ($A_{r+}/A_{d+}$) can be used to determine the conformation of the surfactant tails.[60,123,124] In an all-trans (perfectly ordered) conformation, the $d^+$ reside in a centrosymmetric environment (VSF active) while the $r^+$ reside in a non-centrosymmetric environment (VSF inactive), giving rise to a large $A_{r+}/A_{d+}$ ratio. Conversely, when the alkyl tail contains gauche defects (conformationally disordered), the $d^+$ reside in a non-centrosymmetric environment while the $r^+$ reside in a centrosymmetric environment, leading to a small $A_{r+}/A_{d+}$ ratio. Therefore, a large $A_{r+}/A_{d+}$ ratio indicates the tails are well ordered while a small $A_{r+}/A_{d+}$ ratio indicates the tails are disordered.

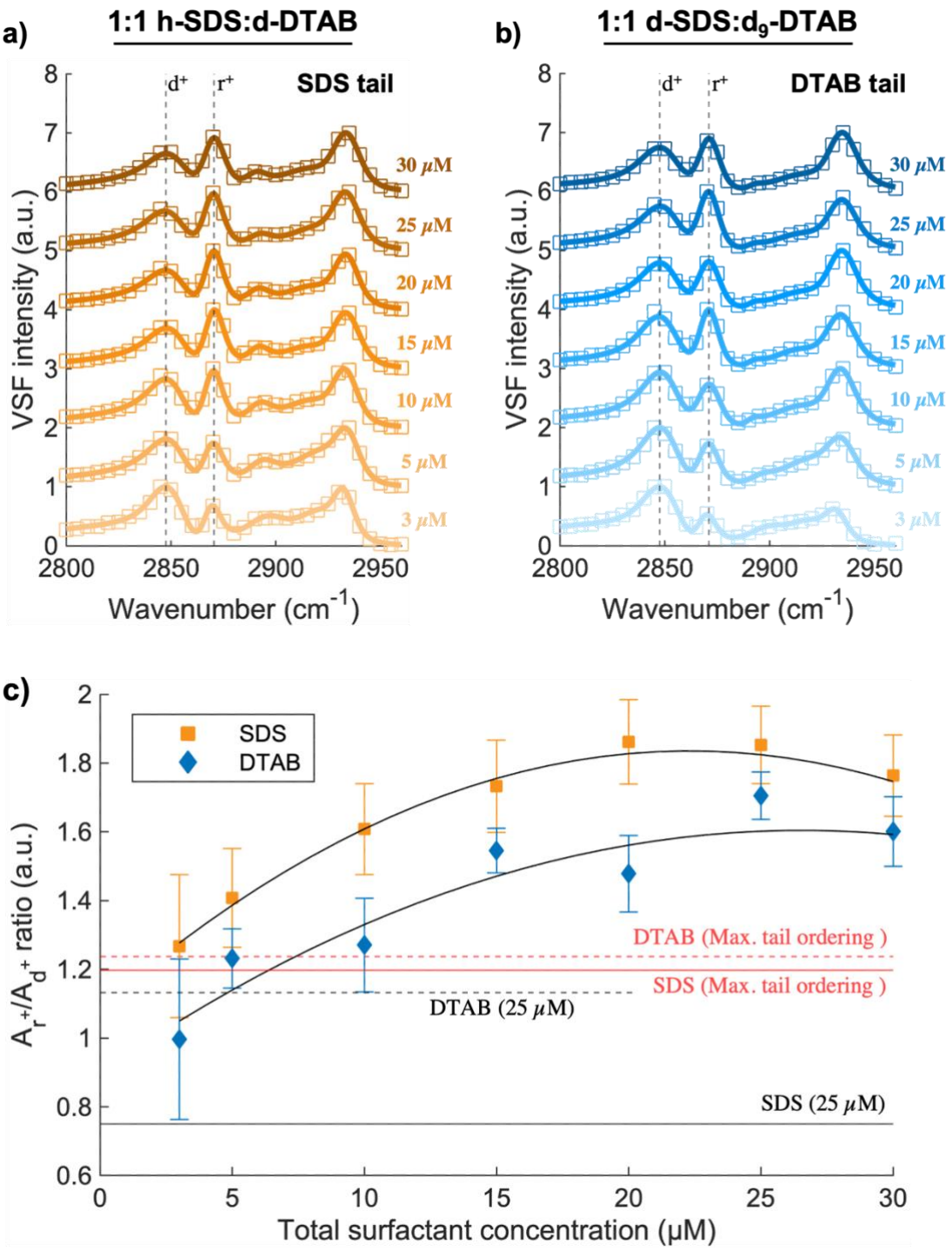


**Figure 4.7.** VSF spectra of 3–30 μM (a) h-SDS:d-DTAB (SDS tail) and (b)1:1 d-SDS:$d_9$-DTAB (DTAB tail) mixtures at the $CCl_4$-$D_2O$ interface. Spectra are offset and scaled to have a maximum intensity of one. The dashed vertical lines denote the $CH_2$ ($d^+$) and $CH_3$ ($r^+$) symmetric stretches while solid lines are fits to the spectra. (c) $A_{r+}/A_{d+}$ ratios of 1:1 h-SDS:d-DTAB (SDS tail, orange squares) and d-SDS:$d_9$-DTAB (DTAB tail, blue diamonds) mixtures obtained from spectra in panels a and b, respectively. The $A_{r+}/A_{d+}$ ratios of pure h-SDS (solid lines) and $d_9$-DTAB (dashed

lines) at concentrations of 25 μM (black lines) and 3 mM (red lines) are included for comparison. Solid black lines overlayed on the squares and diamonds are a guide to the eye. Error bars are the standard deviation of at least three measurements performed on separate days.

Figure 4.7c displays $A_{r+}/A_{d+}$ ratios of 3–30 μM 1:1 h-SDS:d-DTAB (SDS tail, orange squares) and 1:1 d-SDS:$d_9$-DTAB (DTAB tail, blue diamonds). Both the SDS and DTAB tails become more conformationally ordered with concentrations up to 15 μM, as depicted in Figure 4.6a. This result is consistent with VSFS measurements of liquid-like monolayers prepared by 1:1 SDS:DTAB mixtures[93] and molecular dynamic (MD) simulations of liquid-like 1:1 DS:DTA monolayers (free of $Na^+$ and $Br^-$ counterions, respectively),[96] both at the air-water interface. Beyond 15 μM, the tail conformations do not change with concentration since the monolayer is in a solid-like state at and beyond this concentration, as depicted in Figure 4.7a. In both states, the $A_{r+}/A_{d+}$ ratios of both SDS and DTAB are generally well above one, indicating that both alkyl tails of the paired surfactants are by and large conformationally well ordered at all concentrations, congruent with other anionic:cationic mixtures.[93,121,125] This contrasts pure 25 μM h-SDS (solid black line) and $d_9$-DTAB (dashed black line) whose $A_{r+}/A_{d+}$ ratios are near one, indicating that the tails are less conformationally ordered. The tails of both surfactants are similarly disordered at concentrations around 25 μM. These measurements thus demonstrate that the conformational ordering of the surfactant tails is enhanced when SDS and DTAB are paired.

Additionally, the paired surfactants in these micromolar 1:1 SDS:DTAB mixtures are more conformationally ordered than maximally packed monolayers of h-SDS (red solid line) and pure $d_9$-DTAB (red dashed line) that form at total surfactant concentrations of 3 mM (Figure 4.7c) and above.[102] The enhanced conformational tail ordering of the mixtures is primarily due to the tight interfacial packing density of the paired surfactants; tighter packing typically leads to more

conformationally ordered tails. Moreover, in the tightly packed state, the alkyl tails of the paired surfactants interact through van der Waals interactions, further enhancing the tail ordering.

More interestingly, Figure 4.7c also shows that the SDS tails are conformationally more ordered than the DTAB tails at all concentrations of the 1:1 SDS:DTAB mixtures. This result is consistent with MD simulations of an isolated 1:1 DS:DTA pair[96] and a saturated 1:1 DS:DTA monolayer[95] at the air-water interface that show the $DS^-$ tail is consistently longer (more conformationally ordered) than the $DTA^+$ tail. Regardless of the mixture's concentration, one might assume the SDS and DTAB tail conformations to be identical since the tails are the same length and they interact through van der Waals interactions[62] which presumably causes them to be conjoined and be conformationally in unison. Thus, the observed difference in the tail conformations of the paired surfactants (Figure 4.7c) suggest two plausible explanations.

The first explanation is that the miniscule number of unpaired surfactants adsorbed at the interface (see the discussion of Figure 4.5) disrupts the interfacial packing of the paired surfactants. Unpaired surfactants in the mixed SDS:DTAB monolayers likely act as point defects that disrupt the local interfacial packing, and thus diminishes the conformational tail ordering of its paired form and itself. If true, the DTAB tails are conformationally less ordered than the SDS tails because unpaired DTAB molecules are adsorbed at the interface. To test this hypothesis, we selectively examined the conformation of both SDS and DTAB tails of 7:3 and 3:7 DTAB:SDS mixtures (data shown in Chapter V). Regardless of which surfactant was in excess, the SDS tail is more ordered, confirming that unpaired surfactants adsorbed at the interface in the 1:1 SDS:DTAB mixtures does not contribute to the difference in the SDS and DTAB tail conformations.

The second explanation is that the SDS headgroup of the paired surfactant immerses further into the water to create a staggered arrangement, as depicted in Figure 4.8. In this arrangement,

the DTAB tail is displaced towards the oil phase while the SDS tail is displaced towards the aqueous phase. Consequently, the SDS tail segment near the headgroup and the DTAB tail segment near the terminal methyl group experience no or limited van der Waals interactions with the tail of the co-paired surfactant. These tail segments are thus more likely to contain gauche defects. However, neutron reflectivity (NR)[97] and VSFS[126] experiments, as well as MD simulations[96] of surfactant monolayers indicate that gauche defects are predominantly located near the terminal methyl group. These works, in combination with our findings, lead us to believe that the portion of the DTAB tail that protrudes from the monolayer is less conformationally ordered than the segment of the SDS tail near the headgroup, as shown in Figure 4.8. Additionally, a staggered arrangement has been observed in NR experiments of n-dodecylsulfate surfactant mixtures:n-hexylammonium surfactant mixtures (1:1 DS:AM)[94] as well as MD simulations of 1:1 DS:DTA monolayers.[95,96] Therefore, we believe that the 1:1 SDS:DTAB monolayers at the oil-water interface are likely organized in this staggered arrangement.

We consider a collection of experiments[94,123,124,127] and simulations[95,96,98,100] that either examined 1:1 anionic:cationic mixtures or pure anionic/cationic surfactants adsorbed at either an oil-water[100,124] or the air-water interface.[94-96,98,127] While there is no consensus on whether the anionic or cationic surfactant headgroup immerses deeper into the aqueous phase, our experiments suggest that differences in the SDS and DTAB tail conformations of the 1:1 SDS:DTAB mixtures is due to the SDS headgroup immersing deeper into the aqueous phase of the oil-water interface, as depicted in Figure 4.8. If DTAB immersed deeper, as observed in NR experiments[94] and MD simulations[95,96] of 1:1 SDS:DTAB mixtures at the air-water interface, we would expect the DTAB tail to be more conformationally ordered than the SDS tail. This hypothesis could be evaluated with VSFS measurements of isotopically labeled 1:1 SDS:DTAB mixtures adsorbed at either the

air-water or a solid-water interface. At the air-water interface, the DTAB tail is expected to be more conformationally ordered while at the solid-water interface (where one would expect the surfactant headgroup to be in a non-staggered arrangement), the SDS and DTAB tail conformations are expected to be the same. Alternatively, NR measurements could reveal the headgroup arrangement of the 1:1 SDS:DTAB mixtures adsorbed at the oil-water interface.

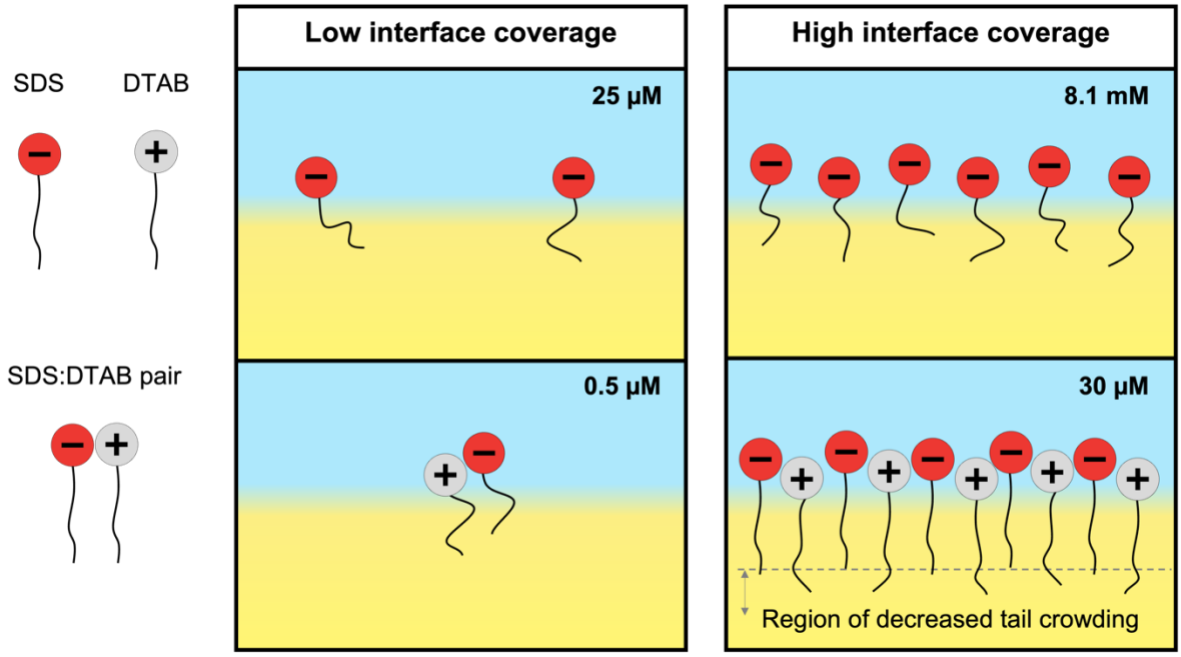


**Figure 4.8.** Cartoon depiction of monolayers formed by pure SDS and 1:1 SDS:DTAB mixtures at low and high interface coverage.

## Summary and Conclusions

Surfactant mixtures are commonly employed across various industries to stabilized foams and emulsions.[18,22,35,72-84] Their deployment as foaming agents is however often limited by the foam's susceptibility to destabilize in oily environments.[17,18,21,35,42,72] To fully exploit their potential, it is necessary to identify surfactant mixtures that can stabilize foams in the presence of oil and to extensively characterize the structure-function relationship of their mixed surfactant monolayers adsorbed at an oil-water interface. In order to ascertain the molecular details, we used interfacial tensiometry in tandem with vibrational sum frequency spectroscopy to directly investigate the

composition, 2D phase, and alkyl tail conformations of monolayers formed by 1:1 SDS:DTAB mixtures with molecular specificity. We show that when mixed, the adsorption of SDS and DTAB at the oil-water interface is enhanced. This enhancement results from the adsorption of paired surfactants at the interface.[43,85] Despite being abundant in solution, a negligible number of unpaired surfactants are also adsorbed at the interface. This disparity in the interface coverage results from the paired surfactant's high interface activity[109] and means the monolayers essentially contain only paired surfactants for practical purposes. These paired surfactants are in a liquid-like state at concentrations below 15 μM and a solid-like state at higher concentrations. The conformational ordering of the SDS and DTAB alkyl tails change with concentration only in a liquid-like state. Regardless of the phase, SDS and DTAB tail conformations are different even though one would expect them to be conformationally the same due to van der Waals interactions. We attribute this observation to the SDS headgroup of the paired surfactants immersing further into the water. This staggered arrangement may contribute to the oil resistance of mixed SDS:DTAB foams by hindering water drainage from the pseudoemulsion film, thereby stabilizing the lamella in oily environments, as previously mentioned.[40] The hindered drainage would result from the SDS headgroups having a more extensive hydration shell in this arrangement and stronger interactions (hydrogen bonds) with water, compared to the DTAB headgroups. It is unclear whether these 1:1 SDS:DTAB mixtures behave similarly at the oil-water and air-water interfaces of the pseudoemulsion film, given the limited literature that provides the molecular-level details of the mixtures adsorbed at an air-water interface. Nevertheless, our findings provide valuable molecular-level insights into how anionic:cationic surfactant mixtures may stabilize the oil-water interface of the pseudoemulsion film and thus foams in the presence of oil, which has many applications to the oil,[10,73] gas,[73,87] and firefighting industries.[22,88]

# CHAPTER V:

# Interfacial Behavior of Non-Equimolar SDS:DTAB Mixtures

This work under review in the journal *Langmuir* Konnor Jones identified the study's obejctives, designed and performed the experiments, analyzed and interpreted the data, and wrote the manusript. Geraldine Richmond was the principal investigator for this work and provide general guidance prior her leave of absence that began on Nov. 8, 2021, serving as Undersecretary of Science and Innovation, Department of Energy. Larry Scatena served as the principal investigator during Dr. Richmond's leave, overseeing the project through completion by providing general feedback and editorial assistance.

## Introduction

Surfactants are a workhorse in a myriad of industries including oil,[35,72] gas,[18,73] detergents,[74,75] firefighting,[22,76] pharmaceuticals,[77,78] cosmetics,[79,80] personal care,[82,128] food,[84,129] and mineral processing.[130] Surfactant mixtures are either intentionally or unintentionally used in nearly all cases. Intentionally employing these mixtures involves deliberately mixing surfactants to concurrently acquire interfacial properties that cannot be obtained with pure (unmixed) surfactants. On the other hand, unintentional mixtures arise when using impure surfactants or in an uncontrolled environment like oil and gas reservoirs. This can undesirably alter the properties of the surfactant-containing system as well. Regardless of how mixtures are created, the resultant mixture engenders unique and complex interfacial behaviors that can alter the properties of the interface to which they are adsorbed. For example in applications such as oil recovery,[10,73] gas production,[73,87] and fire suppression,[22,88] the unique interfacial properties of mixed surfactant

systems can promote the formation and enhance the longevity of aqueous foams which are heavily employed in these industries.

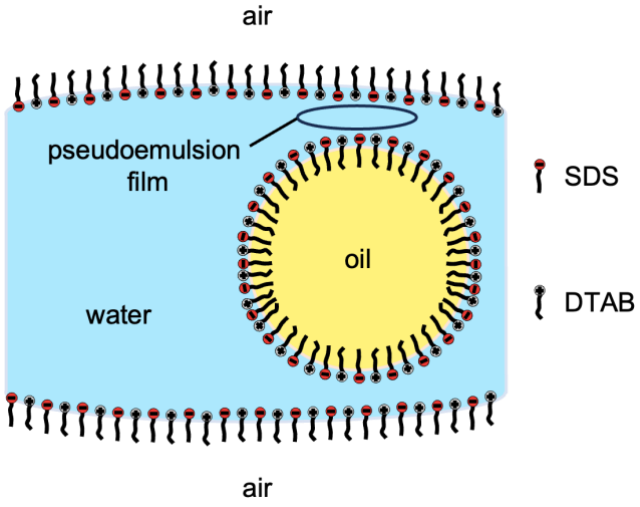


**Figure 5.1.** Cartoon depiction of the pseudoemulsion film inside a lamella.

Liquid foams can generally be described as dispersions of gas bubbles in an aqueous solution, separated by liquid films called lamellae. Lamellae are the determinant of foam stability and maintaining its stability while a foam is deployed is a significant challenge to optimizing their efficacy. The difficulty in stabilizing lamellae has curtailed the deployment of these foams, especially with oil-based applications as oil tends to rupture the lamella and thereby destroy the foam.[17,18,21,35,42,72] Therefore, it is necessary to optimize their efficacy, which can be done by identifying surfactant mixtures and their molecular-level characteristics that adequately stabilize the aqueous film that is interposed between the oil and the lamella (pseudoemulsion film, depicted in Figure 5.1), which is believed to govern foam stability in oily environments.[35,40,89-91] Given that the pseudoemulsion film consists of an air-water and an oil-water interface, it is important to identify the structure-property relationship of mixed surfactant monolayers layers at both interfaces to thoroughly understand how they each influence the film's stability.

The interfaces of thin films, both air-water and oil-water, are exceedingly difficult to selectively probe and assess their individual contributions to pseudoemulsion film stability. Therefore, the oil-water and air-water interfaces formed between bulk fluids are instead studied, as they easily be investigated with traditional techniques (e.g. tensiometry), are instead studied.[43,85,131] Interfacial tensiometry and rheology measurements as well as foam stability observations conjointly indicate that stable foams exhibit strong interfacial viscoelasticity,[30,42,43] ultra-low interfacial tension,[42,43,85] and high disjoining pressure,[30,43] all of which are characteristic of densely packed surfactant monolayers. Mixed anionic:cationic surfactant mixtures can exhibit such characteristics[30,35,43] and are likely the reasons they can form more oil tolerant foams compared to pure anionic and cationic surfactants. The tight interfacial packing of anionic:cationic surfactant mixtures is attributed to the electroneutral headgroup and enhanced interfacial activity of the paired surfactants. The diminished repulsive electrostatics between the paired surfactant headgroups leads to short-range steric and van der Waals interactions regulating the interfacial surfactant packing. In terms of interfacial activity, paired surfactants can be orders of magnitude more interfacially active than unpaired surfactants, which leads to the disproportionate adsorption of paired surfactants that and therefore a monolayer that is densely packed and presumably composed of primarily paired surfactants. It is then reasonable to expect the foam film properties to be largely governed by the characteristics of the paired surfactants with minimal influence from the co-adsorbed unpaired surfactants. However, foam film stability[43] measurements of sodium dodecyl sulfate:dodecyltrimethylammonium bromide (SDS:DTAB), across a range of anionic:cationic surfactant mixing ratios without oil demonstrate film stability is significantly dependent on whether the anionic or cationic surfactant is in excess. For the SDS:DTAB mixtures, foam films are stable when SDS is in excess but unstable when DTAB is in excess, even though

the interfacial tension and rheology properties of the mixtures are equivalent. This is similarly observed for mixed SDS:DTAB stabilized foams in the presence of oil.[35] Hence, this observation implies that unidentified molecular-level nuances of these surfactant monolayers governs foam stability.

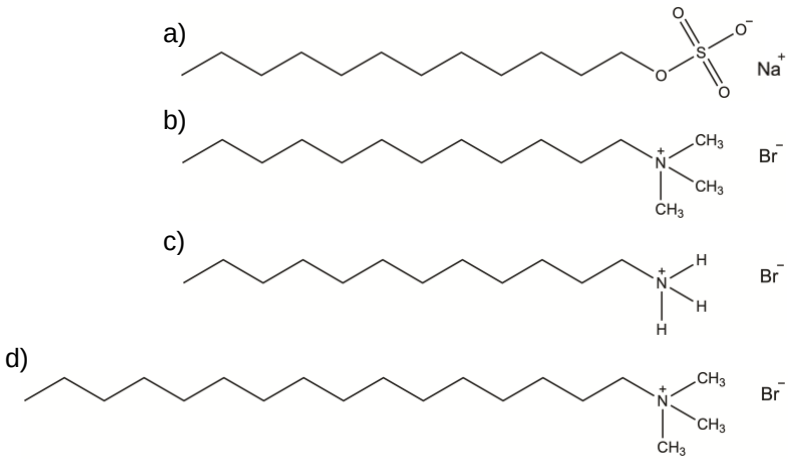


**Figure 5.2.** Molecular structure of (a) SDS, (b) DTAB, (c) DAC, and (d) CTAB.

In order to identify the underlying mechanism(s) that regulate foam stability and the oil tolerance of foams created by anionic:cationic surfactant mixtures across a range of mixing ratios, the work herein directly investigates the composition and molecular conformation of mixed anionic:cationic surfactant monolayers adsorbed at the oil-water interface. This work builds on our previous investigation into the comparably simpler equimolar anionic:cationic surfactant mixture.[132] Such detailed information about the interfacial properties of surfactant mixtures is lacking since few experimental techniques can selectively probe buried liquid-liquid interfaces with molecular specificity. Additionally, techniques that examine liquid-liquid interfaces, whether they are interface specific or not, are technically more challenging to employ and thus less regularly utilized compared to those that probe the liquid-gas interface. This work, along with our earlier investigation with equimolar surfactant mixtures, provide unique insights into the

molecular-level nuances of anionic:cationic surfactant mixtures at an oil-water interface that may regulate the oil resistivity of mixed anionic:cationic surfactant stabilized foams encountered in commercial applications.

In this work, the SDS:DTAB mixtures (molecular structures displayed in Figure 5.2) are examined at an oil-water interface. This mixture is ideal to study since both surfactants are structurally simple and have been extensively studied and employed as foaming agents.[35,42,43] Carbon tetrachloride is used as a model oil because it minimally absorbs light in the visible and mid infrared (IR) spectral regions, which is a requisite to employ vibrational sum frequency spectroscopy (VSFS). VSFS, a surface-specific spectroscopic technique, is leveraged to determine (1) individual SDS and DTAB tail conformations by performing isotopic labeling experiments and (2) elucidate the composition of the adsorbed surfactant monolayers by monitoring the charge-sensitive interfacial water spectral region. Interfacial tensiometery measurements are carried out to determine the relative population of the adsorbed surfactants in the monolayers. From these measurements, the monolayers are found to largely contain paired surfactants and few unpaired surfactants across all mixture compositions: surfactant mixing ratios and total surfactant concentrations. The interfacial concentration of both paired and unpaired surfactants is found to change with the mixture's composition and be distinctly dependent on the relative interfacial activity of the two surfactants in the mixture. This finding is particularly important since the unpaired surfactants disrupt the tight interfacial packing of the mixed surfactant monolayer by acting as point defects. The conclusions obtained from these experiments provide valuable insights into the interfacial behavior of cationic:anionic surfactant mixtures adsorbed at the oil-water interface across range of compositions, which can be indispensable to order to judiciously develop and deploy foams in oil-based applications.

**Relative Interfacial Population of Paired and Unpaired Surfactants**

Figure 5.3a shows interfacial pressure measurements of 25 μM SDS/DTAB mixtures (green markers) as a function of the surfactant mixing ratio (SDS:DTAB). The interfacial pressure of pure 25 μM SDS (10:0) and DTAB (0:10) is close to that of the neat interface (0 mN/m), indicating that few surfactants are adsorbed at the interface at this concentration. Although though the total surfactant concentration is fixed, the interfacial pressures quickly increase as the SDS:DTAB ratio shifts to 9:1 and 1:9, respectively, signifying the interface becomes populated with an appreciable number of surfactants as the SDS and DTAB are mixed. The population of adsorbed surfactants continues to increase, albeit to a lesser extent, as the SDS:DTAB ratios shifts up to 7:3 and 3:7 (Regime 1). In contrast, the interfacial pressures are equivalent for the 7:3 through 3:7 SDS:DTAB mixtures (Regime 2), suggesting the maximum interfacial population has been reached. These regimes are also present when the total surfactant concentration of the mixtures is 5 and 15 μM and presumably result from changes in the relative number of stoichiometric 1:1 SDS:DTAB surfactant pairs (paired surfactants) and unpaired surfactants that populate the interface. The SDS:DTAB paired surfactants, being nearly 300 times more interfacially active than unpaired SDS and DTAB, [133] are expected to constitute most of the adsorbed surfactants and thus chiefly regulate the interfacial pressure of the SDS:DTAB mixtures. However, it is unclear whether the unpaired surfactants adsorbed at the interface markedly contribute to the increases in the interfacial pressures since changing the SDS:DTAB ratio varies the percentage of both stoichiometric 1:1 paired and unpaired surfactants in the solution, as depicted in Figure 5.3b.

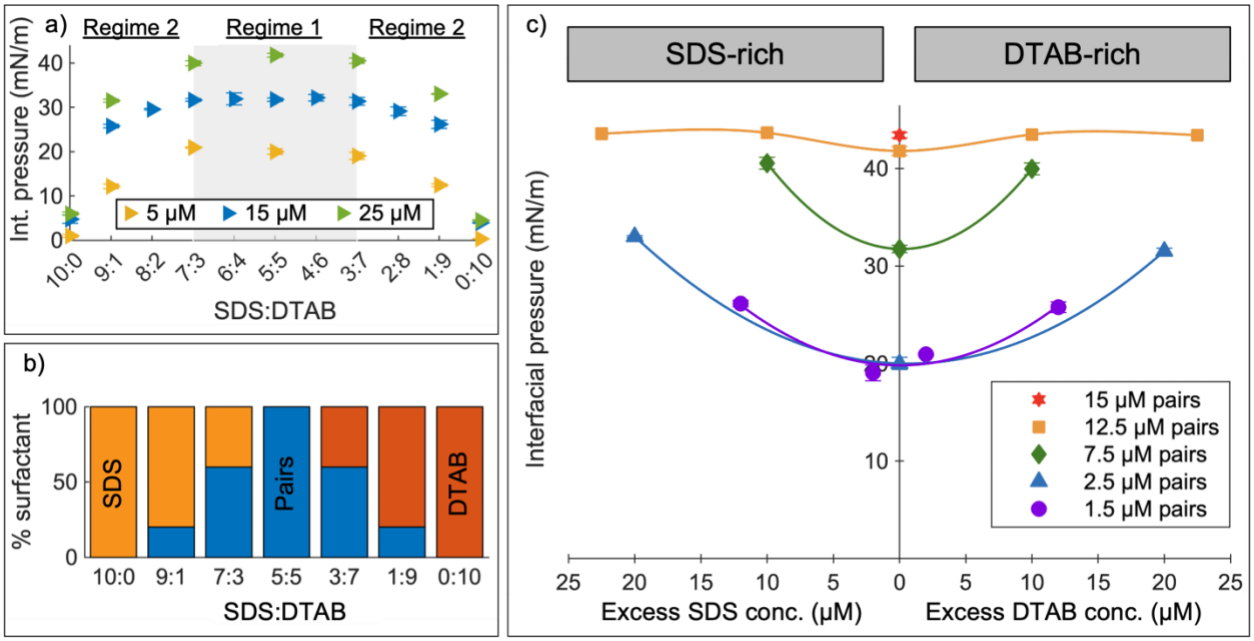


**Figure 5.3.** (a) Interfacial pressure of SDS:DTAB mixtures as a function of SDS:DTAB mixing ratio. The total surfactant concentration is 5, 15, and 25 μM. Spectra that are fit are an average of at least three spectra that are collected on different days. (b) Percentage of unpaired SDS/DTAB and paired surfactants in the solution as a function of SDS:DTAB mixing ratio. (c) Select interfacial pressure measurements in Figure 5.3a reformatted so the paired surfactant concentration is fixed while the unpaired SDS/DTAB concentration is varied. Error bars in both Figure 5.3a and 5.3c are the standard deviation of at least three measurements performed on separate days. Solid lines are used as a guide to the eye. Error bars are the standard deviation of at least three measurements performed on separate days.

To the best of our knowledge, no previous works have rigorously investigated whether the unpaired surfactants appreciably influence the interfacial pressure of anionic:cationic surfactant mixtures adsorbed at a liquid interface, be it the oil-water or air-water interface. The best attempt yet is by Fauser and coworkers[43] utilizing SDS:DTAB mixtures at air-water surface. They found the surface tension values at different SDS:DTAB mixing ratios generally coincide with the surface tension of equimolar SDS:DTAB mixtures containing an equivalent stoichiometric paired surfactant concentration (e.g., surface tension of 50 μM 7:3 SDS:DTAB and 30 μM 1:1 SDS:DTAB mixtures is equivalent). From this finding, they concluded that the excess SDS/DTAB concentration appreciably affects the surface tensions of mixtures in Regime 1, but not Regime 2.

In essence, this implies that surface adsorption is governed by the paired surfactants and is largely insensitive to the unpaired surfactants in solution. While this scenario is plausible, it is based on measurements that cannot discern between paired and unpaired surfactants. Despite their cleverly planned surface tension measurements, it is still unclear whether the unpaired surfactants contribute to the changes in the interfacial pressures, including those measurements in Figure 5.3a.

In order to improve the interpretability of the interfacial pressure measurements, as a function of mixing ratio, the values in Figure 5.3a are reformatted so the stoichiometric paired surfactant concentration is fixed while the unpaired SDS/DTAB concentration is varied. Figure 5.3c shows the reformatted measurements in which equimolar mixtures lie along the y-axis while mixtures that contain excess SDS (SDS-rich) or DTAB (DTAB-rich) lie left and right of the y-axis, respectively. The interfacial pressure measurements are grouped according to the concentration of stoichiometric paired surfactants that can quantitatively form, each represented by a specific marker/color combination. Table 1 shows how the mixtures in Figure 5.3a are grouped and mapped to Figure 5.3c. Only mixtures containing 1.5, 2.5, 7.5, or 12.5 μM paired surfactants are reformatted since there are an insufficient number of data points (less than three) of mixtures at other paired surfactant concentrations to gain meaningful insights. Note that the paired surfactant concentrations represent half of the total surfactant concentration of a 1:1 SDS:DTAB mixture, as each paired surfactant consists of one SDS and one DTAB molecule. Figure 5.3c also includes interfacial pressure values for mixtures not included in Figure 5.3a; the additional mixtures are denoted in Table 1 with an asterisk. These measurements were made to expand the 12.5 μM paired surfactant mixtures plot.

**Table 5.1.** Compositions of the SDS:DTAB mixtures displayed in Figures 5.3a and 5.3c.

| **SDS:DTAB mixture (Figure 5.3a)** | **SDS:DTAB mixture (Figure 5.3c)** | |
|---|---|---|
| | Pairs | Excess |
| 15 μM 9:1 | 1.5 μM pairs | 12 μM SDS |
| 5 μM 7:3 | | 2 μM SDS |
| 5 μM 3:7 | | 2 μM DTAB |
| 15 μM 1:9 | | 12 μM DTAB |
| 25 μM 9:1 | 2.5 μM pairs | 20 μM SDS |
| 5 μM 5:5 | | |
| 25 μM 1:9 | | 20 μM DTAB |
| 25 μM 7:3 | 7.5 μM pairs | 10 μM SDS |
| 15 μM 5:5 | | |
| 25 μM 3:7 | | 10 μM DTAB |
| 47.5 μM 6.8:3.2 * | 12.5 μM pairs | 22.5 μM SDS |
| 35 μM 6.4:3.8 * | | 10 μM SDS |
| 25 μM 5:5 | | |
| 35 μM 3.8:6.4 * | | 10 μM DTAB |
| 47.5 μM 3.2:6.8 * | | 22.5 μM DTAB |

Figure 5.3c shows the interfacial pressure of the equimolar mixtures monotonically increase with concentration up to its CMC of 15 μM (30 μM total surfactant concentration).[43,132] Additionally, at any fixed paired surfactant concentration, the interfacial pressure of these SDS:DTAB mixtures generally increases with excess SDS/DTAB concentration. For the 1.5–7.5 μM paired mixtures, the increase is large due to the concentrations being well below CMC (15 μM SDS mixed with 15 μM DTAB) and full monolayer coverage, leaving vacancies at the interface where additional surfactants adsorb as SDS/DTAB grows in excess. Conversely, the interfacial pressure of the 12.5 μM paired mixtures marginally increases then plateaus with increasing excess SDS/DTAB concentration. This behavior is attributed to the nearly saturated monolayer formed by the 12.5 μM equimolar mixture. The interfacial pressures of the 1.5–7.5 μM paired mixtures are expected to similarly plateau when the excess SDS/DTAB concentration is exceedingly large: well above 22.5 μM, as observed for Fauser and coworker's[43] reformatted surface tension measurements (Figure B.1). Accordingly, these interfacial pressure measurements in Figure 5.3c

clearly show how the adsorbed surfactant population of these SDS:DTAB mixtures varies in response to the concentration of excess SDS/DTAB.

Based on the observations in Figure 5.3c, one may attribute the increase in interfacial pressures to unpaired surfactants adsorbing to the interface; however, these changes in interfacial pressure are likely due to the adsorption of paired surfactants. This can be rationalized by considering the finite association constant of 1:1 anionic:cationic surfactant pairs.[62,63] More paired surfactants form as excess SDS or DTAB is added to an equimolar SDS:DTAB mixture, in accordance with Le Chatelier's principle. This shift in equilibrium leads to an increase in the paired surfactant bulk concentration and therefore interfacial concentration, as described by the Gibbs equation. This is consistent with the observed interfacial pressure changes of the SDS:DTAB mixtures compared to pure SDS and DTAB whereby adding 10 μM excess SDS or DTAB to the equimolar mixtures causes the interfacial pressure to increase by an average of 10 mN/m. Such a relatively large increase cannot solely be due to the unpaired surfactants considering the interfacial pressure of pure 25 μM SDS and DTAB is ~4 mN/m. Therefore, the increase in paired surfactant concentration of the SDS- and DTAB-rich mixtures at least partially accounts for the increased population of adsorbed surfactants.

We employ vibrational sum frequency spectroscopy (VSFS) to better determine the relative interfacial concentration of unpaired surfactants and their respective contribution to the interfacial pressure measurements of the SDS:DTAB mixtures, if any. Figure 5.4 shows the VSF spectra of 1.5, 2.5, 7.5 μM d-SDS:h-DTAB mixtures with excess SDS (panels a and c) or DTAB (panels b and d) at the $H_2O$-$CCl_4$ interface. Panels a and b also display the VSF spectrum of the neat $H_2O$-$CCl_4$ interface. Panels c and d are an expanded y-axis view of the spectra that also include the VSF spectrum of pure 5 μM SDS at the $H_2O$-$CCl_4$ interface. Since the pure 5 μM SDS and DTAB VSF

spectrum are similar, the DTAB spectrum is omitted to enhance figure clarity. The resolved features in the C-H stretching region (2800–3000 $cm^{-1}$) of the mixed SDS:DTAB spectra originate from the hydrogenated DTAB tail and headgroup[116] while the features in the in the O-H stretching region (3000–3700 $cm^{-1}$) in both the pure and mixed surfactant spectra arise from water.[108] Specific assignments for the C-H features as well as the other water spectral features that are not discussed in this chapter are listed in Tables B.1 and B.2. C-H stretching modes in VSF spectra are commonly used to determine the composition of interfacial monolayers[120,134-137] since VSF signal intensity is proportional to the number density, as described in eq. 2.13 However, the C-H features lack the specificity to differentiate between paired and unpaired surfactants and the sensitivity to discern subtle changes in the relative number of adsorbed unpaired SDS/DTAB encountered in the mixed SDS:DTAB monolayers. Therefore, the C-H features are not analyzed in this section to determine the composition of the surfactant monolayers. On the other hand, the two coordinated water symmetric stretching modes (centered at ~3200 and ~3400 $cm^{-1}$) of the interfacial water spectrum are highly sensitive to the interfacial charge of unpaired surfactants adsorbed at the interface,[137] even at nanomolar surfactant concentrations.[103] This sensitivity makes the interfacial water spectrum particularly well-suited to determine the composition of the mixed SDS:DTAB monolayers adsorbed at the oil-water interface and is thus examined in detail below.

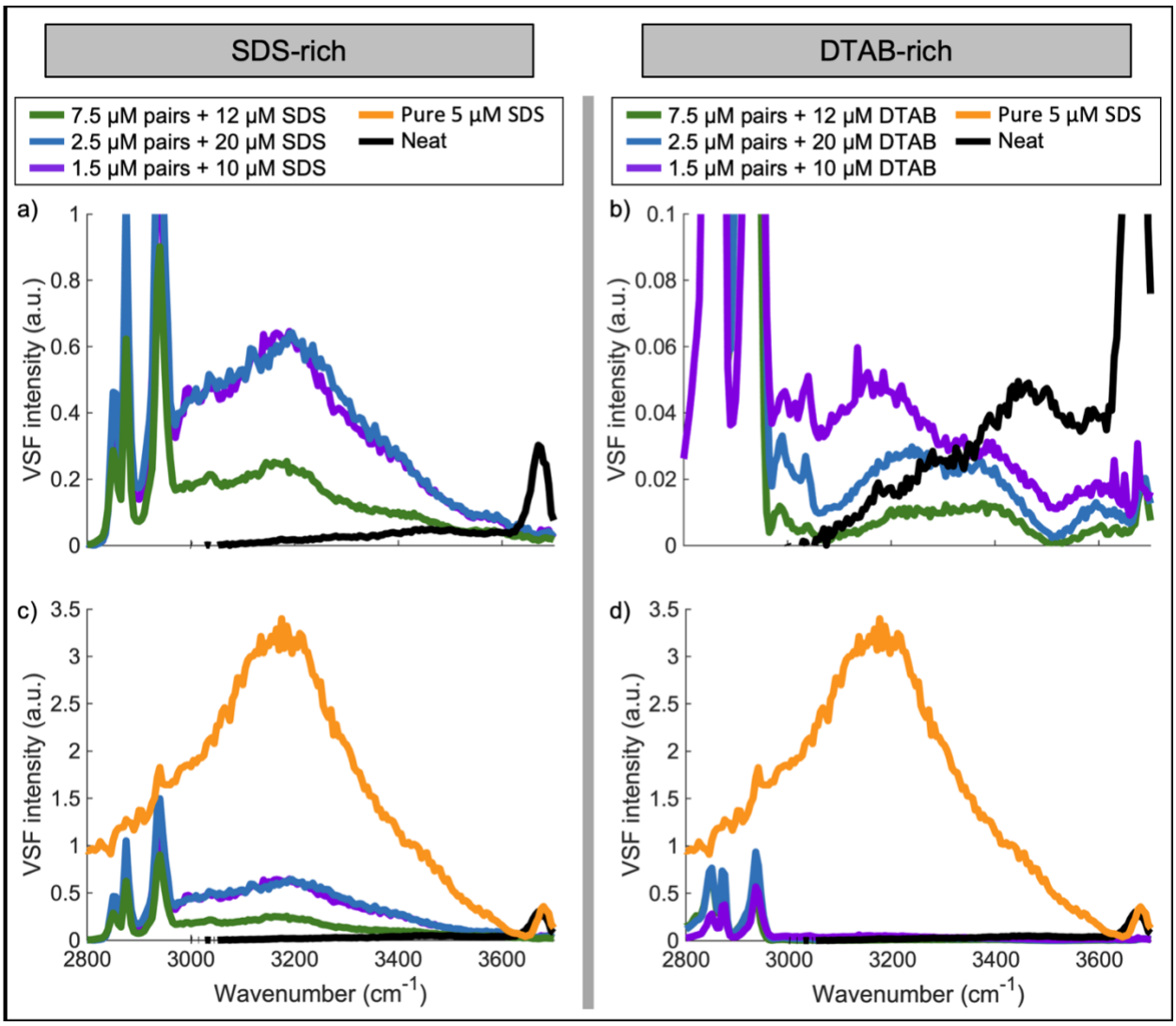


**Figure 5.4.** VSF spectra of (a) SDS-rich and (b) DTAB-rich d-SDS:h-DTAB mixtures. The VSF spectrum of pure 5 μM SDS and the neat $CCl_4$-$H_2O$ interface are displayed in both panels. VSF spectra of (c) SDS-rich and (d) DTAB-rich d-SDS:h-DTAB mixtures. An expanded y-axis view of panels a and b. Panels c and d do not include the pure 5 μM SDS spectrum.

Analysis of the d-SDS:h-DTAB VSF spectra in Figures 5.4a and 5.4b show the coordinated water features are generally more intense and redshifted compared to the neat oil-water interface. This enhancement and redshift results from the restructuring and strengthening of the hydrogen bonding network within the Stern layer or the entire electric double layer. In the Stern layer, charge-dipole and hydrogen bond interactions with surfactant headgroups orient the water molecules whereas in the diffuse layer, the potential setup by charged unpaired surfactants

adsorbed at the interface orients the water. This enhanced structure in the two water regions strengthens the hydrogen-bonding network, which leads to an increase in integrated area and redshift proportional to the network's hydrogen-bonding strength. The paired surfactants are expected to marginally enhance the water signal since their electroneutral headgroup likely orients water solely within the Stern layer, as observed for zwitterionic surfactants,[117] which essentially act as electroneutral paired surfactants. The Stern layer water signal is expected to be redshifted due to the interaction with the headgroup, but because the interaction is weaker than the water-water interaction in the diffuse layer, unpaired surfactants at the interface are characterized by more redshifted water signal.

Given that the enhancement of the coordinated water features is by and large proportional to the number of charged unpaired surfactants adsorbed at the interface, the relative number of unpaired surfactants in the mixed SDS:DTAB monolayers can be gauged by comparing their spectra to the neat oil-water interface and pure 5 μM SDS/DTAB VSF spectra in the water region. The coordinated water features in the spectra of the SDS-rich d-SDS:h-DTAB mixtures (Figure 5.4a) are significantly larger than those of the neat interface, suggesting that unpaired surfactants are adsorbed at the interface when SDS is in excess. On the other hand, the features are less intense than pure 5 μM SDS. Considering that few surfactants are adsorbed at the interface for pure 5 μM SDS (~1% interface coverage), as evidenced by the interfacial pressure measurements in Figure 5.3a, comparison with pure 5 μM SDS these VSF spectra indicate that the adsorbed monolayers formed by SDS-rich mixtures contain very few unpaired surfactants; less than 1% of the interface is covered with unpaired surfactants. On the other hand, the coordinated water features of the DTAB-rich mixtures (Figures 5.4b and 5.4d) are less intense than those of both pure 5 μM SDS and the neat oil-water interface. This suggest that either the interfacial charge is significantly

screened by counterions in the electric double layer or these surfactant monolayers solely contain paired surfactants. Counterions in the electric double layer decrease the Debye screening length, limiting the number of water molecules that are oriented by the interfacial electric field and giving rise to the low integrated areas. However, this is unlikely given that counterion concentration ranges from 3—30 μM, meaning the interfacial electric field is negligibly screened. Thus, one may be led to believe that paired surfactants solely populate the interface. However, the redshift of the coordinated water features of the DTAB-rich mixtures is greater than anticipated for water directly interacting with the SDS or DTAB headgroup (water within the Stern layer).[117,132] As extensively discussed elsewhere,[132] such a large redshift can occur for water molecules within the diffuse layer, not the Stern layer, thus indicating that unpaired surfactants may contribute to the water signa, albeit minimally. Thus, findings from the VSF spectra in Figure 5.4 indicate that both the SDS- and DTAB-rich SDS:DTAB monolayers contain very few unpaired surfactants.

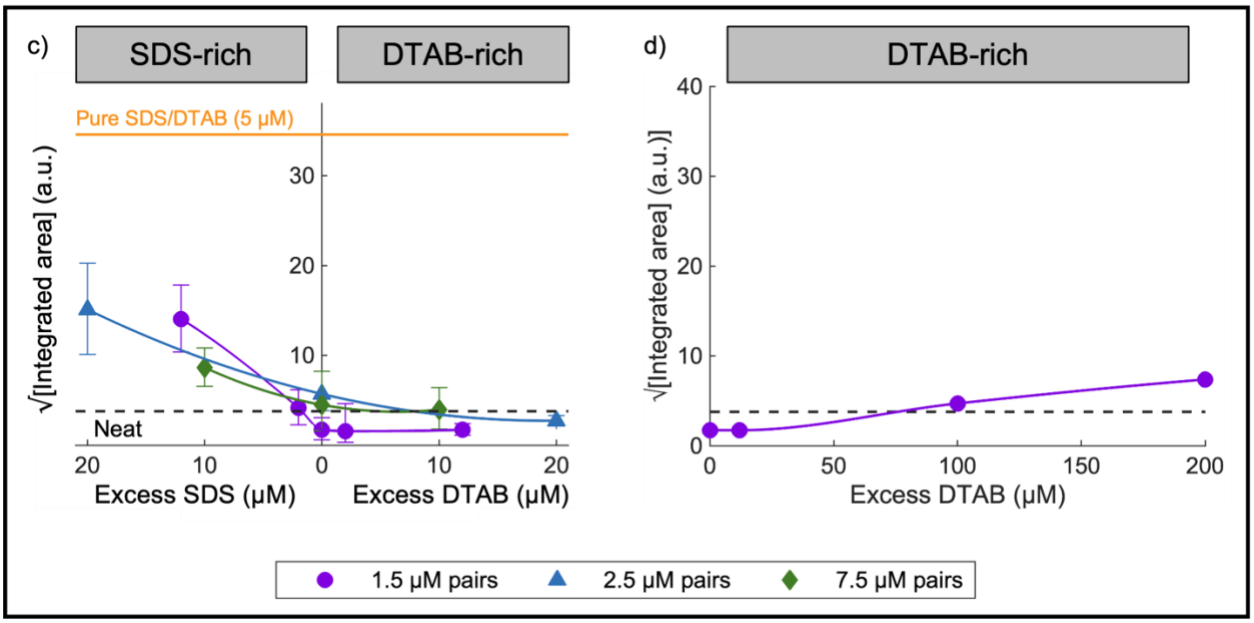


**Figure 5.5.** (a) Coordinated water integrated areas of d-SDS:h-SDS mixtures at the $H_2O$-$CCl_4$ interface as a function of (a) excess SDS/DTAB or (b) excess DTAB concentration. The integrated areas of the neat $H_2O$-$CCl_4$ interface and pure 5 μM SDS/DTAB are also included. Solid lines are a guide to the eye. Error bars are the integrated areas that are calculated using the upper and lower bounds of the fit parameters

In order to more rigorously assess the composition of the mixed SDS:DTAB monolayers, we quantify the relative number of charged unpaired surfactants adsorbed at the interface by means of the integrated area of the coordinated water features for d-SDS:h-DTAB mixtures at the $H_2O$-$CCl_4$ interface. Figure 5.5a shows the square root of the integrated areas for the 1.5, 2.5, and 7.5 μM d-SDS:h-DTAB mixtures ranges from 1.5 to 15. The square root of these values is analyzed since the VSF signal scales quadratically with number density. This analysis assumes the average orientation of the interfacial water molecules does not change with electric field strength. This assumption is reasonable given that the intensity of the coordinated water spectrum between the power spectrum (measured with homodyne VSFS, which is employed herein) and the imaginary spectrum (measured with heterodyne VSFS) are similar;[119] molecular orientation does not influence the intensity of the imaginary spectrum. To associate these values to the relative number of adsorbed unpaired surfactants, we consider the neat oil-water interface as well as pure SDS and DTAB for which the number of unpaired surfactants adsorbed at the interface is known. The majority of the integrated areas of the mixtures are comparable to the neat interface (~4), again suggesting that few unpaired surfactants are adsorbed at the interface. This finding is substantiated by the integrated areas of the SDS:DTAB mixtures being nearly two-times smaller than pure 5 μM SDS/DTAB (~35). Given that the interfacial pressure of pure 5 μM SDS/DTAB is ~0.7 mN/m (~1% interface coverage), areas smaller than 40 are indicative of sparingly few adsorbed unpaired surfactants. The comparatively small integrated areas of the SDS:DTAB mixtures thereby indicate that less than 0.5% of the interface is covered with unpaired surfactants. Hence, the coordinated water integrated areas in Figure 5.5a, together with the interfacial pressure measurements in Figure 5.3c, show that the monolayers prepared by the SDS:DTAB mixtures mainly consist of paired

surfactants and a nearly negligible number of unpaired surfactants, consistent with the findings from the visual analysis of these spectra.

Further inspection of Figure 5.5a reveals that the integrated areas of the SDS-rich mixtures are larger than the DTAB-rich mixtures for the same interfacial surfactant concentration. This suggests that more unpaired surfactants are adsorbed at the interface of the SDS-rich mixtures compared to DTAB-rich mixtures, as anticipated by solution theory.[52] Solution theory predicts that at opposite mixing ratios (e.g. 7:3 and 3:7), the SDS-rich monolayers contain more unpaired SDS than DTAB-rich monolayers contain unpaired DTAB. This prediction is based on SDS being more interfacially active than DTAB. For SDS-rich mixtures, the integrated areas also indicate that the interfacial concentration of unpaired surfactants increases with excess SDS concentration. In contrast, the integrates areas of the DTAB-rich mixtures suggest the interfacial concentration of unpaired surfactants either does not change or decreases with excess DTAB concentration, contrary to model predictions. Interestingly, the areas of the DTAB-rich mixtures are smaller than that of the neat oil-water interface, suggesting that these monolayers are minimally charged, even when the excess DTAB concentration is ~13 times larger than the stoichiometric paired surfactant concentration. This behavior is unanticipated considering our analysis and interpretation of the interfacial pressure measurements (Figure 5.3c) suggest that both unpaired and paired surfactants may adsorb at the interface with increasing excess surfactants. Thus, the cause for the consistently diminutive interfacial charge of the DTAB-rich mixtures is unclear.

In order to assess the underlying mechanism governing the nearly negligible interfacial charge for the DTAB-rich mixtures, we also examine the coordinated water integrated areas of 1.5 μM d-SDS:h-DTAB + 100/200 μM h-DTAB mixtures in Figure 5.5b. The charge of the surfactant monolayers clearly increases with increasing excess DTAB. Surprisingly, the mixture with 200

μM excess DTAB is only comparable to the mixture that contains only 12 μM excess SDS. The increased interfacial charge of the DTAB-rich mixtures (Figure 5.5d) unquestionably results from the adsorption of unpaired DTAB, as evidenced by the fits to the coordinated water features. The fit's phase reports on the average orientation of water's molecular dipole relative to the interface, which is governed by the interfacial charge.[108,138] For the 100 and 200 μM excess DTAB mixtures, the phase indicated that the water's molecular dipole points towards the interface, indicative of a positively charged interface. In contrast to the SDS-rich mixtures, the excess DTAB concentration must be nearly an order of magnitude larger for an appreciable number of unpaired DTAB to populate the interface. The different behavior of the DTAB- and SDS-rich mixtures is likely due to DTAB being half as interfacially active as SDS. The VSFS measurements in Figure 5.5a and 5.5b thus substantiate the finding from Figure 5.4: that the monolayers of the DTAB-rich mixtures listed in Table 1 contain a much smaller number of unpaired DTAB compared to when SDS is in excess. Hence, the coordinated water integrated areas in Figures 5.5a and 5.5b strongly support the idea that more unpaired surfactants are adsorbed at the interface in the SDS-rich mixtures compared to the DTAB-rich mixtures.

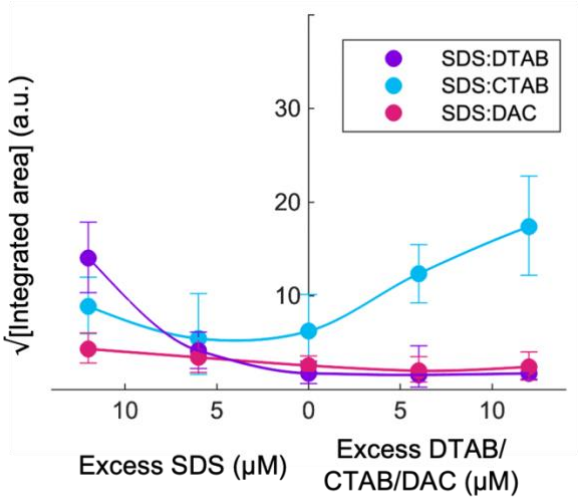


**Figure 5.6.** Square root of the coordinated water integrated areas for 1.5 μM d-SDS:h-DTAB, d-SDS:h-CTAB, and d-SDS:h-DAC mixtures at the $CCl_4$-$H_2O$ as a function of excess function of

excess SDS and cationic (CTAB/DAC/DTAB) concentration. Error bars are the integrated areas calculated using the upper and lower bounds of the fit parameters. Solid lines are a guide to the eye.

To more thoroughly assess whether the interfacial activity plays a major role in regulating the composition of the monolayers created by mixtures with excess SDS/DTAB, we examine the interfacial water spectral region of SDS:CTAB (cetylrimethylammonium bromide) mixtures. CTAB is used because it is roughly eight times more interfacially active than SDS whereas DTAB is nearly half as interfacially active than SDS, as evidenced by their respective CMC.[107,108] Moreover, as depicted in Figure 5.2, CTAB is structurally similar to DTAB in that both surfactants contain the same headgroup and linear alkyl tails, albeit different lengths. Figure 5.6 shows the square root of the coordinated water integrated areas for 1.5 μM d-SDS:h-CTAB mixtures as a function of excess SDS/CTAB concertation. A 1.5 μM paired surfactant concentration was selected since is it below the CMC of the equimolar SDS:CTAB mixture (~5 μM)[139,140] and it can be directly compared to the 1.5 μM SDS:DTAB mixtures, which are also included in Figure 5.6. The areas do not change with excess SDS concentration but increase with excess CTAB concentration. This behavior indicates that the monolayers of the CTAB-rich mixtures are more charged (contain more unpaired surfactants) compared to the monolayers of the SDS-rich mixtures, completely opposite to the SDS:DTAB mixtures. Given that the only difference between CTAB and DTAB is their tail length, which causes CTAB to be more interfacially active compared to DTAB, this result substantiates the notion that more unpaired surfactants are adsorbed at the interface in the SDS-rich mixtures compared to the DTAB-rich mixtures.

The SDS and DTAB headgroups may be another factor that may regulate the composition of the mixed SDS:DTAB surfactant monolayers. To assess the impact surfactant headgroup identity has on the SDS:DTAB mixtures, we examine SDS:DAC (dodecylammonium chloride)

mixtures. DAC is used because its interfacial activity is comparable to DTAB, as gauged by their respective CMC of 14.5 mM[141] and 14.6 mM.[107] Notably, DAC was used because, unlike dodecylammonium bromide (DAB), it is commercially available at high-purity grades. Substituting bromide with chloride is deemed inconsequential at micromolar concentrations. Figure 5.6 shows the square root of the coordinated water integrated areas for 1.5 μM d-SDS:h-DAC mixtures at the $H_2O$-$CCl_4$ interface as a function of excess SDS/DAC concertation. A paired surfactant concentration of 1.5 μM is selected since it is below the CMC of the equimolar SDS:DAC mixture (∼15 μM, see Figure B.2) and facilitates comparison to the 1.5 μM SDS:DTAB and SDS:CTAB mixtures. The profile of the mixed SDS:DAC integrated plot mimics that of the SDS:DTAB mixtures: the values increase with excess SDS concentration and does not change with excess DAC concentration. These changes indicate that more surfactants adsorb at the interface as the mixtures become more SDS-rich and a seemingly undetectable number of surfactants adsorb at the interface in the DAC-rich mixtures. The congruous behavior of the SDS:DAC and SDS:DTAB mixtures suggest that the anionic and cationic surfactant headgroups in the SDS:DTAB mixture minimally regulates the composition of the mixed SDS:DTAB monolayers. Hence, our measurements of the SDS:DTAB, SDS:CTAB, and SDS:DAC mixtures leads us to conclude that the monolayers of the SDS-rich SDS:DTAB mixtures contain more unpaired surfactants compared to the monolayers of the DTAB-rich mixtures because SDS is more interfacially active than DTAB.

**Interfacial Packing of SDS:DTAB Mixtures**

To determine if the adsorbed unpaired surfactants affect the interfacial packing of the mixed SDS:DTAB monolayers, we continue to leverage the unique capabilities of VSFS to selectively examine the conformation of the SDS and DTAB alkyl tails, which is sensitive to the

surfactant's local packing environment. Specifically, the number of gauche defects along the tail is inversely proportional to the surfactant's local packing environment: the number of gauche defects along decreases with a tighter packing environment. For these measurements, $D_2O$ is used as the aqueous phase so the coordinated water features lie outside the C-H stretching region, thereby leaving the C-H features of the surfactants' tails largely unobscured. To ensure that the C-H features solely originate from either the SDS or DTAB tail, the surfactant mixtures are selectively deuterated using two deuteration schemes: (1) hydrogenated SDS mixed with fully deuterated DTAB (h-SDS:d-DTAB) and (2) fully deuterated SDS mixed with partially deuterated DTAB (d-SDS:$d_9$-DTAB), where $d_9$-DTAB possesses a deuterated headgroup and a hydrogenated tail. Thus, the h-SDS:d-DTAB spectrum reports on the SDS tail whereas the d-SDS:$d_9$-DTAB spectrum reports on the DTAB tail.

Figures 5.7a and 7b shows VSF spectra of d-SDS:$d_9$-DTAB and h-SDS:d-DTAB and mixtures at the $D_2O$-$CCl_4$ interface, respectively, across a range of mixing ratios and paired surfactant concentrations. The spectral features have been previously assigned and are listed in Table B2. Inspection of the spectra clearly reveals that the relative intensity of the features changes with excess SDS/DTAB and paired surfactant concentration, which results from the surfactant monolayer restructuring and spectral interferences. Relative amplitude changes of the methyl ($A_{r^+}$, 2875 $cm^{-1}$) and methylene ($A_{d^+}$, 2850 $cm^{-1}$) symmetric stretches (extracted from the spectral fits) are of particular interest since their amplitude ratio ($A_{r^+}/A_{d^+}$) is a sensitive proxy of surfactant tail conformation.[60,123,142] In an all-trans (perfectly ordered) conformation, the $d^+$ are in a centrosymmetric environment (VSF inactive) while the $r^+$ are in a non-centrosymmetric environment (VSF active), which gives rise to a large $A_{r^+}/A_{d^+}$ ratio. Conversely, when the alkyl tail contains gauche defects (conformationally disordered), the $d^+$ are in a non-centrosymmetric

environment whereas the $r^+$ are in a centrosymmetric environment, which gives rise to a small $A_{r^+}/A_{d^+}$ ratio. Therefore, a large $A_{r^+}/A_{d^+}$ ratio is indicative of well-ordered alkyl tails while a small $A_{r^+}/A_{d^+}$ ratio is indicative of disordered alkyl tails.

Figure 5.7 displays $A_{r^+}/A_{d^+}$ ratios of equimolar, SDS-rich, and DTAB-rich h-SDS:d-DTAB (SDS tail, panel a) and d-SDS:$d_9$-DTAB (DTAB tail, panel a) mixtures as a function of excess SDS/DTAB concentration. The paired surfactant concentration of the mixtures is 1.5, 2.5, and 7.5 μM. The conformations of the SDS and DTAB tails in equimolar SDS:DTAB mixtures have previously been characterized with VSFS[132] and therefore are discussed only provide a basis for understanding the behavior of SDS- and DTAB-rich mixtures. Briefly, for equimolar mixtures, both the SDS and DTAB tails are ~55% more conformationally ordered than maximally packed monolayers of pure h-SDS and $d_9$-DTAB that form at concentrations of 3 mM and above.[102] The enhanced interfacial packing of the equimolar mixtures is largely due to the electroneutral headgroup of the paired surfactants, which minimizes long-range, repulsive electrostatic interactions among the headgroups, lending to short-range steric and Van der Waals interactions primarily regulating their interfacial packing. In equimolar mixtures, both SDS and DTAB tails become more ordered with concentration up to 7.5 μM. This behavior is a consequence of the surfactant monolayers being in a liquid-like state.[92,132] In this state, the monolayer packs more densely as additional surfactants adsorb to the interface, resulting in conformationally more ordered alkyl tails. Above 7.5 μM ($A_{r^+}/A_{d^+}$ ratios not shown), the tail conformations do not change with concentration, even though surfactants continue to adsorb to the interface (as monitored by interfacial pressure measurements), since the monolayers are in a solid-like state wherein packing is limited by steric interactions. These monolayers presumably are tightly packed domains, which have been observed for SDS:CTAB mixtures at the air-water interface.[121]

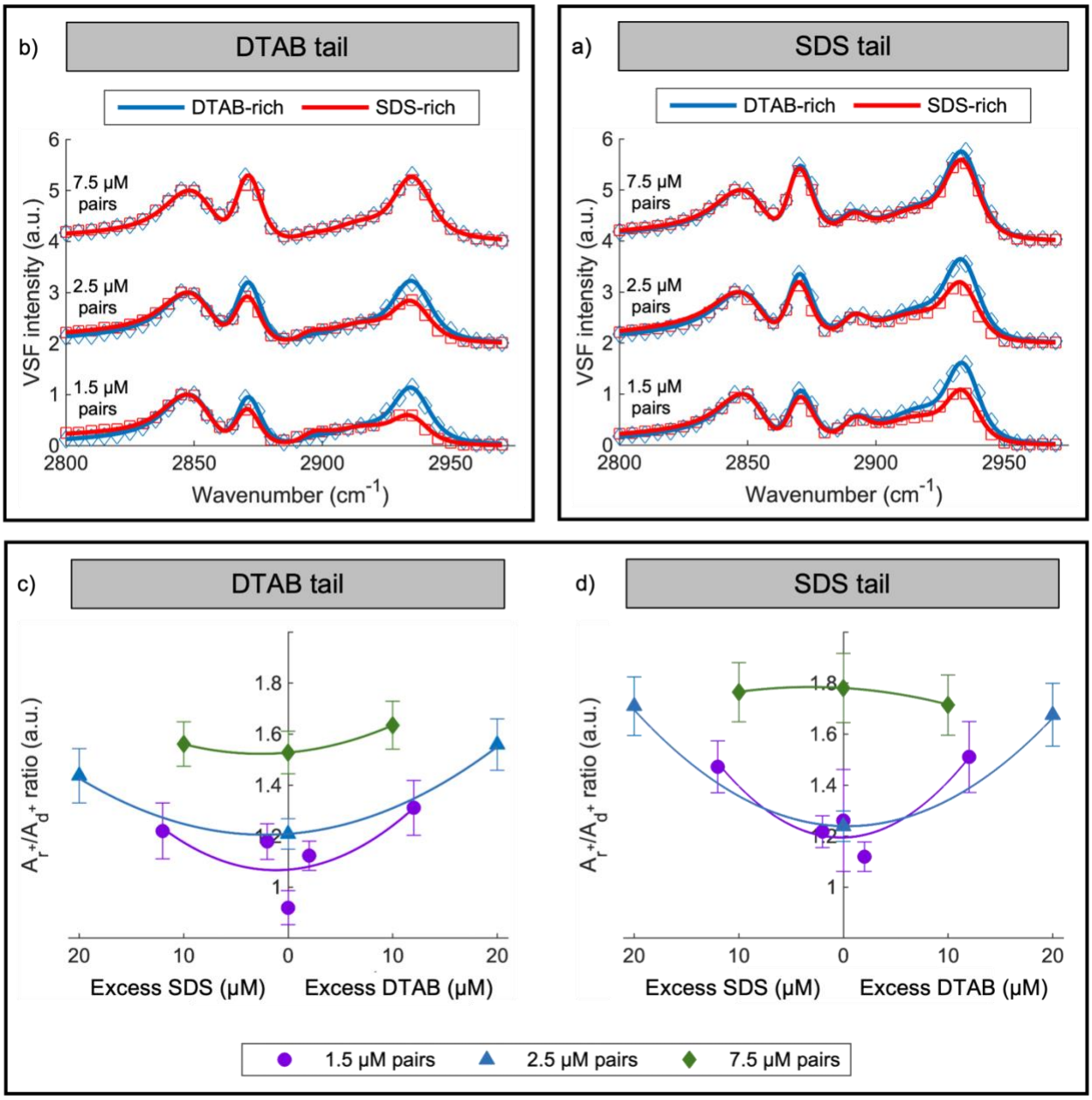


**Figure 5.7.** VSF spectra of DTAB- and SDS-rich (a) d-SDS:$d_9$-DTAB (DTAB tail) and (b) h-SDS:d-DTAB (SDS tail) mixtures at the $CCl_4$-$D_2O$ interface. The 1.5 μM mixtures contain 12 μM excess SDS/DTAB. Spectra are offset and scaled for the ~2850 $cm^{-1}$ feature to have a maximum intensity of one. $A_{r+}/A_{d+}$ ratios of (c) d-SDS:$d_9$-DTAB (DTAB tail) and (d) h-SDS:d-DTAB:d-SDS (SDS tail) obtained from spectra in panels a and b, respectively. Solid lines overlaying the markers are a guide to the eye. Error bars are the standard deviation of at least three measurements performed on separate days.

Inspection of the DTAB $A_{r+}/A_{d+}$ ratios (Figure 5.7c) for the 1.5 and 2.5 μM pair mixtures reveals that the DTAB tail generally become more ordered with increasing excess SDS/DTAB concentration. This behavior arises from the adsorption of additional surfactants to the interface, embedding in the liquid-like monolayer. As excess SDS/DTAB is added to the mixtures, both paired and unpaired surfactants adsorb at the interface, as evidenced by the interfacial pressure (Figure 5.3c) and VSFS water (Figures 5.4 and 5.5) measurements. The adsorption of additional surfactants increases the interfacial packing density as well as surfactant tail ordering. Contrarily, the DTAB tail ordering of the 7.5 μM pair mixtures is the same without and with the excess SDS/DTAB. This behavior is attributed to the surfactant monolayer of the equimolar 7.5 μM pair mixture already being in a solid-like state.

Further inspection of the DTAB $A_{r+}/A_{d+}$ ratios of the 1.5 and 2.5 μM paired mixtures reveals that the DTAB tails are more ordered in DTAB-rich mixtures compared to SDS-rich mixtures. This finding is unexpected given that the surfactant tail ordering is typically correlated to the interfacial surfactant population and this population is the same for mixtures at a fixed paired surfactant concentration at equivalent excess SDS/DTAB concentrations (e.g. 2.5 μM SDS:DTAB + 20 μM SDS and 2.5 μM SDS:DTAB + 20 μM DTAB mixtures), as determined by the interfacial pressure measurements in Figure 5.3. This dissimilarity in the $A_{r+}/A_{d+}$ ratios leads to two possible explanations. Given that the $A_{r+}/A_{d+}$ ratio reports on the average tail conformation of the adsorbed surfactants, it is possible that, for the monolayers of the DTAB-rich mixtures, the unpaired DTAB tails are well ordered and markedly increase the $A_{r+}/A_{d+}$ ratios. However, this scenario is unlikely given that the unpaired and paired surfactants' contribution to the VSF spectra is weighted by their interfacial number density (population) and the mixed SDS:DTAB monolayers contain a nearly negligible number of unpaired surfactants. The more plausible explanation stems from the fact that

more unpaired surfactants are adsorbed at the interface in the SDS-rich mixtures compared to the DTAB-rich mixtures. The unpaired surfactants in the monolayers likely act as point defects, disrupting the interfacial surfactant packing. This disruption presumably is proportional to the number of unpaired surfactants adsorbed at the interface. We therefore posit that the difference in unpaired surfactants in the mixed SDS:DTAB monolayers engenders the dissimilar DTAB tail ordering of SDS- and DTAB-rich mixtures.

Figure 5.7d shows SDS $A_{r+}/A_{d+}$ ratios obtained from the h-SDS:d-DTAB spectra in Figure 5.7b. The SDS tail behavior generally mimics DTAB: in 1.5 and 2.5 μM paired mixtures, the tails generally become more ordered with increasing excess SDS/DTAB concentration whereas for 7.5 μM paired mixtures, the tail ordering does not vary. As discussed earlier, the different tail ordering behavior of the 1.5/2.5 μM mixtures compared to the 7.5 μM mixtures results from the monolayers being in a liquid- or solid-like state, respectively.[92,132] Notably, the $A_{r+}/A_{d+}$ ratios for the 1.5 and 2.5 μM mixtures stay nearly constant the SDS- and DTAB-rich mixtures, which contrasts the behavior observed for the DTAB tails. This different behavior of the SDS and DTAB tails is unexpected given that the $A_{r+}/A_{d+}$ ratios predominantly report on the paired surfactants. The conformation of the DTAB and SDS tail of a paired surfactant are expected to equally change with excess SDS/DTAB concentration, as observed for the equimolar mixtures,[132] since the tails interact through van der Waals interactions[62] which presumably causes them to be conjoined and be conformationally in unison. Regardless of the accuracy of this expectation, since the SDS and DTAB tails are identical, their conformations should be similar in identical packing environments. Hence, the different behavior of the SDS and DTAB tails (similar SDS tail conformation and dissimilar DTAB tail conformation) between SDS- and DTAB-rich mixtures indicates that paired SDS and DTAB at the interface experience different packing environments, possibly a staggered

headgroup arrangement as postulated for equimolar SDS:DTAB mixtures Discerning the details of the arrangement requires additional VSFS measurements and employing interfaically specific techniques that possess high spatial resolution.

## CONCLUSIONS

Anionic:cationoic surfactant mixtures are a commonly employed in many industries to stabilize liquid foams, either through deliberate mixing or by using impure reagents. However, their use as foaming agents is often limited, especially in oil related industries, by foam's susceptibility to destabilize in oily environments. To fully exploit their potential, it is necessary to identify surfactant mixtures that can stabilize foams in the presence of oil. Anionic:cationic surfactant mixtures can make oil tolerant foams, but it is difficult to predict which surfactant mixtures are viable foaming agents for these applications since the underlying mechanism of this behavior is unknown. In order to ascertain the molecular details, we used interfacial tensiometry concurrently with vibrational sum frequency spectroscopy to directly investigate the composition, and surfactant tail conformations of monolayers formed by DTAB:SDS mixtures across a range of surfactant mixing ratios and total surfactant concentrations. We directly show that both paired and unpaired surfactants are adsorbed at the interface although the paired surfactants constitute an overwhelmingly percentage of the mixed SDS:DTAB monolayers adsorbed at the interface. This disparity in the interfacial coverage is due to the paired surfactants being substantially more interfacially active compared to unpaired SDS and DTAB. The very few unpaired surfactants in the monolayer act as point defects to disrupt the packing of neighboring paired surfactants. The SDS-rich monolayers pack less tightly than the DTAB-rich monolayers due to the SDS-rich monolayers containing more unpaired surfactants, which is a consequence of SDS being more surface active than DTAB, as confirmed by VSFS measurements of SDS:CTAB and SDS:CTAB

mixtures. Measurements of these two other surfactant mixtures reveals that the interfacial activity of the unpaired constituent surfactants plays a bigger role in governing the structure of the surfactant monolayers compared to their effective headgroup charge. These findings have implications for nearly all scenarios in which surfactant mixtures are employed to create oil-tolerant foams.

# CHAPTER VI:

# CONCLUSION

Liquid foams are employed in the oil related industries;[14-16] however, their efficacy is limited by their tendency to rupture in oily environments. This rupturing is linked to the destruction of the pseudoemulsion film,[38] which highlights the need for surfactants to stabilize the pseudoemulsion film. Anionic:cationic surfactant mixtures stabilize the pseudoemulsion film and can thereby produce oil-tolerant foams.[35] The oil tolerance is attributed to the high dilatational elasticity of the surfactant mixtures,[30,35,43] which is indicative of tightly packed surfactants monolayers at the interface of the pseudeomulsion film. Given the dilatational elasticity is equivalent across anionic:cationic surfactant mixing ratios,[43,86] this property fails to explain why the oil tolerance significantly varies with the mixing ratio. Hence, this variability in oil tolerance suggests the underlying mechanism driving the oil tolerance is more complex than what can be gleaned from measuring the macroscopic properties of the interface.

In order to investigate molecular factors that contribute to the oil tolerance of foams stabilized by anionic:cationic surfactant mixtures, vibrational sum frequency (VSFS) and interfacial tensiometry were employed to determine the composition and structure of mixed anionic:cationic surfactant monolayers. This work was separated into two parts: the first (Chapter IV) focused on the equimolar SDS:DTAB mixtures while the second part (Chapter V) examined the more complex, non-equimolar SDS:DTAB mixtures. The work discussed in Chapter IV reveals that the surfactant monolayers formed by equimolar SDS:DTAB mixtures contain mostly stoichiometric 1:1 SDS:DTAB surfactant pairs and very few unpaired SDS/DTAB, engendering a negligible interfacial charge. Tail conformation measurements suggest that these paired surfactants in the monolayer are in staggered arrangement with the SDS headgroup immersing further into the

aqueous phase compared to the DTAB headgroup. Work in Chapter V shows that the monolayers of non-equimolar mixtures are similarly weakly charged, and the surfactants exhibit the same staggered arrangement. Moreover, the interfacial charge only slightly changes with SDS:DTAB ratio, indicating that the monolayer composition is largely independent of the surfactant mixing ratio. The few unpaired surfactant in the monolayer slightly disrupts the interfacial surfactant packing by acting as point defects.

Given that the physiochemical properties of the mixed SDS:DTAB monolayers are very similar across all SDS:DTAB mixing ratios, but their foam stability and oil tolerance is significantly different,[35,43] these findings suggest that small changes in the physiochemical properties of the pseudoemulsion film's interfaces significantly change the oil tolerance of foams. In terms of the interfacial charge and packing, the observations imply that the charge, rather than the packing, of the mixed surfactant monolayers adsorbed at the oil-water interface contributes to the oil tolerance of foams stabilized by these surfactant mixtures. At the surfactant concentrations needed to prepare stable foams (50 μM or above[43]), the surfactant monolayer charge changes with surfactant mixing ratio whereas the interfacial surfactant packing does not change. In particular, the SDS-rich mixtures are appreciably charged whereas the DTAB-rich mixtures are marginally charged. Repulsive electrostatic interactions between the surfactant monolayers formed at the air-water and oil-water interfaces of the pseudoemulsison film for SDS-rich SDS:DTAB mixtures presumably stabilize the film and is the reason foams stabilized by these mixtures are oil tolerant. Along the same line, the marginally charged surfactant monolayer prepared by the DTAB-rich SDS:DTAB mixtures is possibly the reason these mixtures do not form oil-tolerant foams.[35,43] Moreover, the staggered arrangement that is observed across all SDS:DTAB mixing ratios may contribute to the oil resistance of mixed SDS:DTAB foams by hindering water drainage from the

pseudoemulsion film, thereby stabilizing the lamella in oily environments. The hindered drainage would result from the SDS headgroups having a more extensive hydration shell in this arrangement and stronger interactions (hydrogen bonds) with water, compared to the DTAB headgroups. These findings have implications for nearly all scenarios in which anionic:cationic surfactant mixtures are employed to create oil-tolerant foams.

There are many conceivable ways to immediately extend and build upon the work of this dissertation. For brevity, only four of the most logical avenues are briefly discussed. The first is to more extensively study the SDS:CTAB mixtures at the oil-water, which were briefly examined in Chapter V. Studying this system would help evaluate the accuracy of interpretations of the mixed SDS:DTAB measurements. The SDS:CTAB mixture a good choice because the surfactant headgroups do not change, meaning that one should not have worry about changes in the headgroup immersions depths, which must be considered for different headgroups. Moreover, the interfacial behavior of SDS:CTAB mixtures have been studied.[121,143] The second avenue is to employ VSFS to study the DTAB and SDS headgroups. Both headgroups are sensitive to their solvation environment[116,144] and can thus provide more information about the system than the alkyl tails alone. Notably, such experiments require accompanying electronic structure calculations to interpret the VSF spectra since the vibrational modes may be affected when SDS and DTAB form a 1:1 stoichiometric pair. Previous work from this lab has already established a foundation for these calculations.[116] Thirdly, combining the experimental measurements within this dissertation with theoretically calculated VSF spectra of the surfactant tails.[104,126] Such calculations would help identify the location of gauche defects along the surfactant tails and thereby refine the molecular-level pictures that have been developed from the interfacial pressure and spectroscopic measurements. Lastly, X-ray and neutron reflectometry measurements would provide invaluable

structural information about this surfactant mixture given the techniques' high spatial resolution.[145,146] This structural information in combination with chemical information obtained from the VSFS measurements herein would provide a tremendous wealth of information about oil tolerant foams.

Regardless of whether the foam stability community heeds these suggestions of how to progress the work of this dissertation, the long-term goals of this field are clear and can be separated into two categories. The first is to more widely employ techniques that can directly elucidate the molecular-level factors that drives the stability and oil tolerance of foams. To date, these factors have been largely inferred from measurements that employ techniques that are not molecularly specific (e.g., interfacial tensiometry and rheology).[30,43,85,86,147] Hence, the molecular details are not definitively known, making it difficult to truly characterize the structure-property relationship that is needed to judiciously create more oil tolerant foams. The second category is to develop a way of selectively studying the oil-water and air-water interfaces of the pseudeomulsion film. This capability is very technically challenging but is needed to determine whether water confinement affects[148] markedly influence the stability of the pseudoemulsion. Because of the origin of these effects, it is not possible to ascertain this information from model oil-water and air-water interfaces formed between bulk fluids. Achieving any of these long- or short-term goals would be particularly important to elucidating the interfacial structure-property relationship oil tolerant foams, which is of value from both an industrial application and a fundamental science perspective.

# APPENDIX A:

# SUPPLEMENTARY INFORMATION FOR CHAPTER IV

### Concentration of surfactants solubilized in $CCl_4$

Figure A.1 shows the same interfacial pressure isotherm from Figure 4.2, but with the total surfactant concentration converted to a logarithmic scale. The critical micelle concentration (CMC) is identified as the intersection of linear regressions (black lines) fitted to the isotherm before and after the inflection point. This value agrees well with the CMC obtained from surface tension measurements at the air-water interface,[43] suggesting the concentration of surfactants that transfer into the oil phase during the interfacial tension (IFT) and vibrational sum frequency spectroscopy (VSFS) measurements is negligible. If an appreciable concentration of surfactants transferred into the $CCl_4$, the isotherm in Figure A.1 would be shifted towards higher concentrations, resulting in a larger CMC, compared to the value obtained from the air-water surface tension isotherm.[149]

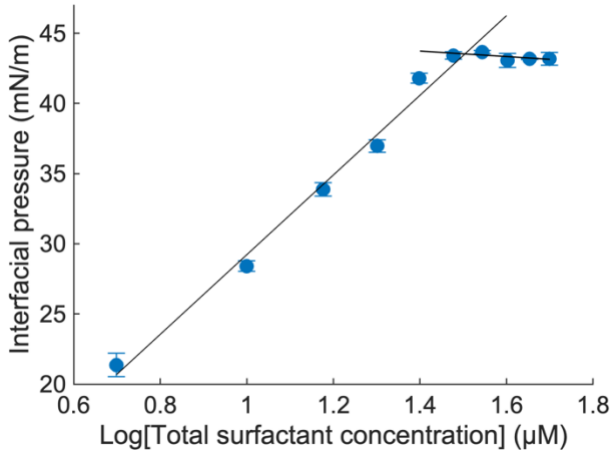


**Figure A.1.** Interfacial pressure measurements in Figure 4.2 plotted against the log of total surfactant concentration for 1:1 SDS:DTAB mixtures. Lines are linear regressions before and after the inflection point.

The surfactant concentration in the $CCl_4$ under these experimental conditions was further evaluated with Fourier transform infrared (FTIR) and quantitative $^1H$ nuclear magnetic resonance (qHNMR) spectroscopies. The appearance of small features in the C-H stretching region confirmed surfactants transfer into the oil phase during the IFT experiments.

The qHNMR measurements were performed to quantify the concentration of surfactants that transfer into the oil phase. To determine the proton chemical shifts of the surfactants in $CCl_4$, a precursory $^1H$ NMR spectrum of $CCl_4$ saturated with hexadecyltrimethylammonium bromide (CTAB) was collected. CTAB was used because its longer alkyl tail enhances its solubility in $CCl_4$, compared to both pure DTAB and SDS. The enhanced solubility allows for a higher surfactant concentration, making it easier to identify its proton signals of the $CH_2$ and $CH_3$ groups in the spectrum. The chemical shifts for the proton signals are expected to minimally change (ca. 0.2 ppm or less) when SDS and DTAB electrostatically pair, as observed for 1:1 SDS:CTAB mixture in chloroform ($CDCl_3$). Unlike the clearly visible and intense features of the 1 μM internal standard BTMSB, the surfactant features were not observed in the 1:1 SDS:DTAB mixture spectrum, indicating a surfactant concentration in the $CCl_4$ is well below 1 μM in both the IFT and VSFS experiments.

**Surfactant headgroup area calculations**

The maximum interfacial excess ($\Gamma_{max}$) was obtained from the pre-CMC regression in Figure A.1 by applying the Gibbs equation:[110]

$$\Gamma_{\max} = \frac{1}{nRT}\left(\frac{\partial \Pi}{\partial \ln(c)}\right)_T \quad \text{(A.1)}$$

where $n$ = 1 to account the number of species in excess at the interface, $R$ is the ideal gas constant, $T$ = 298 K (room temperature), Π is the interfacial pressure, and c is the total surfactant

concentration. The interface excess at a given interfacial pressure ($\Gamma_i$) are obtained by inserting the maximum interface excess and the interfacial pressure values into the Frumkin equation:[53]

$$\Pi = -RT\Gamma_{\max}\left[\ln\left(1-\frac{\Gamma_i}{\Gamma_{\max}}\right)+ a\left(\frac{\Gamma_i}{\Gamma_{\max}}\right)^2\right] \quad \text{(A.2)}$$

in which the interaction parameter ($a$) is set to zero. The average surfactant headgroup area (A) is obtained from the interface excess according to:

$$\mathrm{A} = \frac{10^{20}}{N_A\Gamma} \quad \text{(A.3)}$$

where $N_A$ is Avogadro's number.

**Table A.1.** Peak assignments for VSF spectra of 1:1 h-SDS:d-DTAB (SDS tail) and d-SDS:d$_9$-DTAB (DTAB tail) mixtures at the $D_2O$-$CCl_4$ interface, (Figure 4.7).

| Peak assignment | Frequency ($cm^{-1}$) |
|---|---|
| $CH_2$ symmetric stretch ($d^+$) | 2853 |
| $CH_3$ symmetric stretch ($r^+$) | 2871 |
| $CH_2$ asymmetric stretch ($d^-$) | 2886 |
| $CH_2$ fermi resonance ($d^+_{FR}$) | 2917 |
| $CH_3$ fermi resonance ($r^+_{FR}$) | 2933 |
| $D_2O$ combination band | 2838 |

**Table A.2.** Fit parameters for the neat $H_2O$-$CCl_4$ interface (Figure 4.5).

| Peak Assignment | Parameter | |
|---|---|---|
| Coordinated water O-H stretch | Amplitude | 0.15 ± 0.01 |
| | Phase | 0 |
| | Lorentzian | 5 |
| | Frequency | 3296 ± 20 |
| | Gaussian | 120 ± 24 |
| Coordinated water O-H stretch | Amplitude | 0.17 ± 0.04 |
| | Phase | 0 |
| | Lorentzian | 5 |
| | Frequency | 3435 ± 9 |
| | Gaussian | 80 ± 9 |
| Free OH | Amplitude | 1.33 ± 0.03 |
| | Phase | 3.14 |
| | Lorentzian | 12 |
| | Frequency | 3675.9 ± 0.2 |
| | Gaussian | 11.3 ± 0.3 |
| Nonresonant | Amplitude | 0 |

| | | |
|---|---|---|
| | Phase | 0 |

**Table A.3.** Fit parameters for d-SDS:h-DTAB mixtures (Figure 4.5) at the $H_2O$-$CCl_4$ interface.

| Peak Assignment | Parameter | 30 μM | 25 μM | 20 μM | 15 μM | 10 μM | 5 μM | 3 μM |
|---|---|---|---|---|---|---|---|---|
| $CH_2$ S.S. | Amplitude | 0.77 ± 0.01 | 0.76 ± 0.01 | 0.78 ± 0.01 | 0.75 ± 0.01 | 0.73 ± 0.01 | 0.63 ± 0.01 | 0.30 ± 0.01 |
| | Phase | 0 | 0 | 0 | 0 | 0 | 0 | 0 |
| | Lorentzian | 2 | 2 | 2 | 2 | 2 | 2 | 2 |
| | Frequency | 2850.7 ± 0.3 | 2850.7 ± 0.3 | 2850.5 ± 0.2 | 2850.3 ± 0.3 | 2850.0 ± 0.3 | 2850.7 ± 0.3 | 2846.0 ± 0.5 |
| | Gaussian | 12.3 ± 0.5 | 12.4 ± 0.5 | 12.0 ± 0.4 | 11.1 ± 0.4 | 11.3 ± 0.3 | 10.0 ± 0.3 | 11.1 ± 0.6 |
| $CH_3$ S.S. | Amplitude | 1.06 ± 0.03 | 1.07 ± 0.04 | 1.07 ± 0.05 | 0.87 ± 0.03 | 0.79 ± 0.03 | 0.58 ± 0.02 | 0.3 ± 0.2 |
| | Phase | 0 | 0 | 0 | 0 | 0 | 0 | 0 |
| | Lorentzian | 2 | 2 | 2 | 2 | 2 | 2 | 2 |
| | Frequency | 2870.9 ± 0.1 | 2871.0 ± 0.1 | 2871.1 ± 0.1 | 2870.9 ± 0.1 | 2870.8 ± 0.2 | 2870.3 ± 0.2 | 2870 ± 1 |
| | Gaussian | 4.5 ± 0.2 | 4.0 ± 0.3 | 3.7 ± 0.3 | 4.3 ± 0.3 | 4.2 ± 0.3 | 4.9 ± 0.3 | 2 ± 2 |
| $CH_2$ F.R. | Amplitude | 0.81 ± 0.05 | 0.78 ± 0.05 | 0.75 ± 0.04 | 0.67 ± 0.05 | 0.57 ± 0.04 | 0.37 ± 0.02 | 0.34 ± 0.03 |
| | Phase | 3.14 | 3.14 | 3.14 | 3.14 | 3.14 | 3.14 | 3.14 |
| | Lorentzian | 2 | 2 | 2 | 2 | 2 | 2 | 2 |
| | Frequency | 2914.5 ± 0.5 | 2914.9 ± 0.6 | 2915.3 ± 0.6 | 2914.4 ± 0.7 | 2913.1 ± 0.9 | 2909 ± 1 | 2912 ± 6 |
| | Gaussian | 4.0 ± 0.4 | 4.1 ± 0.5 | 4.4 ± 0.4 | 4.2 ± 0.5 | 5.3 ± 0.6 | 8.1 ± 0.8 | 8 ± 3 |
| $CH_3$ F.R. | Amplitude | 1.44 ± 0.01 | 1.40 ± 0.01 | 1.37 ± 0.01 | 1.18 ± 0.01 | 0.98 ± 0.01 | 0.71 ± 0.01 | 0.37 ± 0.02 |
| | Phase | 0 | 0 | 0 | 0 | 0 | 0 | 0 |
| | Lorentzian | 2 | 2 | 2 | 2 | 2 | 2 | 2 |
| | Frequency | 2935.9 ± 0.1 | 2935.9 ± 0.1 | 2936.0 ± 0.2 | 2935.7 ± 0.2 | 2935.9 ± 0.4 | 2935.9 ± 0.4 | 2934 ± 2 |
| | Gaussian | 8.0 ± 0.1 | 7.6 ± 0.2 | 7.3 ± 0.2 | 7.7 ± 0.2 | 8.9 ± 0.3 | 8.7 ± 0.3 | 8.9 ± 0.7 |
| Coordinated water O-H stretch | Amplitude | 0.35 ± 0.05 | 0.34 ± 0.03 | 0.32 ± 0.03 | 0.28 ± 0.04 | 0.2 ± 0.1 | 0.154 ± 0.006 | 0.095 ±0.006 |
| | Phase | 3.14 | 3.14 | 3.14 | 3.14 | 3.14 | 3.14 | 0 |
| | Lorentzian | 5 | 5 | 5 | 5 | 5 | 5 | 5 |
| | Frequency | 3190 ± 9 | 3201 ± 12 | 3206 ± 15 | 3203 ± 18 | 3199 ± 20 | 3202 ± 12 | 3171 ± 24 |

| | | | | | | | | |
|---|---|---|---|---|---|---|---|---|
| | Gaussian | 96 ± 8 | 107 ± 11 | 112 ± 12 | 110 ± 15 | 93 ± 19 | 109 ± 19 | 167 ± 57 |
| Coordinated water O-H stretch | Amplitude | 0.23 ± 0.01 | 0.21 ± 0.02 | 0.21 ± 0.03 | 0.20 ± 0.03 | 0.21 ± 0.03 | 0.06 ± 0.02 | 0.02 ± 0.03 |
| | Phase | 3.14 | 3.14 | 3.14 | 3.14 | 3.14 | 3.14 | 0 |
| | Lorentzian | 5 | 5 | 5 | 5 | 5 | 5 | 5 |
| | Frequency | 3374 ± 20 | 3382 ± 17 | 3383 ± 20 | 3371 ± 25 | 3352 ± 42 | 3356 ± 19 | 3351 ± 30 |
| | Gaussian | 139 ± 39 | 110 ± 30 | 112 ± 28 | 110 ± 29 | 140 ± 50 | 68 ± 27 | 65 ± 69 |
| $N\text{-}CH_3$ S.S. | Amplitude | 0.08 ± 0.02 | 0.06 ± 0.02 | 0.08 ± 0.02 | 0.09 ± 0.01 | 0.12 ± 0.01 | 0.12 ± 0.02 | 0.08 ± 0.03 |
| | Phase | 0 | 0 | 0 | 0 | 0 | 0 | 0 |
| | Lorentzian | 2 | 2 | 2 | 2 | 2 | 2 | 2 |
| | Frequency | 2985 ± 2 | 2984 ± 3 | 2983 ± 2 | 2982 ± 2 | 2984 ± 2 | 2980 ± 2 | 2980 ± 3 |
| | Gaussian | 10 ± 4 | 12 ± 5 | 13 ± 4 | 18 ± 5 | 20 ± 4 | 13 ± 3 | 10 ± 6 |
| $N\text{-}CH_3$ A.S. | Amplitude | 0.09 ± 0.01 | 0.08 ± 0.02 | 0.07 ± 0.02 | 0.05 ± 0.01 | 0.04 ± 0.03 | 0.05 ± 0.02 | 0.03 ± 0.04 |
| | Phase | 3.14 | 3.14 | 3.14 | 3.14 | 3.14 | 3.14 | 0 |
| | Lorentzian | 2 | 2 | 2 | 2 | 2 | 2 | 2 |
| | Frequency | 3051 ± 3 | 3050 ± 3 | 3049 ± 3 | 3053 ± 4 | 3050 ± 5 | 3050 ± 7 | 3033 ± 13 |
| | Gaussian | 20 ± 4 | 19 ± 5 | 17 ± 5 | 18 ± 8 | 10 ± 9 | 21 ± 11 | 10 ± 22 |
| Water located between surfactant tails | Amplitude | 0.08 ± 0.03 | 0.09 ± 0.02 | 0.09 ± 0.02 | 0.09 ± 0.02 | 0.10 ± 0.02 | | |
| | Phase | 3.14 | 3.14 | 3.14 | 3.14 | 3.14 | | |
| | Lorentzian | 5 | 5 | 5 | 5 | 5 | | |
| | Frequency | 3573 ± 15 | 3564 ± 17 | 3569 ± 14 | 3565 ± 13 | 3578 ± 11 | | |
| | Gaussian | 59 ± 27 | 64 ± 27 | 61 ± 23 | 60 ± 22 | 57 ± 18 | | |
| Free OH | Amplitude | | | | | | | 0.5 ± 0.1 |
| | Phase | | | | | | | 3.14 |
| | Lorentzian | | | | | | | 12 |
| | Frequency | | | | | | | 3686 ± 2 |
| | Gaussian | | | | | | | 10 ± 3 |
| Unassigned $H_2O$ feature | Amplitude | | | | | | 0.204 ± 0.005 | 0.172 ± 0.005 |
| | Phase | | | | | | 3.14 | 0 |
| | Lorentzian | | | | | | 5 | 5 |
| | Frequency | | | | | | 2703 ± 8 | 2785 ± 6 |

| | | | | | | | | |
|---|---|---|---|---|---|---|---|---|
| | Gaussian | | | | | | 93 ± 11 | 110 ± 12 |
| Nonresonant | Amplitude | 0 | 0 | 0 | 0 | 0 | 0 | 0 |
| | Phase | 0 | 0 | 0 | 0 | 0 | 0 | 0 |

**Table A.4.** Fit parameters for 1:1 h-SDSd-DTAB (Figure 4.7a) mixtures at the $D_2O$-$CCl_4$ water interface.

| Peak Assignment | Parameter | 30 μM | 25 μM | 20 μM | 15 μM | 10 μM | 5 μM | 3 μM |
|---|---|---|---|---|---|---|---|---|
| $CH_2$ S.S. | Amplitude | 0.79 ± 0.03 | 0.81 ± 0.03 | 0.68 ± 0.03 | 0.59 ± 0.03 | 0.62 ± 0.03 | 0.54 ± 0.03 | 0.38 ± 0.04 |
| | Phase | 0 | 0 | 0 | 0 | 0 | 0 | 0 |
| | Lorentzian | 2 | 2 | 2 | 2 | 2 | 2 | 2 |
| | Frequency | 2854.6 ± 0.3 | 2854.6 ± 0.3 | 2854.6 ± 0.3 | 2854.6 ± 0.3 | 2854.6 ± 0.3 | 2854.6 ± 0.3 | 2854.6 ± 0.3 |
| | Gaussian | 10.1 ± 0.3 | 10.1 ± 0.3 | 10.1 ± 0.3 | 10.1 ± 0.3 | 10.1 ± 0.3 | 10.1 ± 0.3 | 10.1 ± 0.3 |
| $CH_3$ S.S. | Amplitude | 1.39 ± 0.05 | 1.50 ± 0.05 | 1.25 ± 0.05 | 1.02 ± 0.05 | 1.00 ± 0.05 | 0.75 ± 0.05 | 0.48 ± 0.06 |
| | Phase | 0 | 0 | 0 | 0 | 0 | 0 | 0 |
| | Lorentzian | 2 | 2 | 2 | 2 | 2 | 2 | 2 |
| | Frequency | 2870.3 ± 0.2 | 2870.3 ± 0.2 | 2870.3 ± 0.2 | 2870.3 ± 0.2 | 2870.3 ± 0.2 | 2870.3 ± 0.2 | 2870.3 ± 0.2 |
| | Gaussian | 4.7 ± 0.1 | 4.7 ± 0.1 | 4.7 ± 0.1 | 4.7 ± 0.1 | 4.7 ± 0.1 | 4.7 ± 0.1 | 4.7 ± 0.1 |
| $CH_2$ A.S. | Amplitude | 0.52 ± 0.06 | 0.44 ± 0.06 | 0.43 ± 0.05 | 0.36 ± 0.05 | 0.39 ± 0.06 | 0.35 ± 0.06 | 0.23 ± 0.07 |
| | Phase | 3.14 | 3.14 | 3.14 | 3.14 | 3.14 | 3.14 | 3.14 |
| | Lorentzian | 2 | 2 | 2 | 2 | 2 | 2 | 2 |
| | Frequency | 2890.3 ± 0.4 | 2890.3 ± 0.4 | 2890.3 ± 0.4 | 2890.3 ± 0.4 | 2890.8 ± 0.7 | 2890.8 ± 0.7 | 2890.8 ± 0.7 |
| | Gaussian | 4.8 ± 0.4 | 4.8 ± 0.4 | 4.8 ± 0.4 | 4.8 ± 0.4 | 5.2 ± 0.7 | 5.2 ± 0.7 | 5.2 ± 0.7 |
| $CH_2$ F.R. | Amplitude | 0.49 ± 0.05 | 0.48 ± 0.04 | 0.40 ± 0.04 | 0.34 ± 0.04 | 0.37 ± 0.06 | 0.37 ± 0.06 | 0.23 ± 0.05 |
| | Phase | 0 | 0 | 0 | 0 | 0 | 0 | 0 |
| | Lorentzian | 2 | 2 | 2 | 2 | 2 | 2 | 2 |
| | Frequency | 2921 ± 2 | 2921 ± 2 | 2921 ± 2 | 2921 ± 2 | 2922 ± 3 | 2922 ± 3 | 2922 ± 3 |
| | Gaussian | 13 ± 2 | 13 ± 2 | 13 ± 2 | 13 ± 2 | 13 ± 4 | 13 ± 4 | 13 ± 4 |
| $CH_3$ F.R. | Amplitude | 0.9 ± 0.1 | 0.97 ± 0.09 | 0.77 ± 0.08 | 0.64 ± 0.07 | 0.6 ± 0.1 | 0.5 ± 0.1 | 0.3 ± 0.1 |
| | Phase | 0 | 0 | 0 | 0 | 0 | 0 | 0 |
| | Lorentzian | 2 | 2 | 2 | 2 | 2 | 2 | 2 |

| | | | | | | | | |
|---|---|---|---|---|---|---|---|---|
| | Frequency | 2933.5 ± 0.2 | 2933.5 ± 0.2 | 2933.5 ± 0.2 | 2933.5 ± 0.2 | 2933.0 ± 0.3 | 2933.0 ± 0.3 | 2933.0 ± 0.3 |
| | Gaussian | 6.6 ± 0.4 | 6.6 ± 0.4 | 6.6 ± 0.4 | 6.6 ± 0.4 | 6.1 ± 0.9 | 6.1 ± 0.9 | 6.1 ± 0.9 |
| $D_2O$ combination band | Amplitude | 0.30 ± 0.03 | 0.38 ± 0.03 | 0.32 ± 0.03 | 0.25 ± 0.03 | 0.28 ± 0.03 | 0.22 ± 0.03 | 0.17 ± 0.03 |
| | Phase | 3.14 | 3.14 | 3.14 | 3.14 | 3.14 | 3.14 | 3.14 |
| | Lorentzian | 5 | 5 | 5 | 5 | 5 | 5 | 5 |
| | Frequency | 2823 ± 10 | 2829 ± 6 | 2828 ± 8 | 2831 ± 9 | 2825 ± 8 | 2818 ± 13 | 2807 ± 25 |
| | Gaussian | 90 ± 13 | 75 ± 8 | 812 ± 11 | 81 ± 14 | 75 ± 14 | 86 ± 25 | 96 ± 54 |
| Nonresonant | Amplitude | 0 | 0 | 0 | 0 | 0 | 0 | 0 |
| | Phase | 0 | 0 | 0 | 0 | 0 | 0 | 0 |

**Table A.5.** Fit parameters for 1:1 d-SDS:$d_9$-DTAB (Figure 4.7b) mixtures at the $D_2O$-$CCl_4$ water interface.

| Peak Assignment | Parameter | 30 μM | 25 μM | 20 μM | 15 μM | 10 μM | 5 μM | 3 μM |
|---|---|---|---|---|---|---|---|---|
| $CH_2$ s.s. | Amplitude | 0.48 ± 0.02 | 0.74 ± 0.02 | 0.48 ± 0.02 | 0.84 ± 0.02 | 0.48 ± 0.03 | 0.60 ± 0.03 | 0.26 ± 0.03 |
| | Phase | 0 | 0 | 0 | 0 | 0 | 0 | 0 |
| | Lorentzian | 2 | 2 | 2 | 2 | 2 | 2 | 2 |
| | Frequency | 2853.4 ± 0.3 | 2853.4 ± 0.3 | 2853.4 ± 0.3 | 2853.4 ± 0.3 | 2853.4 ± 0.3 | 2853.4 ± 0.3 | 2853.4 ± 0.3 |
| | Gaussian | 10.0 ± 0.2 | 10.0 ± 0.2 | 10.0 ± 0.2 | 10.0 ± 0.2 | 10.0 ± 0.2 | 10.0 ± 0.2 | 10.0 ± 0.2 |
| $CH_3$ s.s. | Amplitude | 0.78 ± 0.04 | 1.27 ± 0.04 | 0.71 ± 0.04 | 1.29 ± 0.04 | 0.61 ± 0.05 | 0.74 ± 0.05 | 0.26 ± 0.06 |
| | Phase | 0 | 0 | 0 | 0 | 0 | 0 | 0 |
| | Lorentzian | 2 | 2 | 2 | 2 | 2 | 2 | 2 |
| | Frequency | 2871.0 ± 0.1 | 2871.0 ± 0.1 | 2871.0 ± 0.1 | 2871.0 ± 0.1 | 2871.0 ± 0.1 | 2871.0 ± 0.1 | 2871.0 ± 0.1 |
| | Gaussian | 5.0 ± 0.1 | 5.0 ± 0.1 | 5.0 ± 0.1 | 5.0 ± 0.1 | 5.0 ± 0.1 | 5.0 ± 0.1 | 5.0 ± 0.1 |
| $CH_2$ a.s. | Amplitude | 0.34 ± 0.05 | 0.45 ± 0.07 | 0.32 ± 0.06 | 0.34 ± 0.07 | 0.29 ± 0.07 | 0.28 ± 0.08 | 0.23 ± 0.06 |
| | Phase | 3.14 | 3.14 | 3.14 | 3.14 | 3.14 | 3.14 | 3.14 |
| | Lorentzian | 2 | 2 | 2 | 2 | 2 | 2 | 2 |
| | Frequency | 2892.0 ± 0.8 | 2892.0 ± 0.8 | 2892.0 ± 0.8 | 2892.0 ± 0.8 | 2892.0 ± 0.8 | 2892.0 ± 0.8 | 2892.0 ± 0.8 |
| | Gaussian | 3.8 ± 0.6 | 3.8 ± 0.6 | 3.8 ± 0.6 | 3.8 ± 0.6 | 3.8 ± 0.6 | 3.8 ± 0.6 | 3.8 ± 0.6 |

| | | | | | | | | |
|---|---|---|---|---|---|---|---|---|
| $CH_2$ F.R. | Amplitude | 0.28 ± 0.02 | 0.45 ± 0.02 | 0.27 ± 0.02 | 0.50 ± 0.04 | 0.27 ± 0.03 | 0.39 ± 0.05 | 0.17 ± 0.04 |
| | Phase | 0 | 0 | 0 | 0 | 0 | 0 | 0 |
| | Lorentzian | 2 | 2 | 2 | 2 | 2 | 2 | 2 |
| | Frequency | 2920 ± 1 | 2920 ± 1 | 2920 ± 1 | 2920 ± 1 | 2920 ± 1 | 2920 ± 1 | 2920 ± 1 |
| | Gaussian | 15 ± 2 | 15 ± 2 | 15 ± 2 | 15 ± 2 | 15 ± 2 | 15 ± 2 | 15 ± 2 |
| $CH_3$ F.R. | Amplitude | 0.57 ± 0.05 | 0.76 ± 0.07 | 0.53± 0.05 | 0.77 ± 0.08 | 0.46 ± 0.05 | 0.43 ± 0.07 | 0.14 ± 0.07 |
| | Phase | 0 | 0 | 0 | 0 | 0 | 0 | 0 |
| | Lorentzian | 2 | 2 | 2 | 2 | 2 | 2 | 2 |
| | Frequency | 2933.6 ± 0.2 | 2933.6 ± 0.2 | 2933.6 ± 0.2 | 2933.6 ± 0.2 | 2933.6 ± 0.2 | 2933.6 ± 0.2 | 2930 ± 2 |
| | Gaussian | 7.0 ± 0.4 | 7.0 ± 0.4 | 7.0 ± 0.4 | 7.0 ± 0.4 | 7.0 ± 0.4 | 7.0 ± 0.4 | 5.0 ± 4.3 |
| $D_2O$ combination band | Amplitude | 0.16 ± 0.02 | 0.25 ± 0.02 | 0.16 ± 0.02 | 0.26 ± 0.03 | 0.15 ± 0.02 | 0.17 ± 0.03 | 0.14 ± 0.03 |
| | Phase | 3.14 | 3.14 | 3.14 | 3.14 | 3.14 | 3.14 | 3.14 |
| | Lorentzian | 5 | 5 | 5 | 5 | 5 | 5 | 5 |
| | Frequency | 2781 ± 17 | 2788 ± 9 | 2782 ± 19 | 2802 ± 12 | 2770 ± 40 | 2776 ± 37 | 2778 ± 36 |
| | Gaussian | 68 ± 24 | 78 ± 15 | 73 ± 28 | 108 ± 22 | 100 ± 60 | 125 ± 76 | 56 ± 45 |
| Nonresonant | Amplitude | 0 | 0 | 0 | 0 | 0 | 0 | 0 |
| | Phase | 0 | 0 | 0 | 0 | 0 | 0 | 0 |

**Table A.6.** Fit parameters to the coordinated water O-H stretch features for select 1:1 d-SDS:h-DTAB mixtures at the $CCl_4$-$H_2O$ interface (Table A.3) and POPC at the air-HOD interface.[117]

| System | Concentration (μM) | Coordinated water O-H stretch | Coordinated water O-H stretch |
|---|---|---|---|
| POPC | | 3380 | 3452 |
| 1:1 SDS:DTAB | 30 | 3190 | 3374 |
| | 20 | 3206 | 3383 |
| | 10 | 3199 | 3352 |
| | 3 | 3171 | 3351 |

# APPENDIX B:

# SUPPLEMENTARY INFORMATION FOR CHAPTER V

### Literature interfacial pressure measurements of SDS:DTAB mixtures

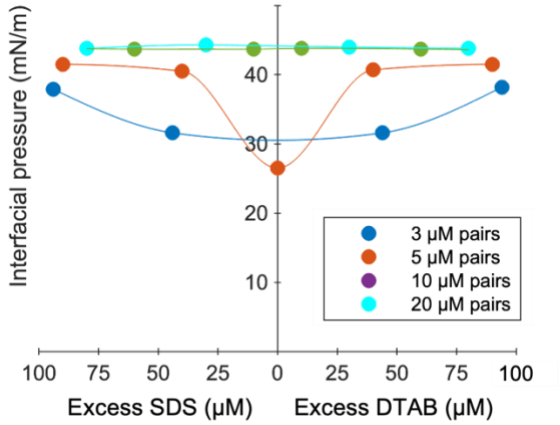


**Figure B.1.** Select interfacial pressure measurements in reference 43 reformatted so the paired surfactant concentration is fixed while the unpaired SDS/DTAB concentration is varied

### Critical micelle concentration of equimolar SDS:DAC mixture

Figure S2 shows the equimolar SDS:DAC mixtures interfacial pressure isotherm. The critical micelle concentration (CMC) is identified as the intersection of linear regressions (black lines) fitted to the isotherm before and after the inflection point.

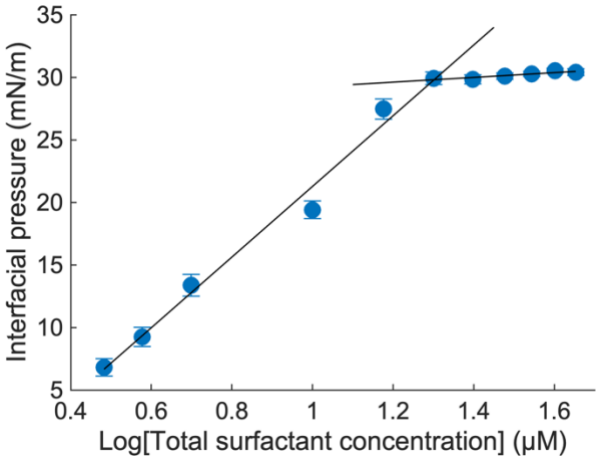


**Figure B.2.** Interfacial pressure isotherm for equimolar SDS:DAC mixtures.

**Table B.1.** Peak assignments for VSF spectra of d-SDS:h-DTAB pair mixtures at the $H_2O$-$CCl_4$ interface (Figure 5.4).

| Peak assignment | Frequency ($cm^{-1}$) |
|---|---|
| $CH_2$ symmetric stretch ($d^+$) | 2853 |
| $CH_3$ symmetric stretch ($r^+$) | 2871 |
| $CH_2$ fermi resonance ($d^+_{FR}$) | 2917 |
| $CH_3$ fermi resonance ($d^+_{FR}$) | 2933 |
| Coordinated water O-H stretch | ~3200 |
| Coordinated water O-H stretch | ~3400 |
| N-$CH_3$ symmetric stretch | 2980 |
| N-$CH_3$ asymmetric stretch | 3040 |
| Water located between surfactant tails O-H stretch | ~2700 |
| Free OH | 3680 |
| Unassigned $H_2O$ feature | ~2750 |

**Table B.2.** Peak assignments for VSF spectra of d-SDS:$d_9$-DTAB (DTAB tail) and h-SDS:d-DTAB (SDS tail) pair mixtures at the $CCl_4$-$D_2O$ interface in Figures 5.7a and 5.7b, respectively.

| Peak assignment | Frequency ($cm^{-1}$) |
|---|---|
| $CH_2$ symmetric stretch ($d^+$) | 2853 |
| $CH_3$ symmetric stretch ($r^+$) | 2871 |
| $CH_2$ asymmetric stretch ($d^-$) | 2886 |
| $CH_2$ fermi resonance ($d^+_{FR}$) | 2917 |
| $CH_3$ fermi resonance ($r^+_{FR}$) | 2933 |
| $D_2O$ combination band | 2838 |

**Table B.3.** Fit parameters for 1.5 µM d-SDS:h-DTAB pair mixtures at the $H_2O$-$CCl_4$ interface, used to calculate the coordinated water integrated areas reported in Figure 5.5.

| Peak Assignment | Parameter | 12 µM SDS excess | 2 µM SDS excess | No excess | 2 µM DTAB excess | 12 µM DTAB excess | 100 µM DTAB excess | 200 µM DTAB excess |
|---|---|---|---|---|---|---|---|---|
| $CH_2$ s.s. | Amplitude | 0.79 ± 0.02 | 0.78 ± 0.03 | 0.30 ± 0.01 | 0.81 ± 0.05 | | 1.04 ± 0.02 | 1.10 ± 0.04 |
| | Phase | 0 | 0 | 0 | 0 | | 0 | 0 |
| | Lorentzian | 2 | 2 | 2 | 2 | | 2 | 2 |
| | Frequency | 2852.5 ± 0.5 | 2853.5 ± 0.3 | 2847.3 ± 0.3 | 2849 ± 0.5 | | 2856.1 ± 0.3 | 2855.8 ± 0.4 |
| | Gaussian | 9.7 ± 0.7 | 9.5 ± 0.2 | 9.2 ± 0.5 | 8.1 ± 0.6 | | 11.7 ± 0.4 | 10.5 ± 0.6 |
| $CH_3$ s.s. | Amplitude | 0.991 ± 0.04 | 0.95 ± 0.03 | 0.21 ± 0.04 | 0.75 ± 0.02 | | 1.50 ± 0.06 | 1.81 ± 0.06 |
| | Phase | 0 | 0 | 0 | 0 | | 0 | 0 |
| | Lorentzian | 2 | 2 | 2 | 2 | | 2 | 2 |

| | | | | | | | | |
|---|---|---|---|---|---|---|---|---|
| | Frequency | 2872.1 ± 0.2 | 2871.7 ± 0.1 | 2869.9 ± 0.6 | 2868.7 ± 0.7 | | 2870.4 ± 0.2 | 2871.1 ± 0.4 |
| | Gaussian | 4.8 ± 0.4 | 4.4 ± 0.2 | 3.0 ± 0.8 | 12 ± 1 | | 4.0 ± 0.2 | 5.1838 ± 0.4 |
| $CH_{2\ F.R.}$ | Amplitude | 0.97 ± 0.08 | 0.42 ± 0.03 | 0.46 ± 0.06 | 0.53 ± 0.06 | | 0.37 ± 0.02 | 0.44 ± 0.03 |
| | Phase | 3.14 | 3.14 | 3.14 | 3.14 | | 3.14 | 3.14 |
| | Lorentzian | 2 | 2 | 2 | 2 | | 2 | 2 |
| | Frequency | 2915± 1 | 2908.3 ± 0.9 | 2913 ± 12 | 2907 ± 2 | | 2905 ± 1 | 2905 ± 2 |
| | Gaussian | 4.1± 0.6 | 6.7 ± 0.6 | 4.4 ± 0.9 | 8 ± 2 | | 17 ± 1 | 20 ± 2 |
| $CH_{3\ F.R.}$ | Amplitude | 1.35 ± 0.02 | 0.85 ± 0.02 | 0.37 ± 0.02 | 0.78 ± 0.04 | | 0.89 ± 0.06 | 0.72 ± 0.06 |
| | Phase | 0 | 0 | 0 | 0 | | 0 | 0 |
| | Lorentzian | 2 | 2 | 2 | 2 | | 2 | 2 |
| | Frequency | 2934.7 ± 0.5 | 2936.8 ± 0.4 | 2933.2 ± 0.8 | 2936 ± 1 | | 2938.5 ± 0.4 | 2938.0 ± 0.4 |
| | Gaussian | 10.4 ± 0.3 | 9.8 ± 0.3 | 8.6 ± 0.7 | 8.8 ± 0.9 | | 6.0 ± 0.4 | 6.4 ± 0.7 |
| Coordinated water O-H stretch | Amplitude | 0.78 ± 0.01 | 0.22 ± 0.01 | 0.098 ± 0.006 | 0.10 ± 0.05 | 0.102 ± 0.003 | 0.20 ± 0.04 | 0.29 ± 0.09 |
| | Phase | 3.14 | 3.14 | 0 | 0 | 0 | 0 | 0 |
| | Lorentzian | 5 | 5 | 5 | 5 | 5 | 5 | 5 |
| | Frequency | 3198 ± 3 | 3223 ± 24 | 3175 ± 23 | 3277 ± 71 | 3266 ± 7 | 3226 ± 8 | 3222 ± 8 |
| | Gaussian | 142 ± 6 | 155 ± 16 | 130 ± 49 | 67 ± 111 | 107 ± 9 | 77 ± 12 | 86 ± 13 |
| Coordinated water O-H stretch | Amplitude | 0.24 ± 0.03 | 0.06 ± 0.03 | 0.04 ± 0.03 | 0.10 ± 0.09 | 0.06 ± 0.01 | 0.23 ± 0.01 | 0.35 ± 0.01 |
| | Phase | 3.14 | 3.14 | 0 | 0 | 0 | 0 | 0 |
| | Lorentzian | 5 | 5 | 5 | 5 | 5 | 5 | 5 |
| | Frequency | 3388 ± 8 | 3405 ± 23 | 3345 ± 37 | 3386 ± 58 | 3379 ± 3 | 3424 ± 13 | 3401 ± 19 |
| | Gaussian | 104 ± 10 | 66 ± 29 | 77 ± 45 | 52 ± 85 | 59 ± 6 | 153 ± 36 | 155 ± 38 |
| $N\text{-}CH_{3\ S.S.}$ | Amplitude | 0.20 ± 0.02 | 0.13 ± 0.01 | 0.08 ± 0.02 | 0.11 ± 0.08 | | 0.07 ± 0.03 | 0.01 ± 0.09 |
| | Phase | 0 | 0 | 0 | 0 | | 0 | 0 |
| | Lorentzian | 2 | 2 | 2 | 2 | | 2 | 2 |
| | Frequency | 2978 ± 1 | 2982 ± 2 | 2984 ± 5 | 2977 ± 17 | | 2979 ± 8 | 2984 ± 31 |
| | Gaussian | 20 ± 3 | 20 ± 3 | 18 ± 8 | 17 ± 28 | | 20 ± 14 | 5 ± 54 |

| | | | | | | | | |
|---|---|---|---|---|---|---|---|---|
| N-$CH_3$ A.S. | Amplitude | | 0.06 ± 0.05 | 0.04 ± 0.02 | | | 0.05 ± 0.02 | 0.12 ± 0.02 |
| | Phase | | 0 | 0 | | | 3.14 | 3.14 |
| | Lorentzian | | 2 | 2 | | | 2 | 2 |
| | Frequency | | 3030 ± 2 | 3031 ± 12 | | | 3051 ± 7 | 3044 ± 3 |
| | Gaussian | | 4 ± 5 | 20 ± 21 | | | 20 ± 12 | 20 ± 6 |
| Water located between surfactant tails | Amplitude | | 0.08 ± 0.05 | | | | | |
| | Phase | | 3.14 | | | | | |
| | Lorentzian | | 5 | | | | | |
| | Frequency | | 3576 ± 32 | | | | | |
| | Gaussian | | 81.463 ± 39 | | | | | |
| Free OH | Amplitude | | 0.2 ± 0.2 | 0.51 ± 0.09 | | | | |
| | Phase | | 3.14 | 3.14 | | | | |
| | Lorentzian | | 12 | 12 | | | | |
| | Frequency | | 3685 ± 74 | 3686 ± 1 | | | | |
| | Gaussian | | 17 ± 50 | 10 ± 2 | | | | |
| Unassigned $H_2O$ feature | Amplitude | | 0.214 ± 0.006 | 0.172 ± 0.004 | 0.39 ± 0.01 | | 0.546 ± 0.004 | 0.774 ± 0.005 |
| | Phase | | 3.14 | 0 | 3.14 | | 3.14 | 3.14 |
| | Lorentzian | | 5 | 5 | 5 | | 5 | 5 |
| | Frequency | | 2721 ± 15 | 2816 ± 5 | 2658 ± 7 | | 2698 ± 4 | 2685 ± 3 |
| | Gaussian | | 107 ± 14 | 97 ± 9 | 103 ± 9 | | 209 ± 8 | 215 ± 6 |
| Nonresonant | Amplitude | 0 | 0 | 0 | 0 | 0 | 0 | 0 |
| | Phase | 0 | 0 | 0 | 0 | 0 | 0 | 0 |

**Table B.4.** Fit parameters for 2.5 μM d-SDS:h-DTAB pair mixtures at the $H_2O$-$CCl_4$ interface, used to calculate the coordinated water integrated areas reported in Figure 5.5.

| Peak Assignment | Parameter | 12 μM SDS excess | Equimolar | 12 μM DTAB excess |
|---|---|---|---|---|
| $CH_2$ S.S. | Amplitude | 0.80 ± 0.06 | 0.748 ± 0.008 | |
| | Phase | 0 | 0 | |
| | Lorentzian | 2 | 2 | |
| | Frequency | 2850 ± 1 | 2849.5 ± 0.4 | |
| | Gaussian | 10 ± 2 | 13 ± 0 | |

| | | | | |
|---|---|---|---|---|
| $CH_{3\ S.S.}$ | Amplitude | 0.84 ± 0.08 | 0.78 ± 0.02 | |
| | Phase | 0 | 0 | |
| | Lorentzian | 2 | 2 | |
| | Frequency | 2868.3 ± 0.7 | 2871.0 ± 0.2 | |
| | Gaussian | 6 ± 1 | 4 ± 0 | |
| $CH_{2\ F.R.}$ | Amplitude | 0.7 ± 0.1 | 0.55 ± 0.06 | |
| | Phase | 3.14 | 3.14 | |
| | Lorentzian | 2 | 2 | |
| | Frequency | 2911 ± 4 | 2919 ± 3 | |
| | Gaussian | 8 ± 3 | 9 ± 0 | |
| $CH_{3\ F.R.}$ | Amplitude | 1.4 ± 0.07 | 1.15 ± 0.04 | |
| | Phase | 0 | 0 | |
| | Lorentzian | 2 | 2 | |
| | Frequency | 2934 ± 1 | 2936.4 ± 0.4 | |
| | Gaussian | 10 ± 0.5 | 8 ± 0 | |
| Coordinated water O-H stretch | Amplitude | 0.79 ± 0.02 | 0.327 ± 0.006 | 0.172 ± 0.001 |
| | Phase | 3.14 | 3.14 | 0 |
| | Lorentzian | 5 | 5 | 5 |
| | Frequency | 3207 ± 8 | 3229 ± 8 | 3246 ± 2 |
| | Gaussian | 172 ± 14 | 145 ± 12 | 123 ± 4 |
| Coordinated water O-H stretch | Amplitude | 0.10 ± 0.06 | 0.056 ± 0.03 | 0.067 ± 0.007 |
| | Phase | 3.14 | 3.14 | 0 |
| | Lorentzian | 5 | 5 | 5 |
| | Frequency | 3428 ± 36 | 3372 ± 14 | 3373 ± 2 |
| | Gaussian | 111 ± 52 | 53 ± 29 | 57 ± 4 |
| $N\text{-}CH_{3\ S.S.}$ | Amplitude | 0.12 ± 0.04 | 0.14 ± 0.02 | |
| | Phase | 0 | 0 | |
| | Lorentzian | 2 | 2 | |
| | Frequency | 2980 ± 4 | 2982 ± 2 | |
| | Gaussian | 20 ± 10 | 15 ± 4 | |
| $N\text{-}CH_{3\ A.S.}$ | Amplitude | 0.1± 0.1 | | |
| | Phase | 3.14 | | |
| | Lorentzian | 2 | | |
| | Frequency | 3040 ± 3 | | |
| | Gaussian | 4 ± 7 | | |
| Nonresonant | Amplitude | 0 | 0 | 0 |
| | Phase | 0 | 0 | 0 |

**Table B.5.** Fit parameters for 7.5 μM d-SDS:h-DTAB pair mixtures at the $H_2O$-$CCl_4$ interface, used to calculate the coordinated water integrated areas reported in Figure 5.5.

| Peak Assignment | Parameter | 12 μM SDS excess | Equimolar | 12 μM DTAB excess |
|---|---|---|---|---|

| | | | | |
|---|---|---|---|---|
| $CH_{2\ S.S.}$ | Amplitude | 0.62 ± 0.01 | 0.58 ± 0.01 | 0.60 ± 0.02 |
| | Phase | 0 | 0 | 0 |
| | Lorentzian | 2 | 2 | 2 |
| | Frequency | 2852.6 ± 0.2 | 2850.7 ± 0.3 | 2852.8 ± 0.4 |
| | Gaussian | 10.7 ± 0.4 | 12.3 ± 0.5 | 10.4 ± 0.3 |
| $CH_{3\ S.S.}$ | Amplitude | 0.97 ± 0.02 | 0.84 ± 0.03 | 0.92 ± 0.03 |
| | Phase | 0 | 0 | 0 |
| | Lorentzian | 2 | 2 | 2 |
| | Frequency | 2872.6 ± 0.1 | 2871.0 ± 0.1 | 2871.3 ± 0.1 |
| | Gaussian | 4.9 ± 0.2 | 4.3 ± 0.3 | 4.6 ± 0.1 |
| $CH_{2\ F.R.}$ | Amplitude | 0.86 ± 0.07 | 0.54 ± 0.05 | 0.46 ± 0.03 |
| | Phase | 3.14 | 3.14 | 3.14 |
| | Lorentzian | 2 | 2 | 2 |
| | Frequency | 2916.7 ± 0.4 | 2911.7 ± 0.7 | 2910.8 ± 0.5 |
| | Gaussian | 3.0 ± 0.4 | 4.4 ± 0.6 | 5.6 ± 0.5 |
| $CH_{3\ F.R.}$ | Amplitude | 1.133 ± 0.009 | 0.94 ± 0.01 | 0.97 ± 0.02 |
| | Phase | 0 | 0 | 0 |
| | Lorentzian | 2 | 2 | 2 |
| | Frequency | 2936.0 ± 0.2 | 2935.7 ± 0.3 | 2935.9 ± 0.1 |
| | Gaussian | 9.2 ± 0.2 | 8.9 ± 0.2 | 8.4 ± 0.1 |
| Coordinated water O-H stretch | Amplitude | 0.479 ± 0.006 | 0.2 ± 0.1 | 0.20 ± 0.03 |
| | Phase | 3.14 | 3.14 | 3.14 |
| | Lorentzian | 5 | 5 | 5 |
| | Frequency | 3194 ± 4 | 3204 ± 11 | 3193 ± 18 |
| | Gaussian | 128 ± 5 | 83 ± 15 | 120 ± 18 |
| Coordinated water O-H stretch | Amplitude | 0.22 ± 0.01 | 0.22 ± 0.03 | 0.14 ± 0.02 |
| | Phase | 3.14 | 3.14 | 3.14 |
| | Lorentzian | 5 | 5 | 5 |
| | Frequency | 3394 ± 6 | 3332 ± 35 | 3383 ± 24 |
| | Gaussian | 106 ± 10 | 129 ± 33 | 122 ± 33 |
| $N\text{-}CH_{3\ S.S.}$ | Amplitude | 0.06 ± 0.01 | 0.11 ± 0.01 | 0.05 ± 0.01 |
| | Phase | 0 | 0 | 0 |
| | Lorentzian | 2 | 2 | 2 |
| | Frequency | 2982 ± 2 | 2984 ± 3 | 2982.3 ± 2 |
| | Gaussian | 12 ± 3 | 20 ± 5 | 12 ± 4 |
| $N\text{-}CH_{3\ A.S.}$ | Amplitude | 0.073 ± 0.008 | 0.10 ± 0.01 | 0.06 ± 0.01 |
| | Phase | 3.14 | 0 | 3.14 |
| | Lorentzian | 2 | 2 | 2 |
| | Frequency | 3050 ± 2 | 3030 ± 3 | 3047 ± 2 |
| | Gaussian | 20 ± 3 | 20 ± 5 | 12 ± 4 |
| Water located between surfactant tails | Amplitude | 0.07 ± 0.01 | 0.06 ± 0.02 | 0.08 ± 0.01 |
| | Phase | 3.14 | 3.14 | 3.14 |
| | Lorentzian | 5 | 5 | 5 |
| | Frequency | 3558 ± 8 | 3565 ± 14 | 3578 ± 9 |

| | | | | |
|---|---|---|---|---|
| | Gaussian | 55 ± 12 | 43 ± 22 | 64 ± 16 |
| Unassigned $H_2O$ feature | Amplitude | | | 0.141 ± 0.005 |
| | Phase | | | 3.14 |
| | Lorentzian | | | 5 |
| | Frequency | | | 2726 ± 15 |
| | Gaussian | | | 115 ± 20 |
| Nonresonant | Amplitude | 0 | 0 | 0 |
| | Phase | 0 | 0 | 0 |

**Table B.6.** Fit parameters for 1.5 μM d-SDS:h-CTAB pair mixtures at the $H_2O$-$CCl_4$ interface, used to calculate the coordinated water integrated areas reported in Figure 5.6.

| Peak Assignment | Parameter | 12 μM SDS excess | 12 μM SDS excess | No excess | 2 μM DTAB excess | 12 μM DTAB excess |
|---|---|---|---|---|---|---|
| $CH_{2\ S.S.}$ | Amplitude | 0.68 ± 0.02 | 0.77 ± 0.01 | 1.25 ± 0.09 | 0.69 ± 0.03 | 0.70 ± 0.05 |
| | Phase | 0 | 0 | 0 | 0 | 0 |
| | Lorentzian | 2 | 2 | 2 | 2 | 2 |
| | Frequency | 2851.9 ± 0.5 | 2851.6 ± 0.3 | 2853.7 ± 0.3 | 2854.0 ± 0.4 | 2854 ± 0.6 |
| | Gaussian | 9.8 ± 0.6 | 10.5 ± 0.4 | 9.1 ± 0.4 | 7.7 ± 0.6 | 6.8 ± 0.9 |
| $CH_{3\ S.S.}$ | Amplitude | 0.75 ± 0.04 | 0.82 ± 0.03 | 1.12 ± 0.06 | 0.87 ± 0.08 | 0.69 ± 0.07 |
| | Phase | 0 | 0 | 0 | 0 | 0 |
| | Lorentzian | 2 | 2 | 2 | 2 | 2 |
| | Frequency | 2872.6 ± 0.3 | 2872.0 ± 0.2 | 2868.3 ± 0.7 | 2873.8 ± 0.4 | 2874.0 ± 0.7 |
| | Gaussian | 4.1 ± 0.4 | 4.5 ± 0.3 | 5.9 ± 0.5 | 5.5 ± 0.7 | 9 ± 1 |
| $CH_{2\ F.R.}$ | Amplitude | 0.71 ± 0.07 | 0.58 ± 0.05 | 0.44 ± 0.05 | 0.01 ± 0.35 | 0.01 ± 1.05 |
| | Phase | 3.14 | 3.14 | 3.14 | 3.14 | 3.14 |
| | Lorentzian | 2 | 2 | 2 | 2 | 2 |
| | Frequency | 2917 ± 2 | 2913 ± 1 | 2905 ± 2 | 2920 ± 38 | 2920 ± 67 |
| | Gaussian | 4.4 ± 0.8 | 5.0 ± 0.7 | 15 ± 2 | 3 ± 163 | 3 ± 376 |
| $CH_{3\ F.R.}$ | Amplitude | 1.01 ± 0.02 | 0.98 ± 0.01 | 0.80 ± 0.09 | 0.47 ± 0.05 | 0.61 ± 0.06 |
| | Phase | 0 | 0 | 0 | 0 | 0 |
| | Lorentzian | 2 | 2 | 2 | 2 | 2 |
| | Frequency | 2935.6 ± 0.5 | 2936.0 ± 0.4 | 2937.5 ± 0.9 | 2931 ± 2 | 2931 ± 2 |
| | Gaussian | 9.4 ± 0.4 | 9.5 ± 0.3 | 7.6 ± 0.6 | 15 ± 2 | 15 ± 2 |
| Coordinated water O-H stretch | Amplitude | 0.47 ± 0.01 | 0.2 ± 0.1 | 0.35 ± 0.04 | 0.627 ± 0.009 | 0.92 ± 0.02 |
| | Phase | 3.14 | 3.14 | 3.14 | 0 | 0 |

| | | | | | | |
|---|---|---|---|---|---|---|
| | Lorentzian | 5 | 5 | 5 | 5 | 5 |
| | Frequency | 3214 ± 7 | 3232 ± 16 | 3132 ± 17 | 3191 ± 8 | 3212 ± 6 |
| | Gaussian | 145 ± 10 | 95 ± 18 | 124 ± 21 | 179 ± 7 | 151 ± 8 |
| Coordinated water O-H stretch | Amplitude | 0.20 ± 0.03 | 0.25 ± 0.01 | 0.12 ± 0.03 | 0.10 ± 0.03 | 0.34 ± 0.05 |
| | Phase | 3.14 | 3.14 | 3.14 | 0 | 0 |
| | Lorentzian | 5 | 5 | 5 | 5 | 5 |
| | Frequency | 3425 ± 12 | 3412 ± 27 | 3372 ± 50 | 3444 ± 18 | 3424 ± 9 |
| | Gaussian | 106 ± 28 | 153 ± 91 | 183 ± 63 | 72 ± 28 | 99 ± 14 |
| $N\text{-}CH_3$ s.s. | Amplitude | 0.11 ± 0.02 | 0.14 ± 0.02 | 0.47 ± 0.05 | 0.05 ± 0.04 | 0.12 ± 0.04 |
| | Phase | 0 | 0 | 0 | 0 | 0 |
| | Lorentzian | 2 | 2 | 2 | 2 | 2 |
| | Frequency | 2983 ± 2 | 2984 ± 2 | 2975 ± 17 | 2977 ± 8 | 2984 ± 5 |
| | Gaussian | 20 ± 4 | 20 ± 4 | 20 ± 7 | 12 ± 13 | 20 ± 8 |
| $N\text{-}CH_3$ a.s. | Amplitude | 0.05 ± 0.03 | 0.07 ± 0.02 | 0.09 ± 0.07 | 0.01 ± 0.3 | 0.01 ± 0.20 |
| | Phase | 0 | 0 | 0 | 0 | 0 |
| | Lorentzian | 2 | 2 | 2 | 2 | 2 |
| | Frequency | 3030 ± 3 | 3030 ± 5 | 3030 ± 5 | 3050 ± 40 | 3046.3 ± 46 |
| | Gaussian | 7 ± 5 | 20 ± 8 | 20 ± 13 | 3 ± 97 | 3 ± 62 |
| Water located between surfactant tails | Amplitude | 0.12 ± 0.04 | 0.13 ± 0.08 | 0.09 ± 0.02 | | |
| | Phase | 3.14 | 3.14 | 3.14 | | |
| | Lorentzian | 5 | 5 | 5 | | |
| | Frequency | 3567 ± 15 | 3589 ± 11 | 3673 ± 12 | | |
| | Gaussian | 69 ± 21 | 65 ± 27 | 52 ± 18 | | |
| Free OH | Amplitude | | | 0.601 ± 0.004 | | |
| | Phase | | | 3.14 | | |
| | Lorentzian | | | 5 | | |
| | Frequency | | | 2733 ± 9 | | |
| | Gaussian | | | 16 ± 11 | | |
| Unassigned $H_2O$ feature | Amplitude | | | | 0.709 ± 0.007 | 0.90 ± 0.01 |
| | Phase | | | | 3.14 | 3.14 |
| | Lorentzian | | | | 5 | 5 |
| | Frequency | | | | 2618 ± 7 | 2639 ± 6 |
| | Gaussian | | | | 171 ± 14 | 177 ± 14 |
| Nonresonant | Amplitude | 0 | 0 | 0 | 0 | 0 |
| | Phase | 0 | 0 | 0 | 0 | 0 |

**Table B.7.** Fit parameters for 1.5 μM d-SDS:h-DAC pair mixtures at the $H_2O$-$CCl_4$ interface, used to calculate the coordinated water integrated areas reported in Figure 5.6.

| Peak Assignment | Parameter | 12 μM SDS excess | 6 μM SDS excess | No excess | 6 μM DTAB excess | 12 μM DTAB excess |
|---|---|---|---|---|---|---|
| $CH_2$ S.S. | Amplitude | 0.15048 ± 0.1 | 1.13 ± 0.03 | 0.16124 ± 0.04 | 0.72085 ± 0.06 | 0.72909 ± 0.01 |
| | Phase | 0 | 0 | 0 | 0 | 0 |
| | Lorentzian | 2 | 2 | 2 | 2 | 2 |
| | Frequency | 2852 ± 5 | 2853.3 ± 0.3 | 2854 ± 1 | 2852 ± 0.5 | 2851 ± 0.3 |
| | Gaussian | 7 ± 8 | 12.0 ± 0.3 | 7 ± 2 | 8.4 ± 0.5 | 10.4 ± 0.4 |
| $CH_3$ S.S. | Amplitude | 0.11 ± 0.09 | 1.00 ± 0.04 | 0.15 ± 0.02 | 0.69 ± 0.02 | 0.58 ± 0.02 |
| | Phase | 0 | 0 | 0 | 0 | 0 |
| | Lorentzian | 2 | 2 | 2 | 2 | 2 |
| | Frequency | 2867 ± 9 | 2869.5 ± 0.2 | 2870 ± 3 | 2868.8 ± 0.7 | 2869.0 ± 0.4 |
| | Gaussian | 10 ± 15 | 4.7 ± 0.3 | 9 ± 6 | 11 ± 2 | 6.7 ± 0.5 |
| $CH_2$ F.R. | Amplitude | 0.19 ± 0.05 | 0.69 ± 0.02 | 0.12 ± 0.02 | 0.56 ± 0.03 | 0.53 ± 0.01 |
| | Phase | 3.14 | 3.14 | 3.14 | 3.14 | 3.14 |
| | Lorentzian | 2 | 2 | 2 | 2 | 2 |
| | Frequency | 2918 ± 21 | 2905 ± 1 | 2899 ± 6 | 2905 ± 1 | 2905 ± 1 |
| | Gaussian | 20 ± 21 | 15 ± 0.9 | 18 ± 8 | 13 ± 1 | 15 ± 1 |
| $CH_3$ F.R. | Amplitude | 0.5 ± 0.4 | 1.13 ± 0.06 | 0.38 ± 0.06 | 0.83 ± 0.05 | 0.9 ± 0.1 |
| | Phase | 0 | 0 | 0 | 0 | 0 |
| | Lorentzian | 2 | 2 | 2 | 2 | 2 |
| | Frequency | 2939 ± 6 | 2935.6 ± 0.4 | 2939 ± 2 | 2935.7 ± 0.6 | 2934.6 ± 0.7 |
| | Gaussian | 6 ± 2 | 5.9 ± 0.4 | 8.1 ± 0.9 | 6.4 ± 0.4 | 5.3 ± 0.4 |
| N-$CH_3$ A.S. | Amplitude | 0.28 ± 0.05 | 0.34 ± 0.03 | 0.212 ± 0.008 | 0.29 ± 0.02 | 0.24 ± 0.01 |
| | Phase | 3.14 | 3.14 | 3.14 | 3.14 | 3.14 |
| | Lorentzian | 2 | 2 | 2 | 2 | 2 |
| | Frequency | 2965 ± 4 | 2962 ± 3 | 2960 ± 3 | 2962 ± 3 | 2953 ± 5 |
| | Gaussian | 20 ± 3 | 13 ± 3 | 20 ± 3 | 13 ± 3 | 18 ± 4 |
| $NH_3^+$ S.S. | Amplitude | 0.26 ± 0.01 | 0.27 ± 0.02 | 0.15 ± 0.01 | 0.02 ± 0.04 | 0.08 ± 0.02 |
| | Phase | 0 | 0 | 0 | 0 | 0 |
| | Lorentzian | 2 | 2 | 2 | 2 | 2 |
| | Frequency | 3096 ± 1 | 3100 ± 19 | 3090 ± 2 | 3156 ± 51 | 3131 ± 7 |
| | Gaussian | 100 ± 3 | 45 ± 10 | 97 ± 3 | 25 ± 79 | 35 ± 11 |
| Coordinated water O-H stretch | Amplitude | 0.06 ± 0.05 | 0.14 ± 0.06 | 0.149 ± 0.007 | 0.05 ± 0.03 | 0.13 ± 0.01 |
| | Phase | 3.14 | 3.14 | 0 | 0 | 0 |
| | Lorentzian | 5 | 5 | 5 | 5 | 5 |

| | | | | | | |
|---|---|---|---|---|---|---|
| | Frequency | 3275 ± 10 | 3250 ± 37 | 3197 ± 4 | 3297 ± 25 | 3262 ± 15 |
| | Gaussian | 65 ± 29 | 83 ± 44 | 77 ± 8 | 47 ± 39 | 101 ± 36 |
| Coordinated water O-H stretch | Amplitude | 0.15 ± 0.02 | 0.16 ± 0.01 | 0.03 ± 0.01 | 0.15 ± 0.01 | 0.12 ± 0.02 |
| | Phase | 3.14 | 3.14 | 0 | 0 | 0 |
| | Lorentzian | 5 | 5 | 5 | 5 | 5 |
| | Frequency | 3390 ± 49 | 3490 ± 22 | 3297 ± 13 | 3450 ± 23 | 3450 ± 18 |
| | Gaussian | 160 ± 50 | 189 ± 74 | 47 ± 16 | 82 ± 23 | 90 ± 28 |
| Dangling O-H Stretch | Amplitude | 0.28 ± 0.01 | 0.17 ± 0.04 | 0.220 ± 0.005 | 0.25 ± 0.01 | 0.24 ± 0.01 |
| | Phase | 3.14 | 3.14 | 3.14 | 3.14 | 3.14 |
| | Lorentzian | 12 | 12 | 12 | 12 | 12 |
| | Frequency | 3692 ± 3 | 3687 ± 7 | 3719 ± 2 | 3700 ± 10 | 3726 ± 6 |
| | Gaussian | 62 ± 3 | 46 ± 13 | 52 ± 2 | 68 ± 11 | 56 ± 8 |
| Unassigned $H_2O$ feature | Amplitude | | 0.603 ± 0.004 | | 0.446 ± 0.004 | 0.392 ± 0.003 |
| | Phase | | 3.14 | | 3.14 | 3.14 |
| | Lorentzian | | 5 | | 5 | 5 ± 0 |
| | Frequency | | 2709 ± 4 | | 2698 ± 4 | 2685 ± 3 |
| | Gaussian | | 126 ± 4 | | 131 ± 5 | 118 ± 4 |
| Nonresonant | Amplitude | 0 | 0 | 0 | 0 | 0 |
| | Phase | 0 | 0 | 0 | 0 | 0 |

**Table B.8.** Fit parameters for 3 μM d-SDS:$d_9$-DTAB mixture at the $CCl_4$-$D_2O$ interface, used obtain the $A_{r+}/A_{d+}$ ratios in Figure 5.7a.

| Peak Assignment | Parameter | |
|---|---|---|
| $CH_2$ S.S. | Amplitude | 0.280 ± 0.007 |
| | Phase | 0 |
| | Lorentzian | 2 |
| | Peak Position | 2852.9 ± 0.6 |
| | Gaussian | 9.4 ± 0.4 |
| $CH_3$ S.S. | Amplitude | 0.26 ± 0.02 |
| | Phase | 0 |
| | Lorentzian | 2 |
| | Peak Position | 2869.5 ± 0.4 |
| | Gaussian | 4.4 ± 0.4 |
| $CH_2$ A.S. | Amplitude | 0.17 ± 0.02 |
| | Phase | 3.14 |
| | Lorentzian | 2 |
| | Peak Position | 2894 ± 2 |
| | Gaussian | 8 ± 1 |
| $CH_2$ F.R. | Amplitude | 0.16 ± 0.03 |
| | Phase | 0 |
| | Lorentzian | 2 |

| | | |
|---|---|---|
| | Peak Position | 2922 ± 4 |
| | Gaussian | 11 ± 5 |
| $CH_{3\ F.R.}$ | Amplitude | 0.2 ± 0.1 |
| | Phase | 0 |
| | Lorentzian | 2 |
| | Peak Position | 2931.4 ± 0.7 |
| | Gaussian | 5 ± 2 |
| $D_2O$ combination band | Amplitude | 0.153 ± 0.004 |
| | Phase | 3.14 |
| | Lorentzian | 5 |
| | Peak Position | 2791 ± 4 |
| | Gaussian | 45 ± 5 |
| Nonresonant | Amplitude | 0 |
| | Phase | 0 |

**Table B.9.** Fit parameters for 5 μM d-SDS:$d_9$-DTAB mixtures at the $CCl_4$-$D_2O$ interface, used obtain the $A_{r+}/A_{d+}$ ratios in Figure 5.7a.

| SDS:DTAB ratio | | 1:9 | 3:7 | 5:5 | 7:3 | 9:1 |
|---|---|---|---|---|---|---|
| 1:1 stoichiometric pairs + excess | | 0.5 μM pairs + 4 μM SDS | 1.5 μM pairs + 2 μM SDS | 2.5 μM pairs | 1.5 μM pairs + 2 μM DTAB | 0.5 μM pairs + 4 μM DTAB |
| Peak Assignment | Parameter | | | | | |
| $CH_{2\ S.S.}$ | Amplitude | 0.28 ± 0.01 | 0.57 ± 0.02 | 0.66 ± 0.02 | 0.66 ± 0.02 | 0.19 ± 0.04 |
| | Phase | 0 | 0 | 0 | 0 | 0 |
| | Lorentzian | 2 | 2 | 2 | 2 | 2 |
| | Peak Position | 2853.8 ± 0.3 | 2853.8 ± 0.3 | 2853.8 ± 0.3 | 2853.8 ± 0.3 | 2853.8 ± 0.3 |
| | Gaussian | 9.8 ± 0.2 | 9.8 ± 0.2 | 9.8 ± 0.2 | 9.8 ± 0.2 | 9.8 ± 0.2 |
| $CH_{3\ S.S.}$ | Amplitude | 0.33 ± 0.02 | 0.67± 0.03 | 0.77 ± 0.03 | 0.75 ± 0.03 | 0.18 ± 0.06 |
| | Phase | 0 | 0 | 0 | 0 | 0 |
| | Lorentzian | 2 | 2 | 2 | 2 | 2 |
| | Peak Position | 2870.6 ± 0.2 | 2870.6 ± 0.2 | 2870.6 ± 0.2 | 2870.6 ± 0.2 | 2870.6 ± 0.2 |
| | Gaussian | 5.0 ± 0.2 | 5.0 ± 0.2 | 5.0 ± 0.2 | 5.0 ± 0.2 | 5.0 ± 0.2 |
| $CH_{2\ A.S.}$ | Amplitude | 0.28 ± 0.02 | 0.24 ± 0.04 | 0.17 ± 0.04 | 0.15 ± 0.04 | 0.14 ± 0.06 |
| | Phase | 3.14 | 3.14 | 3.14 | 3.14 | 3.14 |
| | Lorentzian | 2 | 2 | 2 | 2 | 2 |
| | Peak Position | 2892 ± 1.0 | 2892 ± 1.0 | 2892 ± 1.0 | 2892 ± 1. | 2892 ± 1.0 |

| | | | | | | |
|---|---|---|---|---|---|---|
| | Gaussian | 6.1 ± 0.7 | 6.1 ± 0.7 | 6.1 ± 0.7 | 6.1 ± 0.7 | 6.1 ± 0.7 |
| $CH_{2\ F.R.}$ | Amplitude | 0.25 ± 0.02 | 0.35 ± 0.03 | 0.38 ± 0.04 | 0.37 ± 0.04 | 0.12 ± 0.03 |
| | Phase | 0 | 0 | 0 | 0 | 0 |
| | Lorentzian | 2 | 2 | 2 | 2 | 2 |
| | Peak Position | 2921 ± 2 | 2921 ± 2 | 2921 ± 2 | 2921 ± 2 | 2921 ± 2 |
| | Gaussian | 13 ± 2 | 13 ± 2 | 13 ± 2 | 13 ± 2 | 13 ± 2 |
| $CH_{3\ F.R.}$ | Amplitude | 0.03 ± 0.06 | 0.35 ± 0.08 | 0.47 ± 0.09 | 0.50 ± 0.09 | 0.19 ± 0.05 |
| | Phase | 0 | 0 | 0 | 0 | 0 |
| | Lorentzian | 2 | 2 | 2 | 2 | 2 |
| | Peak Position | 2933.3 ± 0.3 | 2933.3 ± 0.3 | 2933.3 ± 0.3 | 2933.3 ± 0.3 | 2933.3 ± 0.3 |
| | Gaussian | 7.2 ± 0.6 | 7.2 ± 0.6 | 7.2 ± 0.6 | 7.2 ± 0.6 | 7.2 ± 0.6 |
| $D_2O$ combination band | Amplitude | 0.22 ± 0.01 | 0.20 ± 0.01 | 0.20 ± 0.02 | 0.19 ± 0.02 | 0.05 ± 0.03 |
| | Phase | 3.14 | 3.14 | 3.14 | 3.14 | 3.14 |
| | Lorentzian | 5 | 5 | 5 | 5 | 5 |
| | Peak Position | 2790 ± 4 | 2777 ± 16 | 2801 ± 13 | 2814 ± 11 | 2781 ± 116 |
| | Gaussian | 41 ± 6 | 104 ± 29 | 116 ± 22 | 110 ± 18 | 99 ± 195 |
| Nonresonant | Amplitude | 0 | 0 | 0 | 0 | 0 |
| | Phase | 0 | 0 | 0 | 0 | 0 |

**Table B.10.** Fit parameters for 15 μM d-SDS:$d_9$-DTAB pair mixtures at the $CCl_4$-$D_2O$ interface, used obtain the $A_{r+}/A_{d+}$ ratios in Figure 5.7a.

| SDS:DTAB ratio | | 9:1 | 7:3 | 6:4 | 5:5 | 4:6 | 3:7 | 1:9 |
|---|---|---|---|---|---|---|---|---|
| 1:1 stoichiometric pairs + excess | | 1.5 μM pairs + 12 μM SDS | 4.5 μM pairs + 6 μM SDS | 0.5 μM pairs + 3 μM SDS | 7.5 μM pairs | 0.5 μM pairs + 3 μM DTAB | 4.5 μM pairs + 6 μM DTAB | 1.5 μM pairs + 12 μM DTAB |
| $CH_{2\ S.S.}$ | Amplitude | 0.57 ± 0.03 | 0.86 ± 0.03 | 0.64 ± 0.02 | 0.81 ± 0.03 | 0.71 ± 0.03 | 0.78 ± 0.03 | 0.68 ± 0.04 |
| | Phase | 0 | 0 | 0 | 0 | 0 | 0 | 0 |
| | Lorentzian | 2 | 2 | 2 | 2 | 2 | 2 | 2 |
| | Peak Position | 2853.1 ± 0.3 | 2853.0 ± 0.3 | 2853.1 ± 0.3 | 2853 .1 ± 0.3 | 2853.1 ± 0.3 | 2853.1 ± 0.3 | 2853.1 ± 0.3 |
| | Gaussian | 10.1 ± 0.2 | 10.1 ± 0.2 | 10.1 ± 0.2 | 10.1 ± 0.2 | 10.1 ± 0.2 | 10.1 ± 0.2 | 10.1 ± 0.2 |

| | | | | | | | | |
|---|---|---|---|---|---|---|---|---|
| $CH_{3\ S.S.}$ | Amplitude | 0.70 ± 0.05 | 1.19 ± 0.05 | 0.90 ± 0.04 | 1.32 ± 0.05 | 1.07 ± 0.05 | 1.11 ± 0.06 | 0.89 ± 0.05 |
| | Phase | 0 | 0 | 0 | 0 | 0 | 0 | 0 |
| | Lorentzian | 2 | 2 | 2 | 2 | 2 | 2 | 2 |
| | Peak Position | 2870.8 ± 0.1 | 2870.8 ± 0.1 | 2870.8 ± 0.1 | 2870 .8 ± 0.1 | 2870.8 ± 0.1 | 2870.8 ± 0.1 | 2870.8 ± 0.1 |
| | Gaussian | 4.9 ± 0.1 | 4.9 ± 0.1 | 4.9 ± 0.1 | 4.9 ± 0.1 | 4.9 ± 0.1 | 4.9 ± 0.1 | 4.9 ± 0.1 |
| $CH_{2\ A.S.}$ | Amplitude | 0.33 ± 0.07 | 0.42 ± 0.08 | 0.38 ± 0.05 | 0.36 ± 0.08 | 0.29 ± 0.06 | 0.32 ± 0.08 | 0.25 ± 0.08 |
| | Phase | 3.14 | 3.14 | 3.14 | 3.14 | 3.14 | 3.14 | 3.14 |
| | Lorentzian | 2 | 2 | 2 | 2 | 2 | 2 | 2 |
| | Peak Position | 2894 ± 1 | 2894 ± 1 | 2894 ± 1 | 2894 ± 1 | 2894 ± 1 | 2894 ± 1 | 2894 ± 1 |
| | Gaussian | 4.9 ± 0.7 | 4.9 ± 0.7 | 4.9 ± 0.7 | 4.9 ± 0.7 | 4.9 ± 0.7 | 4.9 ± 0.7 | 4.9 ± 0.7 |
| $CH_{2\ F.R.}$ | Amplitude | 0.34 ± 0.03 | 0.49 ± 0.04 | 0.38 ± 0.03 | 0.49 ± 0.06 | 0.41 ± 0.05 | 0.43 ± 0.05 | 0.38 ± 0.06 |
| | Phase | 0 | 0 | 0 | 0 | 0 | 0 | 0 |
| | Lorentzian | 2 | 2 | 2 | 2 | 2 | 2 | 2 |
| | Peak Position | 2921 ± 2 | 2921 ± 2 | 2921 ± 2 | 2921 ± 2 | 2921 ± 2 | 2921 ± 2 | 2921 ± 2 |
| | Gaussian | 14 ± 2 | 14 ± 2 | 14 ± 2 | 14 ± 2 | 14 ± 2 | 14 ± 2 | 14 ± 2 |
| $CH_{3\ F.R.}$ | Amplitude | 0.4 ± 0.1 | 0.8 ± 0.1 | 0.59 ± 0.09 | 0.8 ± 0.1 | 0.7 ± 0.1 | 0.7 ± 0.1 | 0.61 ± 0.09 |
| | Phase | 0 | 0 | 0 | 0 | 0 | 0 | 0 |
| | Lorentzian | 2 | 2 | 2 | 2 | 2 | 2 | 2 |
| | Peak Position | 2933.9 ± 0.2 | 2933.9 ± 0.2 | 2933.9 ± 0.2 | 2933 .9 ± 0.2 | 2933.9 ± 0.2 | 2933.9 ± 0.2 | 2933.9 ± 0.2 |
| | Gaussian | 7.0 ± 0.5 | 7.0 ± 0.5 | 7.0 ± 0.5 | 7.0 ± 0.5 | 7.0 ± 0.5 | 7.0 ± 0.5 | 7.0 ± 0.5 |
| $D_2O$ combination band | Amplitude | 0.21 ± 0.02 | 0.24 ± 0.03 | 0.20 ± 0.02 | 0.25 ± 0.03 | 0.18 ± 0.03 | 0.21 ± 0.03 | 0.17± 0.03 |
| | Phase | 3.14 | 3.14 | 3.14 | 3.14 | 3.14 | 3.14 | 3.14 |
| | Lorentzian | 5 | 5 | 5 | 5 | 5 | 5 | 5 |
| | Peak Position | 2707 ± 110 | 2776 ± 21 | 2778 ± 17 | 2797 ± 16 | 2764 ± 54 | 2788 ± 22 | 2806 ± 21 |

| | | | | | | | | |
|---|---|---|---|---|---|---|---|---|
| | Gaussian | 150 ± 112 | 106 ± 36 | 69 ± 24 | 107 ± 30 | 153 ± 88 | 110 ± 45 | 106 ± 45 |
| Nonresonant | Amplitude | 0 | 0 | 0 | 0 | 0 | 0 | 0 |
| | Phase | 0 | 0 | 0 | 0 | 0 | 0 | 0 |

**Table B.11.** Fit parameters for 25 μM d-SDS:$d_9$-DTAB mixtures at the $CCl_4$-$D_2O$ interface, used obtain the $A_{r+}/A_{d+}$ ratios in Figure 5.7a.

| SDS:DTAB ratio | | 1:9 | 3:7 | 5:5 | 7:3 | 9:1 |
|---|---|---|---|---|---|---|
| 1:1 stoichiometric pairs + excess | | 2.5 μM pairs + 20 μM SDS | 7.5 μM pairs + 10 μM SDS | 12.5 μM pairs | 7.5 μM pairs + 10 μM DTAB | 2.5 μM pairs + 20 μM DTAB |
| Peak Assignment | Parameter | | | | | |
| $CH_2$ S.S. | Amplitude | 0.76 ± 0.03 | 0.83 ± 0.03 | 0.78 ± 0.03 | 0.83 ± 0.03 | 0.81 ± 0.03 |
| | Phase | 0 | 0 | 0 | 0 | 0 |
| | Lorentzian | 2 | 2 | 2 | 2 | 2 |
| | Peak Position | 2854.2 ± 0.4 | 2854.2 ± 0.4 | 2854.2 ± 0.4 | 2854.2 ± 0.4 | 2854.2 ± 0.4 |
| | Gaussian | 10.3 ± 0.3 | 10.3 ± 0.3 | 10.3 ± 0.3 | 10.3 ± 0.3 | 10.3 ± 0.3 |
| $CH_3$ S.S. | Amplitude | 1.09 ± 0.07 | 1.30 ± 0.06 | 1.35 ± 0.07 | 1.36 ± 0.06 | 1.27 ± 0.06 |
| | Phase | 0 | 0 | 0 | 0 | 0 |
| | Lorentzian | 2 | 2 | 2 | 2 | 2 |
| | Peak Position | 2871.1 ± 0.1 | 2871.1 ± 0.1 | 2871.1 ± 0.1 | 2871.1 ± 0.1 | 2871.1 ± 0.1 |
| | Gaussian | 5.1 ± 0.1 | 5.1 ± 0.1 | 5.1 ± 0.1 | 5.1 ± 0.1 | 5.1 ± 0.1 |
| $CH_2$ A.S. | Amplitude | 0.34 ± 0.09 | 0.34 ± 0.07 | 0.29 ± 0.09 | 0.25 ± 0.07 | 0.22 ± 0.08 |
| | Phase | 3.14 | 3.14 | 3.14 | 3.14 | 3.14 |
| | Lorentzian | 2 | 2 | 2 | 2 | 2 |
| | Peak Position | 2892.6 ± 0.9 | 2892.6 ± 0.9 | 2892.6 ± 0.9 | 2892.6 ± 0.9 | 2892.6 ± 0.9 |
| | Gaussian | 4.5 ± 0.7 | 4.5 ± 0.7 | 4.5 ± 0.7 | 4.5 ± 0.7 | 4.5 ± 0.7 |
| $CH_2$ F.R. | Amplitude | 0.47 ± 0.05 | 0.50 ± 0.05 | 0.46 ± 0.05 | 0.55 ± 0.04 | 0.50 ± 0.05 |
| | Phase | 0 | 0 | 0 | 0 | 0 |
| | Lorentzian | 2 | 2 | 2 | 2 | 2 |
| | Peak Position | 2920 ± 2 | 2920 ± 2 | 2920 ± 2 | 2920 ± 2 | 2920 ± 2 |
| | Gaussian | 15 ± 2 | 15 ± 2 | 15 ± 2 | 15 ± 2 | 15 ± 2 |
| $CH_3$ F.R. | Amplitude | 0.61 ± 0.08 | 0.87 ± 0.09 | 0.80 ± 0.08 | 0.86 ± 0.09 | 0.79 ± 0.08 |
| | Phase | 0 | 0 | 0 | 0 | 0 |

| | | | | | | |
|---|---|---|---|---|---|---|
| | Lorentzian | 2 | 2 | 2 | 2 | 2 |
| | Peak Position | 2934.1 ± 0.2 | 2934.1 ± 0.2 | 2934.1 ± 0.2 | 2934.1 ± 0.2 | 2934.1 ± 0.2 |
| | Gaussian | 7.3 ± 0.5 | 7.3 ± 0.5 | 7.3 ± 0.5 | 7.3 ± 0.5 | 7.3 ± 0.5 |
| $D_2O$ combination band | Amplitude | 0.290839 ± 0.0254828 | 0.245993 ± 0.0293321 | 0.272514 ± 0.0304409 | 0.233409 ± 0.0391378 | 0.260477 ± 0.0381514 |
| | Phase | 3.14 | 3.14 | 3.14 | 3.14 | 3.14 |
| | Lorentzian | 5 | 5 | 5 | 5 | 5 |
| | Peak Position | 2795 ± 15 | 2780 ± 30 | 2807 ± 14 | 2809 ± 24 | 2824 ± 13 |
| | Gaussian | 103 ± 30 | 145 ± 40 | 100 ± 22 | 147 ± 29 | 100 ± 17 |
| Nonresonant | Amplitude | 0 | 0 | 0 | 0 | 0 |
| | Phase | 0 | 0 | 0 | 0 | 0 |

**Table B.12.** Fit parameters for 3 μM h-SDS:d-DTAB mixture at the $CCl_4$-$D_2O$ interface, used obtain the $A_{r+}/A_{d+}$ ratios in Figure 5.7b.

| Peak Assignment | Parameter | |
|---|---|---|
| 1:1 stoichiometric pairs + excess | | 1.5 μM pairs |
| $CH_{2\ S.S.}$ | Amplitude | 0.38 ± 0.04 |
| | Phase | 0 |
| | Lorentzian | 2 |
| | Peak Position | 2854.3 ± 0.3 |
| | Gaussian | 10.1 ± 0.3 |
| $CH_{3\ S.S.}$ | Amplitude | 0.48 ± 0.06 |
| | Phase | 0 |
| | Lorentzian | 2 |
| | Peak Position | 2870.3 ± 0.2 |
| | Gaussian | 4.7 ± 0.1 |
| $CH_{2\ A.S.}$ | Amplitude | 0.23 ± 0.07 |
| | Phase | 3.14 |
| | Lorentzian | 2 |
| | Peak Position | 2890.8 ± 0.7 |
| | Gaussian | 5.2 ± 0.7 |
| $CH_{2\ F.R.}$ | Amplitude | 0.23 ± 0.05 |
| | Phase | 00 |
| | Lorentzian | 2 |
| | Peak Position | 2922 ± 3 |
| | Gaussian | 13 ± 4 |
| $CH_{3\ F.R.}$ | Amplitude | 0.3 ± 0.1 |
| | Phase | 0 |
| | Lorentzian | 2 |
| | Peak Position | 2933.0 ± 0.3 |

| | | |
|---|---|---|
| | Gaussian | 6.1 ± 0.9 |
| $D_2O$ combination band | Amplitude | 0.17 ± 0.03 |
| | Phase | 3.14 |
| | Lorentzian | 5 |
| | Peak Position | 2807 ± 25 |
| | Gaussian | 96 ± 54 |
| Nonresonant | Amplitude | 0 |
| | Phase | 0 |

**Table B.13.** Fit parameters for 5 μM h-SDS:d-DTAB mixture at the $CCl_4$-$D_2O$ interface, used obtain the $A_{r+}/A_{d+}$ ratios in Figure 5.7b.

| SDS:DTAB ratio | | 1:9 | 3:7 | 5:5 | 7:3 | 9:1 |
|---|---|---|---|---|---|---|
| 1:1 stoichiometric pairs + excess | | 0.5 μM pairs + 4 μM SDS | 1.5 μM pairs + 2 μM SDS | 2.5 μM pairs | 1.5 μM pairs + 2 μM DTAB | 0.5 μM pairs + 4 μM DTAB |
| Peak Assignment | Parameter | | | | | |
| $CH_2$ S.S. | Amplitude | 0.37 ± 0.01 | 0.68 ± 0.02 | 0.56 ± 0.02 | 0.57 ± 0.02 | 0.19 ± 0.05 |
| | Phase | 0 | 0 | 0 | 0 | 0 |
| | Lorentzian | 2 | 2 | 2 | 2 | 2 |
| | Peak Position | 2854.0 ± 0.3 | 2854.0 ± 0.3 | 2854.0 ± 0.3 | 2854.0 ± 0.3 | 2854.0 ± 0.3 |
| | Gaussian | 9.6 ± 0.3 | 9.6 ± 0.3 | 9.6 ± 0.3 | 9.6 ± 0.3 | 9.6 ± 0.3 |
| $CH_3$ S.S. | Amplitude | 0.43 ± 0.03 | 0.83 ± 0.03 | 0.70 ± 0.03 | 0.64 ± 0.03 | 0.16 ± 0.06 |
| | Phase | 0 | 0 | 0 | 0 | 0 |
| | Lorentzian | 2 | 2 | 2 | 2 | 2 |
| | Peak Position | 2869.0 ± 0.2 | 2869.0 ± 0.2 | 2869.0 ± 0.2 | 2869.0 ± 0.2 | 2869.0 ± 0.2 |
| | Gaussian | 4.7 ± 0.2 | 4.7 ± 0.2 | 4.7 ± 0.2 | 4.7 ± 0.2 | 4.7 ± 0.2 |
| $CH_2$ A.S. | Amplitude | 0.33 ± 0.02 | 0.36 ± 0.03 | 0.33 ± 0.03 | 0.28 ± 0.03 | 0.11 ± 0.06 |
| | Phase | 3.14 | 3.14 | 3.14 | 3.14 | 3.14 |
| | Lorentzian | 2 | 2 | 2 | 2 | 2 |
| | Peak Position | 2892.2 ± 0.5 | 2892.2 ± 0.5 | 2892.2 ± 0.5 | 2892.2 ± 0.5 | 2892.2 ± 0.5 |
| | Gaussian | 8.7 ± 0.5 | 8.7 ± 0.5 | 8.7 ± 0.5 | 8.7 ± 0.5 | 8.7 ± 0.5 |
| $CH_2$ F.R. | Amplitude | 0.27 ± 0.03 | 0.38 ± 0.06 | 0.31 ± 0.05 | 0.32 ± 0.06 | 0.12 ± 0.04 |
| | Phase | 0 | 0 | 0 | 0 | 0 |
| | Lorentzian | 2 | 2 | 2 | 2 | 2 |
| | Peak Position | 2925 ± 2 | 2925 ± 2 | 2925 ± 2 | 2925 ± 2 | 2925 ± 2 |

| | | | | | | |
|---|---|---|---|---|---|---|
| | Gaussian | 10 ± 2 | 10 ± 2 | 10 ± 2 | 10 ± 2 | 10 ± 2 |
| $CH_{3\ F.R.}$ | Amplitude | 0.2 ± 0.1 | 0.5 ± 0.1 | 0.5 ± 0.1 | 0.5 ± 0.1 | 0.19 ± 0.07 |
| | Phase | 0 | 0 | 0 | 0 | 0 |
| | Lorentzian | 2 | 2 | 2 | 2 | 2 |
| | Peak Position | 2934.0 ± 0.3 | 2934.0 ± 0.3 | 2934.0 ± 0.3 | 2934.0 ± 0.3 | 2934.0 ± 0.3 |
| | Gaussian | 6.1 ± 0.5 | 6.1 ± 0.5 | 6.1 ± 0.5 | 6.1 ± 0.5 | 6.1 ± 0.5 |
| $D_2O$ combination band | Amplitude | 0.24 ± 0.01 | 0.24 ± 0.01 | 0.24 ± 0.01 | 0.24 ± 0.01 | 0.24 ± 0.01 |
| | Phase | 3.14 | 3.14 | 3.14 | 3.14 | 3.14 |
| | Lorentzian | 5 | 5 | 5 | 5 | 5 |
| | Peak Position | 2800 ± 4 | 2817 ± 6 | 2817 ± 6 | 2823 ± 7 | 2808 ± 59 |
| | Gaussian | 53 ± 8 | 75 ± 7 | 69 ± 9 | 73 ± 9 | 82 ± 108 |
| Nonresonant | Amplitude | 0 | 0 | 0 | 0 | 0 |
| | Phase | 0 | 0 | 0 | 0 | 0 |

**Table B.14.** Fit parameters for 15 μM h-SDS:d-DTAB mixture at the $CCl_4$-$D_2O$ interface, used obtain the $A_{r+}/A_{d+}$ ratios in Figure 5.7b.

| SDS:DTAB ratio | | 9:1 | 7:3 | 6:4 | 5:5 | 4:6 | 3:7 | 1:9 |
|---|---|---|---|---|---|---|---|---|
| 1:1 stoichiometric pairs + excess | | 1.5 μM pairs + 12 μM SDS | 4.5 μM pairs + 10 μM SDS | 0.5 μM pairs + 4 μM SDS | 7.5 μM pairs | 0.5 μM pairs + 4 μM DTAB | 4.5 μM pairs + 10 μM DTAB | 1.5 μM pairs + 12 μM DTAB |
| $CH_{2\ S.S.}$ | Amplitude | 0.66 ± 0.03 | 0.68 ± 0.03 | 0.76 ± 0.03 | 0.59 ± 0.03 | 0.78 ± 0.03 | 0.67 ± 0.04 | 0.53 ± 0.04 |
| | Phase | 0 | 0 | 0 | 0 | 0 | 0 | 0 |
| | Lorentzian | 2 | 2 | 2 | 2 | 2 | 2 | 2 |
| | Peak Position | 2854.9 ± 0.3 | 2854.9 ± 0.3 | 2854.9 ± 0.3 | 2854.9 ± 0.3 | 2854.9 ± 0.3 | 2854.9 ± 0.3 | 2854.9 ± 0.3 |
| | Gaussian | 9.4 ± 0.3 | 9.4 ± 0.3 | 9.4 ± 0.3 | 9.4 ± 0.3 | 9.4 ± 0.3 | 9.4 ± 0.3 | 9.4 ± 0.3 |
| $CH_{3\ S.S.}$ | Amplitude | 0.98 ± 0.05 | 1.156 ± 0.05 | 1.34 ± 0.05 | 1.05 ± 0.05 | 1.32 ± 0.06 | 1.11 ± 0.05 | 0.80 ± 0.05 |
| | Phase | 0 | 0 | 0 | 0 | 0 | 0 | 0 |
| | Lorentzian | 2 | 2 | 2 | 2 | 2 | 2 | 2 |
| | Peak Position | 2870.5 ± 0.2 | 2870.5 ± 0.2 | 2870.5 ± 0.2 | 2870.5 ± 0.2 | 2870.5 ± 0.2 | 2870.5 ± 0.2 | 2870.5 ± 0.2 |

| | | | | | | | | |
|---|---|---|---|---|---|---|---|---|
| | Gaussian | 4.9 ± 0.1 | 4.9 ± 0.1 | 4.9 ± 0.1 | 4.9 ± 0.1 | 4.9 ± 0.1 | 4.9 ± 0.1 | 4.9 ± 0.1 |
| $CH_{2\ A.S.}$ | Amplitude | 0.40 ± 0.06 | 0.44 ± 0.06 | 0.41 ± 0.06 | 0.36 ± 0.06 | 0.44 ± 0.06 | 0.37 ± 0.06 | 0.33 ± 0.06 |
| | Phase | 3.14 | 3.14 | 3.14 | 3.14 | 3.14 | 3.14 | 3.14 |
| | Lorentzian | 2 | 2 | 2 | 2 | 2 | 2 | 2 |
| | Peak Position | 2890.8 ± 0.3 | 2890.8 ± 0.3 | 2890.8 ± 0.3 | 2890 .8 ± 0.3 | 2890.8 ± 0.3 | 2890.8 ± 0.3 | 2890.8 ± 0.3 |
| | Gaussian | 4.7 ± 0.4 | 4.7 ± 0.4 | 4.7 ± 0.4 | 4.7 ± 0.4 | 4.7 ± 0.4 | 4.7 ± 0.4 | 4.7 ± 0.4 |
| $CH_{2\ F.R.}$ | Amplitude | 0.40 ± 0.04 | 0.40 ± 0.04 | 0.41 ± 0.03 | 0.34 ± 0.03 | 0.48 ± 0.04 | 0.41 ± 0.04 | 0.35 ± 0.04 |
| | Phase | 0 | 0 | 0 | 0 | 0 | 0 | 0 |
| | Lorentzian | 2 | 2 | 2 | 2 | 2 | 2 | 2 |
| | Peak Position | 2922 ± 1 | 2922 ± 1 | 2922 ± 1 | 2922 ± 1 | 2922 ± 1 | 2922 ± 1 | 2922 ± 1 |
| | Gaussian | 14 ± 2 | 14 ± 2 | 14 ± 2 | 14 ± 2 | 14 ± 2 | 14 ± 2 | 14 ± 2 |
| $CH_{3\ F.R.}$ | Amplitude | 0.59 ± 0.07 | 0.70 ± 0.07 | 0.85 ± 0.07 | 0.63 ± 0.06 | 0.91 ± 0.08 | 0.77 ± 0.07 | 0.57 ± 0.06 |
| | Phase | 0 | 0 | 0 | 0 | 0 | 0 | 0 |
| | Lorentzian | 2 | 2 | 2 | 2 | 2 | 2 | 2 |
| | Peak Position | 2933.6 ± 0.2 | 2933.6 ± 0.2 | 2933.6 ± 0.2 | 2933 .6 ± 0.2 | 2933.6 ± 0.2 | 2933.6 ± 0.2 | 2933.6 ± 0.2 |
| | Gaussian | 6.3 ± 0.3 | 6.3 ± 0.3 | 6.3 ± 0.3 | 6.3 ± 0.3 | 6.3 ± 0.3 | 6.3 ± 0.3 | 6.3 ± 0.3 |
| $D_2O$ combination band | Amplitude | 0.29 ± 0.03 | 0.30 ± 0.03 | 0.39 ± 0.03 | 0.27 ± 0.03 | 0.32 ± 0.03 | 0.26 ± 0.03 | 0.21 ± 0.03 |
| | Phase | 3.14 ± 0 | 3.14 ± 0 | 3.14 ± 0 | 3.14 ± 0 | 3.14 ± 0 | 3.14 ± 0 | 3.14 ± 0 |
| | Lorentzian | 5 | 5 | 5 | 5 | 5 | 5 | 5 |
| | Peak Position | 2824 ± 9 | 2823 ± 10 | 2835 ± 6 | 2833 ± 9 | 2831 ± 10 | 2836 ± 10 | 2832 ± 11 |
| | Gaussian | 85 ± 14 | 89 ± 14 | 69 ± 6 | 74 ± 12 | 90 ± 11 | 88 ± 13 | 79 ± 18 |
| Nonresonant | Amplitude | 0 | 0 | 0 | 0 | 0 | 0 | 0 |
| | Phase | 0 | 0 | 0 | 0 | 0 | 0 | 0 |

**Table B.15.** Fit parameters for 25 μM h-SDS:d-DTAB mixture at the $CCl_4$-$D_2O$ interface, used obtain the $A_{r+}/A_{d+}$ ratios in Figure 5.7b.

| SDS:DTAB ratio | | 1:9 | 3:7 | 5:5 | 7:3 | 9:1 |
|---|---|---|---|---|---|---|
| 1:1 stoichiometric pairs + excess | | 0.5 μM pairs + 4 μM SDS | 1.5 μM pairs + 2 μM SDS | 12.5 μM pairs | 1.5 μM pairs + 2 μM DTAB | 0.5 μM pairs + 4 μM DTAB |
| SDS:DTAB ratio | | 1:9 | 3:7 | 5:5 | 7:3 | 9:1 |
| Peak Assignment | Parameter | | | | | |
| $CH_2$ S.S. | Amplitude | 0.80 ± 0.04 | 0.89 ± 0.06 | 0.85 ± 0.04 | 0.86 ± 0.05 | 0.78 ± 0.04 |
| | Phase | 0 | 0 | 0 | 0 | 0 |
| | Lorentzian | 2 | 2 | 2 | 2 | 2 |
| | Peak Position | 2854.7 ± 0.4 | 2854.7 ± 0.4 | 2854.7 ± 0.4 | 2854.7 ± 0.4 | 2854.7 ± 0.4 |
| | Gaussian | 10.2 ± 0.4 | 10.2 ± 0.4 | 10.2 ± 0.4 | 10.2 ± 0.4 | 10.2 ± 0.4 |
| $CH_3$ S.S. | Amplitude | 1.37 ± 0.06 | 1.58 ± 0.06 | 1.50 ± 0.06 | 1.47 ± 0.06 | 1.31 ± 0.06 |
| | Phase | 0 | 0 | 0 | 0 | 0 |
| | Lorentzian | 2 | 2 | 2 | 2 | 2 |
| | Peak Position | 2870.1 ± 0.3 | 2870.1 ± 0.3 | 2870.1 ± 0.3 | 2870.1 ± 0.3 | 2870.1 ± 0.3 |
| | Gaussian | 4.8 ± 0.1 | 4.8 ± 0.1 | 4.8 ± 0.1 | 4.8 ± 0.1 | 4.8 ± 0.1 |
| $CH_2$ A.S. | Amplitude | 0.46 ± 0.06 | 0.49 ± 0.07 | 0.40 ± 0.07 | 0.46 ± 0.07 | 0.43 ± 0.07 |
| | Phase | 3.14 | 3.14 | 3.14 | 3.14 | 3.14 |
| | Lorentzian | 2 | 2 | 2 | 2 | 2 |
| | Peak Position | 2890.4 ± 0.4 | 2890.4 ± 0.4 | 2890.4 ± 0.4 | 2890.4 ± 0.4 | 2890.4 ± 0.4 |
| | Gaussian | 4.6 ± 0.5 | 4.6 ± 0.5 | 4.6 ± 0.5 | 4.6 ± 0.5 | 4.6 ± 0.5 |
| $CH_2$ F.R. | Amplitude | 0.46 ± 0.04 | 0.58 ± 0.06 | 0.49 ± 0.05 | 0.56 ± 0.06 | 0.47 ± 0.05 |
| | Phase | 0 | 0 | 0 | 0 | 0 |
| | Lorentzian | 2 | 2 | 2 | 2 | 2 |
| | Peak Position | 2921 ± 2 | 2921 ± 2 | 2921 ± 2 | 2921 ± 2 | 2921 ± 2 |
| | Gaussian | 13 ± 2 | 13 ± 2 | 13 ± 2 | 13 ± 2 | 13 ± 2 |
| $CH_3$ F.R. | Amplitude | 0.8 ± 0.1 | 1.1 ± 0.1 | 1.0 ± 0.1 | 1.0 ± 0.1 | 0.9 ± 0.1 |
| | Phase | 0 | 0 | 0 | 0 | 0 |
| | Lorentzian | 2 | 2 | 2 | 2 | 2 |
| | Peak Position | 2933.4 ± 0.2 | 2933.4 ± 0.2 | 2933.4 ± 0.2 | 2933.4 ± 0.2 | 2933.4 ± 0.2 |
| | Gaussian | 6.7 ± 0.4 | 6.7 ± 0.4 | 6.7 ± 0.4 | 6.7 ± 0.4 | 6.7 ± 0.4 |
| | Amplitude | 0.43 ± 0.04 | 0.39 ± 0.04 | 0.38 ± 0.04 | 0.35 ± 0.05 | 0.36 ± 0.05 |

| | | | | | | |
|---|---|---|---|---|---|---|
| $D_2O$ combination band | Phase | 3.14 | 3.14 | 3.14 | 3.14 | 3.14 |
| | Lorentzian | 5 | 5 | 5 | 5 | 5 |
| | Peak Position | 2833 ± 6 | 2834 ± 10 | 2834 ± 8 | 2841 ± 9 | 2839 ± 7 |
| | Gaussian | 72 ± 8 | 98 ± 11 | 82 ± 11 | 95 ± 11 | 73 ± 11 |
| Nonresonant | Amplitude | 0 | 0 | 0 | 0 | 0 |
| | Phase | 0 | 0 | 0 | 0 | 0 |

REFERENCES CITED

1. Joye, S. B. The Geology and Biogeochemistry of Hydrocarbon Seeps. *Annu. Rev. Earth Planet. Sci.* **2020,** *48*, 205-231.
2. Andreae, M. O.; Crutzen, P. J. Atmospheric Aerosols: Biogeochemical Sources and Role in Atmospheric Chemistry. *Science* **1997,** *276*, 1052-1058.
3. Dash, J. G.; Rempel, A. W.; Wettlaufer, J. S. The Physics of Premelted Ice and its Geophysical Consequences. *Rev. Mod. Phys.* **2006,** *78*, 695-741.
4. Love, A. H.; Bailey, C. G.; Hanna, M. L.; Hok, S.; Vu, A. K.; Reutter, D. J.; Raber, E. Efficacy of Liquid and Foam Decontamination Technologies for Chemical Warfare Agents on Indoor Surfaces. *J. Hazard. Mater.* **2011,** *196*, 115-22.
5. Kuznetsov, G. V.; Volkov, R. S.; Sviridenko, A. S.; Zhdanova, A. O.; Strizhak, P. A. Containment and Suppression of Compartment Fires using Specialized Liquid Compositions. *Fire Saf. J.* **2024,** *147,* 104187.
6. Hjelt, T.; Ketoja, J. A.; Kiiskinen, H.; Koponen, A. I.; Pääkkönen, E. Foam Forming of Fiber Products: A Review. *J. Dispersion Sci. Technol.* **2021,** *43*, 1462-1497.
7. Solbakken, J. S. Status of Foam as a Liquid Blocking Agent in Porous Media: A Review. *Energies* **2023,** *16*, 5063.
8. Bai, L.; Huan, S.; Rojas, O. J.; McClements, D. J. Recent Innovations in Emulsion Science and Technology for Food Applications. *J. Agric. Food Chem.* **2021,** *69*, 8944-8963.
9. Marti-Mestres, G.; Nielloud, F. Emulsions in Health Care Applications - An Overview. *J. Dispersion Sci. Technol.* **2002,** *23*, 419-439.
10. Zhou, Y.; Yin, D.; Chen, W.; Liu, B.; Zhang, X. A Comprehensive Review of Emulsion and its Field Application for Enhanced Oil Recovery. *Energy Sci. Eng.* **2019,** *7*, 1046-1058.
11. del Amo, B.; Romagnoli, R.; Deyá, C.; González, J. A. High Performance Water-Based Paints with Non-Toxic Anticorrosive Pigments. *Prog. Org. Coat.* **2002,** *45*, 389-397.
12. Deng, J.; Ding, T.; Yan, X., Effect of Two Types of Pomelo Peel Flavonoid Microcapsules on the Performance of Water-Based Coatings on the Surface of Fiberboard. *Coatings* **2024,** *14*, 1032.
13. Ho, J.; Mudraboyina, B.; Spence-Elder, C.; Resendes, R.; Cunningham, M. F.; Jessop, P. G. Water-Borne Coatings that Share the Mechanism of Action of Oil-Based Coatings. *Green Chem.* **2018,** *20*, 1899-1905.
14. Valkovska, D. S.; Kralchevsky, P. A.; Danov, K. D.; Broze, G.; Mehreteab, A. The Effect of Oil Solubility on the Oil Drop Entry at Water−Air Interface. *Langmuir* **2000,** *16*, 8892-8902.
15. Magrabi, S. A.; Dlugogorski, B. Z.; Jameson, G. J., A Comparative Study of Drainage Characteristics in AFFF and FFFP Compressed-Air Fire-Fighting Foams. *Fire Saf. J.* **2002,** *37*, 21-52.
16. Abdelaal, A.; Aljawad, M. S.; Alyousef, Z.; Almajid, M. M. A Review of Foam-Based Fracturing Fluids Applications: From Lab Studies to Field Implementations. *J. Nat. Gas. Sci. Eng.* **2021,** *95, 104236*.
17. Denkov, N. D. Mechanisms of Foam Destruction by Oil-Based Antifoams. *Langmuir* **2004,** *20*, 9463-505.
18. Qu, C.; Wang, J.; Yin, H.; Lu, G.; Li, Z.; Feng, Y. Condensate Oil-Tolerant Foams Stabilized by an Anionic-Sulfobetaine Surfactant Mixture. *ACS Omega* **2019,** *4*, 1738-1747.

19. Collivignarelli, M. C.; Baldi, M.; Abbà, A.; Caccamo, F. M.; Carnevale Miino, M.; Rada, E. C.; Torretta, V. Foams in Wastewater Treatment Plants: From Causes to Control Methods. *Appl. Sci.* **2020,** *10*, 2716.
20. Frank, A.; Scholz, W. Defoamers in the Coatings Industry. *Chimia* **2002,** *56*, 177-183.
21. Simjoo, M.; Rezaei, T.; Andrianov, A.; Zitha, P. L. J. Foam stability in the presence of oil: Effect of surfactant concentration and oil type. *Colloids Surf., A* **2013,** *438*, 148-158.
22. Banerjee, A.; Liu, Y. Essential Factor of Perfluoroalkyl Surfactants Contributing to Efficacy in Firefighting Foams. *Langmuir* **2021,** *37*, 8937-8944.
23. Weaire, D. L.; Hutzler, S. *The Physics of Foams*; Clarendon Press: Oxford, 1999.
24. Cantat, I.; Cohen-Addad, S.; Elias, F.; Graner, F.; Höhler, R.; Pitois, O.; Elias, F.; Saint-Jalmes, A.; Rouyer, F. *Foams: Structure and Dynamics*; Oxford Press, 2013.
25. Engelhardt, K.; Rumpel, A.; Walter, J.; Dombrowski, J.; Kulozik, U.; Braunschweig, B.; Peukert, W. Protein Adsorption at the Electrified Air-Water Interface: Implications on Foam Stability. *Langmuir* **2012,** *28*, 7780-7787.
26. Tcholakova, S.; Mitrinova, Z.; Golemanov, K.; Denkov, N. D.; Vethamuthu, M.; Ananthapadmanabhan, K. P. Control of Ostwald Ripening by Using Surfactants with High Surface Modulus. *Langmuir* **2011,** *27*, 14807-14819.
27. Kristen, N.; von Klitzing, R. Effect of Polyelectrolyte/Surfactant Combinations on the Stability of Foam Films. *Soft Matter* **2010,** *6*, 849-861.
28. Mikhailovskaya, A.; Chatzigiannakis, E.; Renggli, D.; Vermant, J.; Monteux, C. From Individual Liquid Films to Macroscopic Foam Dynamics: A Comparison between Polymers and a Nonionic Surfactant. *Langmuir* **2022,** *38*, 10768-10780.
29. Engelhardt, K.; Lexis, M.; Gochev, G.; Konnerth, C.; Miller, R.; Willenbacher, N.; Peukert, W.; Braunschweig, B. pH Effects on the Molecular Structure of Beta-Lactoglobulin Modified Air-Water Interfaces and its Impact on Foam Rheology. *Langmuir* **2013,** *29*, 11646-11655.
30. Varade, D.; Carriere, D.; Arriaga, L. R.; Fameau, A. L.; Rio, E.; Langevin, D.; Drenckhan, W. On the origin of the stability of foams made from catanionic surfactant mixtures. *Soft Matter* **2011,** *7* , 6557-6570.
31. Robinson, J. V.; Woods, W. W. A Method of Selecting Foam Inhibitors. *J. Soc. Chem. Ind.* **2010,** *67*, 361-365.
32. Harkins, W. D. A General Thermodynamic Theory of the Spreading of Liquids to Form Duplex Films and of Liquids or Solids to Form Monolayers. *J. Chem. Phys.* **1941,** *9*, 552-568.
33. Lau, H. C.; O'Brien, S. M. Effects of Spreading and Nonspreading Oils on Foam Propagation Through Porous Media. *SPE Reservoir Eng.* **1988,** *3*, 893-896.
34. Garrett, P. R.*The Science of Defoaming Theory, Experiment and Applications*; CRC Press: Boca Raton, 2013.
35. Wang, C.; Fang, H.; Gong, Q.; Xu, Z.; Liu, Z.; Zhang, L.; Zhang, L.; Zhao, S. Roles of Catanionic Surfactant Mixtures on the Stability of Foams in the Presence of Oil. *Energy Fuels* **2016,** *30*, 6355-6364.
36. Wang, H.; Wang, Z.; Lv, Q.; Li, C.; Du, Z.; Sun, S.; Hu, S. Mechanism of Foam Film Destruction Induced by Emulsified Oil: A Coarse-Grained Simulation Study. *J. Phys. Chem. C* **2018,** *122*, 26438-26446.
37. Pugh, R. J. *Bubble and Foam Chemistry*; Cambridge: Cambridge University, 2016.
38. Wasan, D. T.; Koczo, K.; Nikolov, A. D. Mechanisms of Aqueous Foam Stability and Antifoaming Action with and without Oil. ACS Symposium Series; American Chemical Society: Washington, DC, 1994; No. 242.

39. Manlowe, D. J.; Radke, C. J. A Pore-Level Investigation of Foam/Oil Interactions in Porous Media. *SPE Reservoir Eng.* **1990,** *5*, 495-502.
40. Gao, F.; Yan, H.; Wang, Q.; Yuan, S. Mechanism of Foam Destruction by Antifoams: A Molecular Dynamics Study. *Phys. Chem. Chem. Phys.* **2014,** *16*, 17231-17237.
41. Lobo, L.; Wasan, D. T. Mechanisms of Aqueous Foam stability in the Presence of Emulsified Non-Aqueous-Phase Liquids: Structure and Stability of the Pseudoemulsion Film. *Langmuir* **2002,** *9*, 1668-1677.
42. Wang, C.; Zhao, L.; Xu, B.-c.; Cao, X.-l.; Guo, L.-l.; Zhang, L.; Zhang, L.; Zhao, S. Effect of Dynamic Interfacial Dilational Properties on the Foam Stability of Catanionic Surfactant Mixtures in the Presence of Oil. *Colloids Surf., A* **2018,** *541*, 78-86.
43. Fauser, H.; Uhlig, M.; Miller, R.; von Klitzing, R. Surface Adsorption of Oppositely Charged SDS:$C_{12}$TAB Mixtures and the Relation to Foam Film Formation and Stability. *J. Phys. Chem. B* **2015,** *119*, 12877-86.
44. Qian, J.; Gao, X.; Pan, B. Nanoconfinement-Mediated Water Treatment: From Fundamental to Application. *Environ. Sci. Technol.* **2020,** *54*, 8509-8526.
45. Otake, K. I.; Otsubo, K.; Komatsu, T.; Dekura, S.; Taylor, J. M.; Ikeda, R.; Sugimoto, K.; Fujiwara, A.; Chou, C. P.; Sakti, A. W.; Nishimura, Y.; Nakai, H.; Kitagawa, H., Confined Water-Mediated High Proton Conduction in Hydrophobic Channel of a Synthetic Nanotube. *Nat. Commun.* **2020,** *11*, 843-849.
46. Premadasa, U. I.; Ma, Y. Z.; Sacci, R. L.; Bocharova, V.; Thiele, N. A.; Doughty, B. Understanding Self-Assembly and the Stabilization of Liquid/Liquid Interfaces: The Importance of Ligand Tail Branching and Oil-Phase Solvation. *J. Colloid Interface Sci.* **2022,** *609*, 807-814.
47. Vacha, R.; Roke, S., Sodium Dodecyl Sulfate at Water-Hydrophobic Interfaces: A Simulation Study. *J. Phys. Chem. B* **2012,** *116*, 11936-11942.
48. Beaman, D. K.; Robertson, E. J.; Richmond, G. L. From Head to Tail: Structure, Solvation, and Hydrogen Bonding of Carboxylate Surfactants at the Organic–Water Interface. *J. Phys. Chem. C* **2011,** *115*, 12508-12516.
49. Osei-Bonsu, K.; Shokri, N.; Grassia, P., Foam Stability in the Presence and Absence of Hydrocarbons: From Bubble- to Bulk-Scale. *Colloids Surf., A* **2015,** *481*, 514-526.
50. Lee, J.; Nikolov, A.; Wasan, D. Stability of Aqueous Foams in the Presence of Oil: On the Importance of Dispersed vs Solubilized Oil. *Ind. Eng. Chem. Res.* **2013,** *52*, 66-72.
51. Phaodee, P.; Sabatini, D. A. Anionic and Cationic Surfactant Synergism: Minimizing Precipitation, Microemulsion Formation, and Enhanced Solubilization and Surface Modification. *J. Surfactants Deterg.* **2021,** *24*, 551-562.
52. Rosen, M. J.; Murphy, D. S., Synergism in Binary Mixtures of Surfactants. *J. Colloid Interface Sci.* **1986,** *110*, 224-236.
53. Rosen, M. J.; Kunjappu, J. T. *Surfactants and Interfacial Phenomena*, 4th ed; John Wiley & Sons, Inc: Hoboken, NJ, 2012.
54. Sloutskin, E.; Tamam, L.; Sapir, Z.; Ocko, B. M.; Bain, C. D.; Kuzmenko, I.; Gog, T.; Deutsch, M. Counterions under a Surface-Adsorbed Cationic Surfactant Monolayer: Structure and Thermodynamics. *Langmuir* **2022,** *38*, 12356-12366.
55. Delcea, M.; Helm, C. A. X-ray and Neutron Reflectometry of Thin Films at Liquid Interfaces. *Langmuir* **2019,** *35*, 8519-8530.
56. Mitrinovic, D. M.; Zhang, Z.; Williams, S. M.; Huang, Z.; Schlossman, M. L. X-ray Reflectivity Study of the Water−Hexane Interface. *The Journal of Physical Chemistry B* **1999,** *103*, 1779-1782.

57. Scoppola, E.; Watkins, E.; Li Destri, G.; Porcar, L.; Campbell, R. A.; Konovalov, O.; Fragneto, G.; Diat, O. Structure of a Liquid/Liquid Interface During Solvent Extraction Combining X-Ray and Neutron Reflectivity Measurements. *Phys. Chem. Chem. Phys.* **2015,** *17*, 15093-15097.
58. Zarbakhsh, A.; Querol, A.; Bowers, J.; Webster, J. R. Structural Studies of Amphiphiles Adsorbed at Liquid-Liquid Interfaces Using Neutron Reflectometry. *Faraday Discuss* **2005,** *129*, 155-167.
59. Bowers, J.; Zarbakhsh, A.; Webster, J. R. P.; Hutchings, L. R.; Richards, R. W. Neutron Reflectivity Studies at Liquid−Liquid Interfaces: Methodology and Analysis. *Langmuir* **2000,** *17*, 140-145.
60. Lambert, A. G.; Davies, P. B.; Neivandt, D. J. Implementing the Theory of Sum Frequency Generation Vibrational Spectroscopy: A Tutorial Review. *Appl. Spectrosc. Rev.* **2005,** *40*, 103-145.
61. Pickering, J. D.; Bregnhoj, M.; Rasmussen, M. H.; Strunge, K.; Weidner, T. Tutorials in Vibrational Sum Frequency Generation Spectroscopy. III. Collecting, Processing, and Analyzing Vibrational Sum Frequency Generation Spectra. *Biointerphases* **2022,** *17*, 041201.
62. Norvaisas, P.; Petrauskas, V.; Matulis, D. Thermodynamics of Cationic and Anionic Surfactant Interaction. *J. Phys. Chem. B* **2012,** *116*, 2138-44.
63. Pradines, V.; Lavabre, D.; Micheau, J. C.; Pimienta, V. Determining the Association Constant and Adsorption Properties of Ion Pairs in Water by Fitting Surface Tension Data. *Langmuir* **2005,** *21*, 11167-11172.
64. Conley, R. T., *Infrared Spectroscopy*. 1996.
65. Morita, A. *Theory of Sum Frequency Generation Spectroscopy*; Springer, Singapore, 2018.66. Gragson, D. E.; Richmond, G. L. Investigations of the Structure and Hydrogen Bonding of Water Molecules at Liquid Surfaces by Vibrational Sum Frequency Spectroscopy. *J. Phys. Chem. B* **1998,** *102*, 3847-3861.
67. Raymond, E. A.; Richmond, G. L. Probing the Molecular Structure and Bonding of the Surface of Aqueous Salt Solutions. *J. Phys. Chem. B* **2004,** *108*, 5051-5059.
68. Yamaguchi, S.; Shiratori, K.; Morita, A.; Tahara, T. Electric Quadrupole Contribution to the Nonresonant Background of Sum Frequency generation at Air/Liquid Interfaces. *J. Chem. Phys.* **2011,** *134*, 184705.
69. Walker, R. A.; Conboy, J. C.; Richmond, G. L. Molecular Structure and Ordering of Phospholipids at a Liquid−Liquid Interface. *Langmuir* **1997,** *13*, 3070-3073.
70. Altman, R. M.; Richmond, G. L. Twist and Stretch: Assignment and Surface Charge Sensitivity of a Water Combination Band and Its Implications for Vibrational Sum Frequency Spectra Interpretations. *J. Phys. Chem. B* **2021,** *125*, 6717-6726.
71. Bain, C. D.; Davies, P. B.; Ong, T. H.; Ward, R. N.; Brown, M. A. Quantitative Analysis of Monolayer Composition by Sum-Frequency Vibrational Spectroscopy. *Langmuir* **2002,** *7*, 1563-1566.
72. Majeed, T.; Kamal, M. S.; Zhou, X.; Solling, T., A Review on Foam Stabilizers for Enhanced Oil Recovery. *Energy Fuels* **2021,** *35*, 5594-5612.
73. Zhou, H.; Qu, C.; Lu, G.; Li, Z.; Wang, X.; Yin, H.; Feng, Y. Deliquification of Low-Productivity Natural Gas Wells with In Situ Generated Foams and Heat. *Energy Fuels* **2021,** *35*, 9873-9882.
74. Bajpai, D.; Tyagi, V. K. Laundry detergents: an overview. *J. Oleo. Sci.* **2007,** *56*, 327-40.

75. Schramm, L. L.; Stasiuk, E. N.; Marangoni, D. G. Surfactants and their applications. *Annu. Rep. Prog. Chem., Sect. C* **2003,** *99*, 3-48.
76. Hinnant, K. M.; Giles, S. L.; Smith, E. P.; Snow, A. W.; Ananth, R. Characterizing the Role of Fluorocarbon and Hydrocarbon Surfactants in Firefighting-Foam Formulations for Fire-Suppression. *Fire Technol.* **2019,** *56*, 1413-1441.
77. Akbar, J. R.; Deubry, R.; Marangoni, D. G.; Wettig, S. D. Interactions between gemini and nonionic pharmaceutical surfactants. *Can. J. Chem.* **2010,** *88*, 1262-1270.
78. Ghosh, S.; Ray, A.; Pramanik, N.; Ambade, B. Can a Catanionic Surfactant Mixture Act as a Drug Delivery Vehicle? *C. R. Chim.* **2016,** *19*, 951-954.
79. Baki, G. *Introduction to Cosmetic Formulation and Technology,* 2nd ed; John Wiley & Sons, Inc. Hoboken, NJ, 2015.
80. Agredo, P.; Rave, M. C.; Echeverri, J. D.; Romero, D.; Salamanca, C. H. An Evaluation of the Physicochemical Properties of Stabilized Oil-In-Water Emulsions Using Different Cationic Surfactant Blends for Potential Use in the Cosmetic Industry. *Cosmetics* **2019,** *6*, 12.
81. Tadros, T. F. *Formulations: In Cosmetic and Personal Care*; De Gruyter, Berlin, Germany, 2016
82. Lippert, F. An Introduction to Toothpaste - Its Purpose, History and Ingredients. *Monogr. Oral. Sci.* **2013,** *23*, 1-14.
83. Tadros, T. F. *Applied Surfactants: Principles and Applications;* Wiley-VCH Verlag GmbH & Co. KGaA. Weinheim, 2005.
84. Kralova, I.; Sjöblom, J. Surfactants Used in Food Industry: A Review. *J. Dispersion Sci. Technol.* **2009,** *30*, 1363-1383.
85. Lucassen-Reynders, E. H.; Lucassen, J.; Giles, D. Surface and Bulk Properties of Mixed Anionic/Cationic Surfactant Systems I. Equilibrium Surface Tensions. *J. Colloid Interface Sci.* **1981,** *81*, 150-157.
86. Wang, C.; Cao, X. L.; Quo, L. L.; Xu, Z. C.; Zhang, L.; Gong, Q. T.; Zhang, L.; Zhao, S. Effect of Molecular Structure of Catanionic Surfactant Mixtures on Their Interfacial Properties. *Colloid Surface., A* **2016,** *509*, 601-612.
87. Zhong, D.-L.; Ding, K.; Lu, Y.-Y.; Yan, J.; Zhao, W.-L. Methane Recovery from Coal Mine Gas Using Hydrate Formation in Water-In-Oil Emulsions. *Appl. Energy* **2016,** *162*, 1619-1626.
88. Man, C.; Shunbing, Z.; Litao, J. I. A.; Xiaoli, W. U. Surfactant-Containing Water Mist Suppression Pool Fire Experimental Analysis. *Procedia Eng.* **2014,** *84*, 558-564.
89. Hadjiiski, A.; Tcholakova, S.; Denkov, N. D.; Durbut, P.; Broze, G.; Mehreteab, A. Effect of Oily Additives on Foamability and Foam Stability. 2. Entry Barriers. *Langmuir* **2001,** *17*, 7011-7021.
90. Koczo, K.; Lobo, L. A.; Wasan, D. T. Effect of Oil on Foam Stability - Aqueous Foams Stabilized by Emulsions. *J. Colloid and Interface Sci.* **1992,** *150*, 492-506.
91. Farajzadeh, R.; Andrianov, A.; Krastev, R.; Hirasaki, G. J.; Rossen, W. R. Foam-Oil Interaction in Porous Media: Implications for Foam Assisted Enhanced Oil Recovery. *Adv. Colloid Interface Sci.* **2012,** *183-184*, 1-13.
92. Gilányi, T.; Mészáros, R.; Varga, I., Phase Transition in the Adsorbed Layer of Catanionic Surfactants at the Air/Solution Interface. *Langmuir* **2000,** *16*, 3200-3205.
93. Varga, I.; Keszthelyi, T.; Meszaros, R.; Hakkel, O.; Gilanyi, T. Observation of a Liquid-Gas Phase Transition in Monolayers of Alkyltrimethylammonium Alkyl Sulfates Adsorbed at the Air/Water Interface. *J Phys Chem B* **2005,** *109*, 872-878.

94. Eastoe, J.; Dalton, J.; Rogueda, P.; Sharpe, D.; Dong, J.; Webster, J. R. P. Interfacial Properties of a Catanionic Surfactant. *Langmuir* **1996,** *12*, 2706-2711.
95. Clavero, E.; Rodriguez, J.; Laria, D. Computer Simulations of Catanionic Surfactants Adsorbed at Air/Water Interfaces. II. Full Coverage. *J. Chem. Phys.* **2007,** *127*, 124704.
96. Rodriguez, J.; Clavero, E.; Laria, D. Computer Simulations of Catanionic Surfactants Adsorbed at Air/Water Interfaces. *J. Phys. Chem. B* **2005,** *109*, 24427-33.
97. Lyttle, D. J.; Lu, J. R.; Su, T. J.; Thomas, R. K.; Penfold, J. Structure of a Dodecyltrimethylammonium Bromide Layer at the Air/Water Interface Determined by Neutron Reflection: Comparison of the Monolayer Structure of Cationic Surfactants with Different Chain Lengths. *Langmuir* **1995,** *11*, 1001-1008.
98. Abranko-Rideg, N.; Darvas, M.; Horvai, G.; Jedlovszky, P. Immersion Depth of Surfactants at the Free Water Surface: A Computer Simulation and ITIM Analysis Study. *J. Phys. Chem. B* **2013,** *117*, 8733-46.
99. Palazzesi, F.; Calvaresi, M.; Zerbetto, F. A Molecular Dynamics Investigation of Structure and Dynamics of SDS and SDBS Micelles. *Soft Matter* **2011,** *7*, 9148-9156.
100. Schweighofer, K. J.; Essmann, U.; Berkowitz, M. Structure and Dynamics of Water in the Presence of Charged Surfactant Monolayers at the Water−$CCl_4$ Interface. A Molecular Dynamics Study. *J. Phys. Chem. B* **1997,** *101*, 10775-10780.
101. Sachin, K. M.; Karpe, S. A.; Kumar, D.; Singh, M.; Dominguez, H.; Ríos-López, M.; Bhattarai, A. A simulation study of self-assembly behaviors and micellization properties of mixed ionic surfactants. *J. Mol. Liq.* **2021,** *336, 116003*.
102. Conboy, J. C.; Messmer, M. C.; Richmond, G. L. Dependence of Alkyl Chain Conformation of Simple Ionic Surfactants on Head Group Functionality As Studied by Vibrational Sum-Frequency Spectroscopy. *J. Phys. Chem. B* **1997,** *101*, 6724-6733.
103. Scatena, L. F.; Richmond, G. L. Isolated Molecular Ion Solvation at an Oil/Water Interface Investigated by Vibrational Sum-Frequency Spectroscopy. *J. Phys. Chem. B* **2004,** *108*, 12518-12528.
104. Hore, D. K.; Beaman, D. K.; Parks, D. H.; Richmond, G. L. Whole-Molecule Approach for Determining Orientation at Isotropic Surfaces by Nonlinear Vibrational Spectroscopy. *J. Phys. Chem. B* **2005,** *109*, 16846-16851.
105. Schabes, B. K.; Hopkins, E. J.; Richmond, G. L. Molecular Interactions Leading to the Coadsorption of Surfactant Dodecyltrimethylammonium Bromide and Poly(styrenesulfonate) at the Oil/Water Interface. *Langmuir* **2019,** *35*, 7268-7276.
106. Góralczyk, D. Effect of the Molar Ratio of Surfactants in the Solution on the Composition and Mutual Interactions in Anionic—Cationic Adsorption Films. *Colloids and Surfaces* **1992,** *66*, 241-248.
107. Shah, S. K.; Chatterjee, S. K.; Bhattarai, A. The Effect of Methanol on the Micellar Properties of Dodecyltrimethylammonium Bromide (DTAB) in Aqueous Medium at Different Temperatures. *Journal of Surfactants and Detergents* **2015,** *19*, 201-207.
108. Gragson, D. E.; McCarty, B. M.; Richmond, G. L. Ordering of Interfacial Water Molecules at the Charged Air/Water Interface Observed by Vibrational Sum Frequency Generation. *J. Am. Chem. Soc.* **1997,** *119*, 6144-6152.
109. Fainerman, V. B.; Lucassen-Reynders, E. H. Adsorption of Single and Mixed Ionic Surfactants at Fluid Interfaces. *Adv. Colloid Interface Sci.* **2002,** *96*, 295-323.
110. Gibbs, J. W. *The Collected Works of J. Willard Gibbs,* Vol 1; Yale University Press: New Haven, Conneticut, 1928.

111. Rosen, M. J.; Dahanayake, M.; Cohen, A. W., Relationship of Structure to Properties in Surfactants. 11. Surface and Thermodynamic Properties of N-dodecyl-pyridinium Bromide and Chloride. *Colloids Surf.* **1982,** *5*, 159-172.
112. Danov, K. D.; Kralchevska, S. D.; Kralchevsky, P. A.; Ananthapadmanabhan, K. P.; Lips, A. Mixed Solutions of Anionic and Zwitterionic Surfactant (Betaine): Surface-Tension Isotherms, Adsorption, and Relaxation Kinetics. *Langmuir* **2004,** *20*, 5445-53.
113. Garcia Rey, N.; Weissenborn, E.; Schulze-Zachau, F.; Gochev, G.; Braunschweig, B. Quantifying Double-Layer Potentials at Liquid-Gas Interfaces from Vibrational Sum-Frequency Generation. *J. Phys. Chem. C* **2019,** *123*, 1279-1286.
114. Mucic, N.; Gochev, G.; Won, J.; Ulaganathan, V.; Fauser, H.; Javadi, A.; Aksenenko, E. V.; Krägel, J.; Miller, R. Adsorption of Equimolar Aqueous Sodium Dodecyl Sulphate/Dodecyl Trimethylammonium Bromide Mixtures at Solution/Air and Solution/Oil Interfaces. *Colloid Polym. Sci.* **2015,** *293*, 3099-3106.
115. Hsiao, Y.; Chou, T. H.; Patra, A.; Wen, Y. C. Momentum-Dependent Sum-Frequency Vibrational Spectroscopy of Bonded Interface Layer at Charged Water Interfaces. *Sci. Adv.* **2023,** *9*, No. eadg2823.
116. Ciszewski, R. K.; Gordon, B. P.; Muller, B. N.; Richmond, G. L. Takes Two to Tango: Choreography of the Coadsorption of CTAB and Hexanol at the Oil-Water Interface. *J. Phys. Chem. B* **2019,** *123*, 8519-8531.
117. Mondal, J. A.; Nihonyanagi, S.; Yamaguchi, S.; Tahara, T. Three Distinct Water Structures at a Zwitterionic Lipid/Water Interface Revealed by Heterodyne-Detected Vibrational Sum Frequency Generation. *J. Am. Chem. Soc.* **2012,** *134*, 7842-50.
118. Gragson, D. E.; Richmond, G. L. Potential Dependent Alignment and Hydrogen Bonding of Water Molecules at Charged Air/Water and $CCl_4$/Water Interfaces. *J. Am. Chem. Soc.* **1998,** *120*, 366-375.
119. Pool, R. E.; Versluis, J.; Backus, E. H.; Bonn, M. Comparative Study of Direct and Phase-Specific Vibrational Sum-Frequency Generation Spectroscopy: Advantages and Limitations. *J. Phys. Chem. B* **2011,** *115*, 15362-15369.
120. Vilangottunjalil, A.; Versluis, J.; Bakker, H. J. Observation of Electrostatically Driven Surface Adsorption in Mixed Surfactant Systems. *J. Phys. Chem. Lett.* **2024,** *15*, 1596-1602.
121. Saha, A.; Upadhyaya, H. P.; Kumar, A.; Choudhury, S.; Naik, P. D. Sum-Frequency Generation Spectroscopy of an Adsorbed Monolayer of Mixed Surfactants at an Air–Water Interface. *J. Phys. Chem. C* **2014,** *118*, 3145-3155.
122. Tyrode, E.; Hedberg, J. A Comparative Study of the CD and CH Stretching Spectral Regions of Typical Surfactants Systems Using VSFS: Orientation Analysis of the Terminal $CH_3$ and $CD_3$ Groups. *J. Phys. Chem. C* **2011,** *116*, 1080-1091.
123. Messmer, M. C.; Conboy, J. C.; Richmond, G. L. Observation of Molecular Ordering at the Liquid-Liquid Interface by Resonant Sum Frequency Generation. *J. Am. Chem. Soc.* **2002,** *117*, 8039-8040.
124. Scheu, R.; Chen, Y.; de Aguiar, H. B.; Rankin, B. M.; Ben-Amotz, D.; Roke, S. Specific Ion Effects in Amphiphile Hydration and Interface sStabilization. *J. Am. Chem. Soc.* **2014,** *136*, 2040-2047.
125. Nguyen, K. T.; Nguyen, T. D.; Nguyen, A. V. Strong Cooperative Effect of Oppositely Charged Surfactant Mixtures on their Adsorption and Packing at the Air-Water Interface and Interfacial Water Structure. *Langmuir* **2014,** *30*, 7047-7051.

126. Yu, C. C.; Seki, T.; Chiang, K. Y.; Wang, Y.; Bonn, M.; Nagata, Y. Depth-Profiling Alkyl Chain Order in Unsaturated Lipid Monolayers on Water. *J. Chem. Phys.* **2024,** *160*, 114902.
127. Lu, J. R.; Simister, E. A.; Lee, E. M.; Thomas, R. K.; Rennie, A. R.; Penfold, J. Direct Determination by Neutron Reflection of the Penetration of Water into Surfactant Layers at the Air/Water Interface. *Langmuir* **1992,** *8*, 1837-1844.
128. Tadros, T. F. *Formulations: In Cosmetic and Personal Care*; De Gruyter, Berlin, Germany, 2016.
129. Tadros, T. F. *Applied Surfactants: Principles and Applications;* Wiley-VCH Verlag GmbH & Co. KGaA. Weinheim, 2005.
130. Ashim, D. Surfactants and Detergents; London, England: IntechOpen,2019
131. Tian, Y.; Zhou, J.; He, C.; He, L.; Li, X.; Sui, H. The Formation, Stabilization and Separation of Oil–Water Emulsions: A Review. *Processes* **2022,** *10*, 738.
132. Jones, K. K.; Scatena, L. F. A tale of Two Tales: Tail Ordering of Stoichiometric 1:1 DTAB:SDS Pairs Adsorbed at the Oil-Water Interface, 10.1021/acs.langmuir.4c03748.
133. Fainerman, V. B.; Vollhardt, D.; Siegel, S. Dynamics of a Mixed Monolayer Consisting of a Soluble Amphiphile and Its Insoluble 2D Condensing Homologue. *J. Phys. Chem. B* **2002,** *106*, 5701-5709.
134. Altman, R. M.; Christoffersen, E. L.; Jones, K. K.; Krause, V. M.; Richmond, G. L. Playing Favorites: Preferential Adsorption of Nonionic over Anionic Surfactants at the Liquid/Liquid Interface. *Langmuir* **2021,** *37*, 12213-12222.
135. Tran, E.; Jones, K. K.; Cano, G. A.; Moore, F. G.; Scatena, L. F. Spectroscopic Studies of Zwitterionic DDAPS at Planar and Droplet Oil/Water Interfaces. *J. Phys. Chem. B* **2022,** *126*, 7720-7730.
136. Casford, M. T. L.; Davies, P. B.; Neivandt, D. J. Study of the Coadsorption of an Anionic Surfactant and an Uncharged Polymer at the Aqueous Solution/Hydrophobic Surface Interface by Sum Frequency Spectroscopy. *Langmuir* **2003,** *19*, 7386-7391.
137. Duignan, T. T.; Peng, M.; Nguyen, A. V.; Zhao, X. S.; Baer, M. D.; Mundy, C. J. Detecting the undetectable: The Role of Trace Surfactant in the Jones-Ray Effect. *J. Chem. Phys.* **2018,** *149*, 194702.
138. Nihonyanagi, S.; Yamaguchi, S.; Tahara, T., Direct Evidence for Orientational Flip-Flop of Water Molecules at Charged Interfaces: A Heterodyne-Detected Vibrational Sum Frequency Generation Study. *J. Chem. Phys.* **2009,** *130*, 204704.
139. Kumari, R.; Kakati, A.; Nagarajan, R.; Sangwai, J. S., Synergistic Effect of Mixed Anionic and Cationic Surfactant Systems on the Interfacial Tension of Crude Oil-Water and Enhanced Oil Recovery. *J. Disp. Sci. Tech.* **2018,** *40*, 969-981.
140. Rajkhowa, S.; Mahiuddin, S.; Ismail, K., An Assessment of the Aggregation and Adsorption Behavior of the Sodium Dodecylsulfate–Cetyltrimethylammonium Bromide Mixed Surfactant System in Aqueous Medium. *J. Solution Chem.* **2016,** *46*, 11-24.
141. Jukeriee, P.; Mysels, K. J. *Critical Micelle Concentration of Aqueous Surfactant Systems*; Washington: U.S. National Bureau of Standards ; 1971.
142. Scheu, R.; Chen, Y.; de Aguiar, H. B.; Rankin, B. M.; Ben-Amotz, D.; Roke, S., Specific Ion Effects in Amphiphile Hydration and Interface Stabilization. *J. Am. Chem. Soc.* **2014,** *136*, 2040-2047.
143. Popova, M. V.; Raev, D. L. Aggregation Behavior of Monomeric Surfactants and a Gemini Cationic Surfactant by NMR and Computer Simulation Data. *Appl. Magn. Reson.* **2018,** *49*, 619-630.

144. Weissenborn, E.; Braunschweig, B. Specific Ion Effects of Dodecyl Sulfate Surfactants with Alkali Ions at the Air-Water Interface. *Molecules* **2019,** *24, 2911*.
145. Zarbakhsh, A.; Bowers, J.; Webster, J. R. P. A New Approach for Measuring Neutron Reflection From a Liquid/Liquid Interface. *Meas. Sci. Technol.* **1999,** *10*, 738-743.
146. Jiang, J.; Sakurai, K. X-ray reflectivity Imager with 15 W power X-Ray Source. *Rev. Sci. Instrum.* **2016,** *87*, 093709.
147. Lyu, Y.; Gu, C.; Fan, X.; Tao, J.; Yao, X.; Dai, C.; Zhao, G., Interfacial Rheology of a Novel Dispersed Particle Gel Soft Heterogeneous Combination Flooding System at the Oil-Water Interface. *Colloids Surf., A* **2018,** *559*, 23-34.
148. Chakraborty, S.; Kumar, H.; Dasgupta, C.; Maiti, P. K. Confined Water: Structure, Dynamics, and Thermodynamics. *Acc. Chem. Res.* **2017,** *50*, 2139-2146.
149. Tadmouri, R.; Zedde, C.; Routaboul, C.; Micheau, J. C.; Pimienta, V. Partition and Water/Oil Adsorption of Some Surfactants. *J. Phys. Chem. B* **2008,** *112*, 12318-12325.